



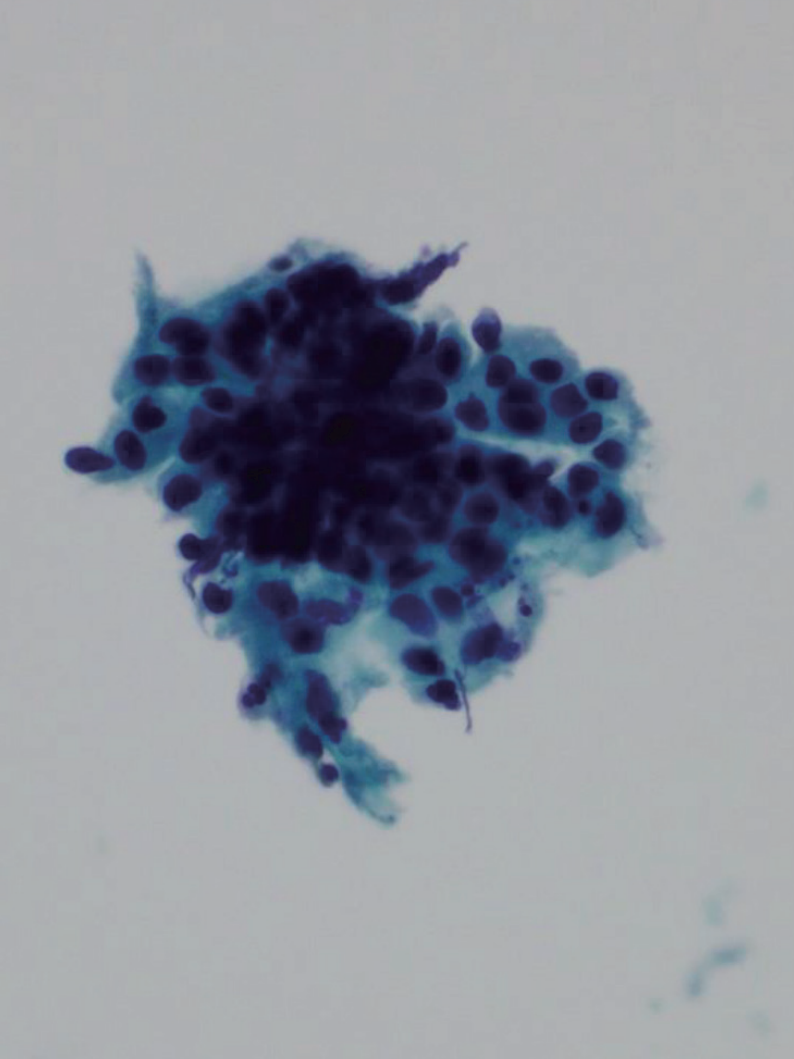
JPTM

Journal of **P**athology
and **T**ranslational **M**edicine

May 2023
Vol. 57 / No.3
jpatholtm.org
pISSN: 2383-7837
eISSN: 2383-7845



Trouble-Makers
in Cervical Cytology



Aims & Scope

The *Journal of Pathology and Translational Medicine* is an open venue for the rapid publication of major achievements in various fields of pathology, cytopathology, and biomedical and translational research. The Journal aims to share new insights into the molecular and cellular mechanisms of human diseases and to report major advances in both experimental and clinical medicine, with a particular emphasis on translational research. The investigations of human cells and tissues using high-dimensional biology techniques such as genomics and proteomics will be given a high priority. Articles on stem cell biology are also welcome. The categories of manuscript include original articles, review and perspective articles, case studies, brief case reports, and letters to the editor.

Subscription Information

To subscribe to this journal, please contact the Korean Society of Pathologists/the Korean Society for Cytopathology. Full text PDF files are also available at the official website (<https://jpatholtm.org>). *Journal of Pathology and Translational Medicine* is indexed by Emerging Sources Citation Index (ESCI), PubMed, PubMed Central, Scopus, KoreaMed, KoMCI, WPRIM, Directory of Open Access Journals (DOAJ), and CrossRef. Circulation number per issue is 50.

Editors-in-Chief

Jung, Chan Kwon, MD (*The Catholic University of Korea, Korea*) <https://orcid.org/0000-0001-6843-3708>

Park, So Yeon, MD (*Seoul National University, Korea*) <https://orcid.org/0000-0002-0299-7268>

Associate Editors

Bychkov, Andrey, MD (*Kameda Medical Center, Japan; Nagasaki University Hospital, Japan*) <https://orcid.org/0000-0002-4203-5696>

Kim, Haeryoung, MD (*Seoul National University, Korea*) <https://orcid.org/0000-0002-4205-9081>

Lee, Hee Eun, MD (*Mayo Clinic, USA*) <https://orcid.org/0000-0001-6335-7312>

Shin, Eunah, MD (*Yongin Severance Hospital, Yonsei University, Korea*) <https://orcid.org/0000-0001-5961-3563>

Editorial Board

Avila-Casado, Maria del Carmen, MD (*University of Toronto, Toronto General Hospital UHN, Canada*)

Bae, Jeong Mo, MD (*Seoul National University, Korea*)

Bae, Young Kyung, MD (*Yeungnam University, Korea*)

Bongiovanni, Massimo, MD (*Lausanne University Hospital, Switzerland*)

Bova, G. Steven, MD (*University of Tampere, Finland*)

Choi, Joon Hyuk (*Yeungnam University, Korea*)

Chong, Yo Sep, MD (*The Catholic University of Korea, Korea*)

Chung, Jin-Haeng, MD (*Seoul National University, Korea*)

Fadda, Guido, MD (*Catholic University of Rome-Foundation Agostino Gemelli University Hospital, Italy*)

Fukushima, Noriyoshi, MD (*Jichi Medical University, Japan*)

Go, Heounjeong (*University of Ulsan, Korea*)

Hong, Soon Won, MD (*Yonsei University, Korea*)

Jain, Deepali, MD (*All India Institute of Medical Sciences, India*)

Kakudo, Kennichi, MD (*Izumi City General Hospital, Japan*)

Kim, Jang-Hee, MD (*Ajou University, Korea*)

Kim, Jung Ho, MD (*Seoul National University, Korea*)

Kim, Se Hoon, MD (*Yonsei University, Korea*)

Komuta, Mina, MD (*Keio University, Tokyo, Japan*)

Kwon, Ji Eun (*Ajou University, Korea*)

Lai, Chiung-Ru, MD (*Taipei Veterans General Hospital, Taiwan*)

Lee, C. Soon, MD (*University of Western Sydney, Australia*)

Lee, Hwajeong, MD (*Albany Medical College, USA*)

Lee, Sung Hak, MD (*The Catholic University, Korea*)

Liu, Zhiyan, MD (*Shanghai Jiao Tong University, China*)

Lkhagvadorj, Sayamaa, MD (*Mongolian National University of Medical Sciences, Mongolia*)

Moran, Cesar, MD (*MD Anderson Cancer Center, U.S.A.*)

Paik, Jin Ho, MD (*Seoul National University, Korea*)

Park, Jeong Hwan (*Seoul National University, Korea*)

Ro, Jae Y., MD (*Cornell University, The Methodist Hospital, U.S.A.*)

Sakhuja, Puja, MD (*Govind Ballabh Pant Hospital, India*)

Shahid, Pervez, MD (*Aga Khan University, Pakistan*)

Song, Joon Seon, MD (*University of Ulsan, Korea*)

Tan, Puay Hoon, MD (*National University of Singapore, Singapore*)

Than, Nandor Gabor, MD (*Semmelweis University, Hungary*)

Tse, Gary M., MD (*The Chinese University of Hong Kong, Hong Kong*)

Yatabe, Yasushi, MD (*Aichi Cancer Center, Japan*)

Zhu, Yun, MD (*Jiangsu Institution of Nuclear Medicine, China*)

Ethic Editor

Choi, In-Hong, MD (*Yonsei University, Korea*)

Huh, Sun, MD (*Hallym University, Korea*)

Statistics Editors

Kim, Dong Wook (*National Health Insurance Service Ilsan Hospital, Korea*)

Lee, Hye Sun (*Yonsei University, Korea*)

Manuscript Editor

Chang, Soo-Hee (*InfoLumi Co., Korea*)

Layout Editor

Kim, Haeja (*iMiS Company Co., Ltd., Korea*)

Website and JATS XML File Producers

Cho, Yoonsang (*M2Community Co., Korea*)

Im, Jeonghee (*M2Community Co., Korea*)

Administrative Assistants

Kim, Da Jeong (*The Korean Society of Pathologists*)

Jeon, Anmi (*The Korean Society for Cytopathology*)

Contact the Korean Society of Pathologists/the Korean Society for Cytopathology

Publishers: Choe, Gheeyoung, MD, Lee, Seung-Sook, MD

Editors-in-Chief: Jung, Chan Kwon, MD, Park, So Yeon, MD

Published by the Korean Society of Pathologists/the Korean Society for Cytopathology

Editorial Office

Room 1209 Gwanghwamun Officia, 92 Saemunan-ro, Jongno-gu, Seoul 03186, Korea

Tel: +82-2-795-3094 Fax: +82-2-790-6635 E-mail: office@jpatholtm.org

#1508 Renaissancetower, 14 Mallijae-ro, Mapo-gu, Seoul 04195, Korea

Tel: +82-2-593-6943 Fax: +82-2-593-6944 E-mail: office@jpatholtm.org

Printed by iMiS Company Co., Ltd. (JMC)

Jungang Bldg. 18-8 Wonhyo-ro 89-gil, Yongsan-gu, Seoul 04314, Korea

Tel: +82-2-717-5511 Fax: +82-2-717-5515 E-mail: ml@smileml.com

Manuscript Editing by InfoLumi Co.

210-202, 421 Pangyo-ro, Bundang-gu, Seongnam 13522, Korea

Tel: +82-70-8839-8800 E-mail: infolumi.chang@gmail.com

Front cover image: Atrophic cervicitis in liquid based preparation (p141).

© Copyright 2023 by the Korean Society of Pathologists/the Korean Society for Cytopathology

© Journal of Pathology and Translational Medicine is an Open Access journal under the terms of the Creative Commons Attribution Non-Commercial License (<https://creativecommons.org/licenses/by-nc/4.0>).

© This paper meets the requirements of KS X ISO 9706, ISO 9706-1994 and ANSI/NISO Z.39.48-1992 (Permanence of Paper).

CONTENTS

REVIEW

- 139 Trouble-makers in cytologic interpretation of the uterine cervix
Eunah Shin, Jaeeun Yu, Soon Won Hong

ORIGINAL ARTICLES

- 147 Expression of specific microRNAs in tissue and plasma in colorectal cancer
Allan Fellizar, Vivencio Refuerzo, John Donnie Ramos, Pia Marie Albano
- 158 Frequent apocrine changes in pleomorphic adenoma with malignant transformation:
a possible pre-malignant step in ductal carcinoma ex pleomorphic adenoma
Joon Seon Song, Yeseul Kim, Yoon-Se Lee, Seung-Ho Choi, Soon Yuhl Nam, Sang Yoon Kim, Kyung-Ja Cho
- 166 Clinicopathologic characterization of cervical metastasis from an unknown primary tumor: a multicenter study in Korea
Miseon Lee, Uiree Jo, Joon Seon Song, Youn Soo Lee, Chang Gok Woo, Dong-Hoon Kim, Jung Yeon Kim, Sun Och Yoon, Kyung-Ja Cho

CASE REPORT

- 178 Thyroid pathology, a clue to PTEN hamartoma tumor syndrome
Yurimi Lee, Young Lyun Oh

NEWSLETTER

- 184 What's new in bone and soft tissue pathology 2023: guidelines for molecular testing
Farres Obeidin

Trouble-makers in cytologic interpretation of the uterine cervix

Eunah Shin, Jaeun Yu, Soon Won Hong

Department of Pathology, Yongin Severance Hospital, Yonsei University College of Medicine, Yongin, Korea

The development and standardization of cytologic screening of the uterine cervix has dramatically decreased the prevalence of squamous cell carcinoma of the uterine cervix. Advances in the understanding of biology of human papillomavirus have contributed to upgrading the histologic diagnosis of the uterine cervix; however, cytologic screening that should triage those that need further management still poses several difficulties in interpretation. Cytologic features of high grade intraepithelial squamous lesion (HSIL) mimics including atrophy, immature metaplasia, and transitional metaplasia, and glandular lesion masquerades including tubal metaplasia and HSIL with glandular involvement are described with accentuation mainly on the differential points. When the cytologic features lie in a gray zone between the differentials, the most important key to the more accurate interpretation is sticking to the very basics of cytology; screening the background and cellular architecture, and then scrutinizing the nuclear and cytoplasmic details.

Key Words: Cytology; Uterine cervix; Atrophy; Metaplasia; Glandular involvement; High grade intraepithelial squamous lesion

Received: December 6, 2022 **Revised:** April 21, 2023 **Accepted:** April 25, 2023

Corresponding Author: Soon Won Hong, MD, PhD, Department of Pathology, Yongin Severance Hospital, Yonsei University College of Medicine, 363 Dongbaekjukjeon-daero, Giheung-gu, Yongin 16995, Korea
Tel: +82-31-5189-8250, Fax: +82-31-5189-8248, E-mail: soonwonh@yuhs.ac

Cytology is an important and well-established diagnostic modality in the screening of uterine cervical cancers. With the implication of the Bethesda System, the cytologic diagnosis of the uterine cervix has been standardized and steadily upgraded worldwide; however, it still poses several difficulties in interpretation due to the fact that the uterine cervix is affected by various indigenous factors, namely hormone, age, and infection. The major difficulties in the interpretation of cervical cytology lie in high grade intraepithelial squamous lesion (HSIL) mimics and glandular lesion masquerades. This review is mainly focused on detailed differential points in discriminating these troublesome entities.

HIGH GRADE INTRAEPITHELIAL SQUAMOUS LESION MIMICS

Cytologic features that are diagnostic of HSIL can be described in two aspects; cytologic features of discrete, singly scattered individual cells and those of tissue fragments. Cells diagnostic of HSIL are usually small and round, but with high nuclear:cytoplasmic (N:C) ratio. The nuclear features include rounded but sharp nu-

clear membrane, coarsely granular chromatin, and longitudinal nuclear groove with lack of nucleoli. The cytoplasm is scant in amount or almost indiscernible. Syncytial tissue fragments are a common architectural presentation of HSIL, and the above diagnostic nuclear details can be found within these syncytial tissue fragments by changing the plane of focus. However, not all HSIL cases consistently show these cytologic features clearcut and not all the diagnostic features are exclusively seen in HSIL. Discrete, singly scattered cells that mimic HSIL can be found in immature squamous metaplasia, intrauterine device associated changes, atrophic cervicitis, and endometrial stromal cells. Tissue fragments that mimic HSIL can be found in squamous metaplasia, tubal metaplasia, endocervical adenocarcinoma in situ (AIS), endometrial adenocarcinoma, and atrophic cervicitis. Acs et al. [1] have reported that when 130 cases with cervical cytologic diagnosis of HSIL or atypical squamous cells of uncertain significance - cannot exclude HSIL (ASC-H) that had corresponding biopsy were reviewed, 13 cases were histologically diagnosed as low grade squamous intraepithelial lesion (LSIL) or reactive. Re-examination of the cervical cytology slides of these 13 cases revealed repair changes, atypical squamous metaplasia, atrophy, tubal metaplasia,

lower uterine sampling, and histiocytes and lymphocytes [1]. Therefore, many conditions work as confounding factors in diagnosing HSIL, and these so-called HSIL mimics, namely atrophic cervicitis, immature or atypical squamous metaplasia, and transitional metaplasia are described more in detail.

Atrophic cervicitis (atrophy)

Abnormal results are reported more frequently in postmenopausal women than in pre-menopausal women, and Kaminski et al. [2] attributed this to the strong correlation between estrogen deficiency and squamous atypia, and concluded that estrogen therapy can revert this squamous atypia to normal cytology. Since atrophic cervicovaginal smears can exhibit various atypical patterns, they can easily mislead to overdiagnosis of squamous atypia or even carcinoma. On the contrary, due to the reduced number of exfoliated cells after menopause, a high false negative rate on cytologic screening is also problematic in postmenopausal women. Additional confounding factors are frequent drying artifacts and inflammation, resulting in low cellularity, nuclear hyperchromasia and poor nuclear preservation [3]. Therefore, it is very critical that cervicovaginal smears in postmenopausal women be examined with extra care to avoid both overdiagnosis and underestimation.

Cervical smears of atrophic cervicitis show tissue fragments composed of uniform cell population with a streaming pattern in the background of cellular and inflammatory debris. These tissue fragments are not true syncytial tissue fragments and they often show folding of the edges. The uniform cell population comprising the tissue fragments are mostly parabasal cells with nuclear enlargement or miniature squamous cells with orangeophilic cytoplasm and pyknotic nuclei. The nuclear details of the atrophic parabasal cells comprising tissue fragments can be highlighted by changing the plane of focus. The entire cell population in the tissue fragments is uniform and very similar to the squamous cells present in the background. The tissue fragments show more crowding of smaller nuclei that are densely stained and have scant cytoplasm with high N:C ratios, often misleading to the diagnosis of HSIL. Moreover, atrophic fragments are not truly syncytial as in HSIL fragments. One of the other helpful diagnostic features would be the similarity between the background cells, which lack the nuclear characteristics of HSIL cells. The singly scattered cells around these tissue fragments are often pleomorphic in shape, but when carefully examined, the nuclei are either smudged or too hyperchromatic (Fig. 1). In a study by Chivukula and Shidham [4], they subcategorized reactive cytomorphologic patterns into microglandular

hyperplasia-like, repair-like and atrophy-like patterns, and they described atrophy-like pattern as either single cells or hyperchromatic crowded groups of parabasal cells. In the single cell pattern, the individual cells had abundant blue cytoplasm and open chromatin with or without nucleoli. In the parabasal pattern, the cells showed small dark nuclei and variable cytoplasm, usually with a low N:C ratio. In contrast, they described HSIL-like pattern as single cells with nuclear hyperchromasia and coarse chromatin. In a study by Mokhtar et al. [5], the authors described a coarse chromatin pattern as a distinct predictive feature of HSIL in follow-up biopsies. An increase in nuclear size of at least twice that of an intermediate cell nucleus with significant hyperchromasia, irregular nuclear contours or chromatin distribution and marked cellular pleomorphism are features that can qualify for atypical squamous cells of uncertain significance in postmenopausal women. Additional feature is a variation in nuclear size [6]. In a study by Acs et al. [1], unequivocal cytologic features of those diagnosed in cytology as atypical squamous cells and later histologically confirmed as squamous intraepithelial lesion (SIL) were atypical parakeratotic/dyskeratotic cells showing irregular and hyperchromatic nuclei, orangeophilic cytoplasm with anisocytosis, and increased N:C ratio. Pseudokoilocytosis characterized by perinuclear halo with slightly increased size of nuclei can also be seen in atrophic smear and mislead to an overdiagnosis of LSIL, however, the nuclear enlargement is mild (1.5–2.5 intermediate cell nuclei), nuclear contours are mostly smooth, and chromatin pattern is evenly distributed and smooth [7]. Nuclear hyperchromasia and irregular nuclear contours are the most reliable cytomorphological criteria [8,9]. The nuclear membrane in HSIL is thickened twice that of non-HSIL cells in the background, and it appears as if the nuclear membrane has been drawn over. It should be noted that degenerated and dried small parabasal cells often appear orangeophilic in postmenopausal smears and it may be difficult to distinguish them from atypical parakeratosis or dyskeratotic cells of HSIL [10]. Nuovo et al. [11], has reported that parakeratosis was the only feature noted at a higher rate in the human papillomavirus-positive cases from postmenopausal women.

Another pseudo-alarming cytologic feature in atrophic smear is the blue blobs, which are round to oval, smudged, and densely cyanophilic bodies with ill-defined borders, mostly seen in postmenopausal smears (Fig. 2) [12]. They have been once thought to be inspissated mucus, but Abdulla et al. [13] have demonstrated positive immunoreactivity to cytokeratin and epithelial membrane antigen and cellular skeletons with residual tonofilaments on transmission electron microscopy, concluding that they

are degenerated parabasal cells. Blue blobs appear in atrophic smear in postmenopausal women due to the lack of mucus and stagnation of exfoliated cells, which are then further degenerated.

Disintegration of chromatin results in the characteristic dense cyanophilic appearance of blue blobs and they eventually become granular background material. Blue blobs should be differenti-

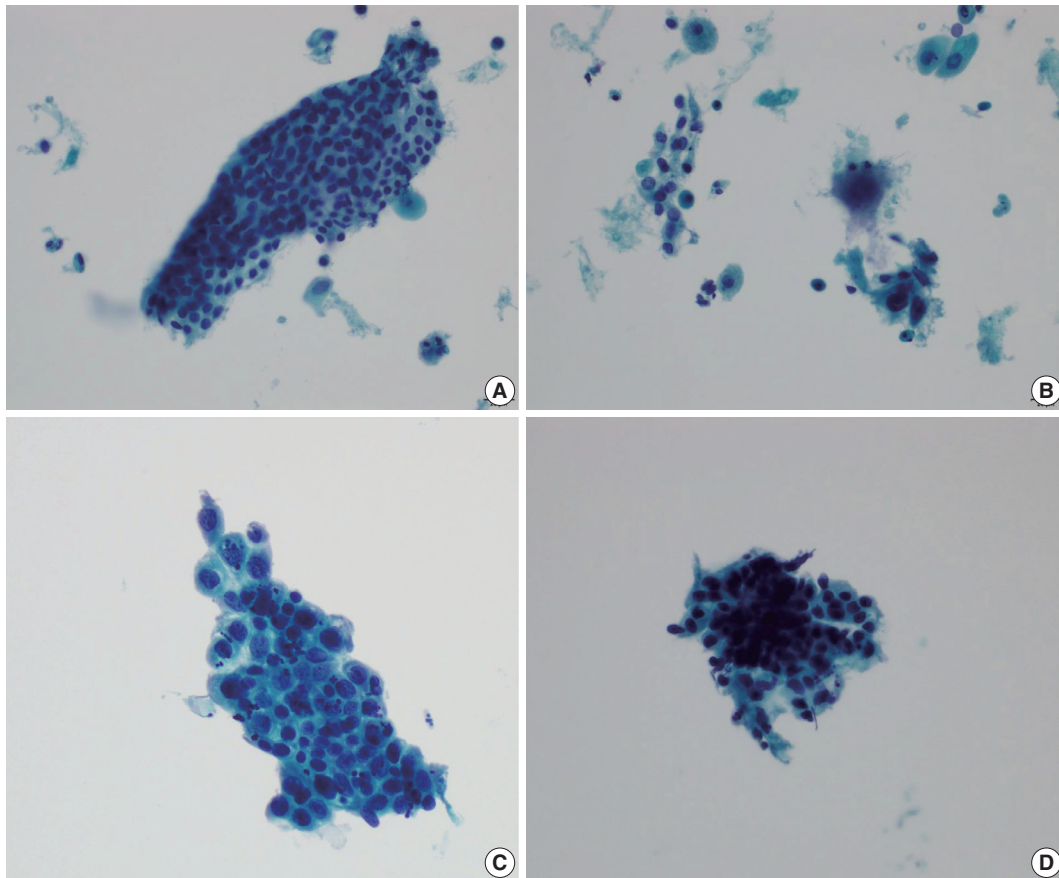


Fig. 1. Atrophic cervicitis in liquid based preparation. (A) A tissue fragment in atrophic cervicitis, showing small nuclei with scant cytoplasm and high nuclear:cytoplasmic ratio. The tissue fragment is not syncytial, with folding of the edge. (B) Inflammatory debris in the background is evident in liquid based preparation. (C) Atrophic parabasal cells showing apoptotic and inflammatory debris within the cell group. (D) The nuclei in atrophic cervicitis are often pyknotic.

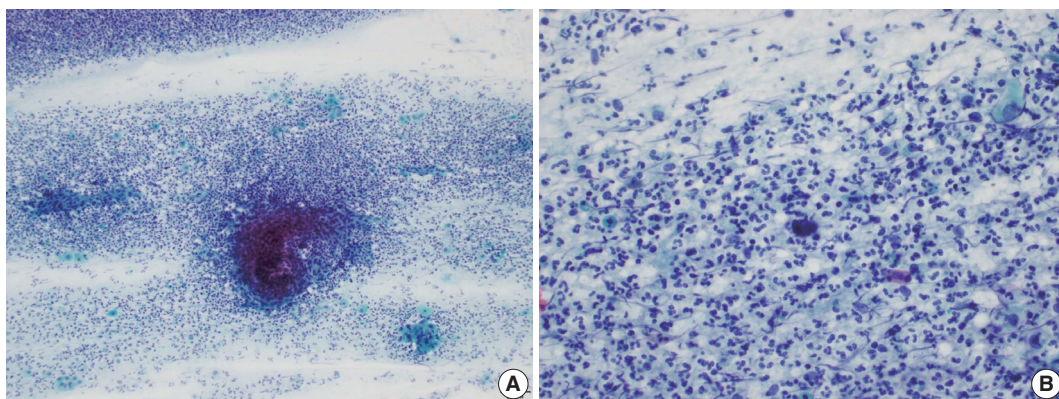


Fig. 2. Atrophic cervicitis in conventional smear. (A) Atrophic cervicitis showing a tissue fragment composed of uniform cell population with a streaming pattern in the background of cellular and inflammatory debris. (B) A blue blob showing small round to oval, smudged, and densely cyanophilic body with an ill-defined border.

ated rightly because they can be mistaken for naked dyskeratotic or malignant cell nuclei. Lack of chromatin and lack of background inflammatory reaction or diathesis should help identify blue blobs from true dyskeratotic cells. The differential diagnostic points of atrophy from HSIL are summarized in Table 1.

Immature squamous metaplasia

Immature metaplastic cells with slight nuclear enlargement are often difficult to differentiate from SIL. A common cytologic presentation of HSIL is syncytial tissue fragments as in immature squamous metaplasia. However, tissue fragments in immature squamous metaplasia is basically monolayered, composed of metaplastic cells characterized by well-defined cell borders, appreciable cytoplasm, uniform nuclei with minimal nuclear enlargement. The cells show low N:C ratio with evenly dispersed chromatin. The singly scattered metaplastic cells also show distinct cytoplasmic border, smooth nuclear membrane and evenly distributed finely granular chromatin pattern. The nucleoli are often present, which is one of the important differential points from SIL. Cytoplasmic processes can also be present. Immature squamous metaplasia is associated with a fine chromatin pattern and dense cytoplasmic differentiation [14]. A fine chromatin pat-

tern along with dense cytoplasmic differentiation is a significant diagnostic feature of immature squamous metaplasia, and the presence of prominent nucleoli is highly predictive of reactive cell change (Fig. 3) [5], and nuclear crowding, overlapping and pleomorphism are not distinctive. The differential diagnostic points between HSIL and immature squamous metaplasia are summarized in Table 2.

Transitional metaplasia

Transitional metaplasia can be mistaken as HSIL because they appear as hyperchromatic crowded groups comprised of small hyperchromatic cells with increased N:C ratio. Differential points include no distinct cytoplasmic border, longitudinal nuclear grooves, and relatively bland chromatin pattern. HSIL cells can show longitudinal nuclear grooves, which can be one of the differential points distinguishing HSIL from glandular abnormality. Therefore, when differentiating tubal metaplasia from HSIL, longitudinal nuclear grooves should be taken into account with other nuclear features, such as presence of nucleoli, but with bland and even chromatin pattern, nearly inconspicuous nuclear membrane, and the presence of relatively ample cytoplasm. Characteristically, the cell groups show a monolayered streaming pattern of ovoid to spindle shaped nuclei [15]. Whirling and streaming pattern of the cells within the cellular cluster can be an additionally helpful point.

GLANDULAR LESION MASQUERADES

Tubal metaplasia

Tubal metaplasia indicates endocervical glandular epithelium replaced by cells resembling the lining epithelial cells of the fal-

Table 1. Differential diagnostic points between atrophy and HSIL

Cytologic features	Atrophy	HSIL
Cell border	Poorly defined	Distinct
Nuclear:cytoplasmic ratio	Low	High
Nucleoli	Often present	Absent
Cell population	Uniform	Heterogeneous
Polarity	Streaming	Haphazard loss of polarity
Background	Same cells	Singly scattered HSIL cells

HSIL, high grade intraepithelial squamous lesion.

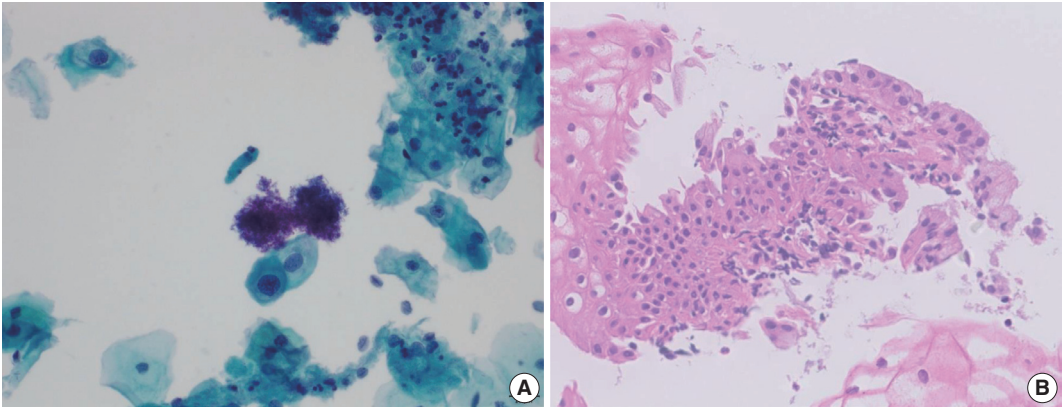


Fig. 3. Cytologic (A) and histologic (B) pictures of immature squamous metaplasia showing fine chromatin pattern with dense cytoplasmic differentiation. The nuclear:cytoplasmic ratio is increased, but short of that in high grade intraepithelial squamous lesion, and the nuclear membrane is not irregular or thickened.

lopian tubes. It is a common diagnostic pitfall, especially in differential diagnosis of endocervical AIS, because the cells are alarming at first glance. Usually, they appear as flat monolayered sheets, pseudostratified strips, or cohesive clusters of cuboidal or columnar cells with basally oriented nuclei and cilia in the other end of the cytoplasm when the cells are arranged parallel to each other (Fig. 4) [16]. However, they can appear hyperchromatic with loss of polarity, and increased N:C ratio, especially when the cells are arranged en face on the slide and cilia cannot be ascertained. The nuclei show finely granular chromatin and nucleoli are usually not seen. Therefore, in order to overcome this diagnostic pitfall and avoid overdiagnosis, an extra care should be taken to locate other cellular clusters that reveal slender columnar cells with tapering in one end and cilia in the other end. In addition, cellular sheets of tubal metaplasia reveal rare or no mitotic figures, no apoptotic bodies, and clean background [16,17].

HSIL with glandular involvement

Benign mimics of glandular lesion are two dimensional with

Table 2. Differential diagnostic points between HSIL and immature squamous metaplasia

Cytologic features	Immature squamous metaplasia	HSIL
Nuclear features		
Chromatin pattern	Evenly distributed finely granular	Clumped coarsely granular
Nuclear membrane	Smooth	Sharp, undulating, grooving
Nucleoli	Often present	Absent
Cytoplasmic features		
Cytoplasmic processes	Present	Absent
Amount	Appreciable	Scanty, often indiscernible
N:C ratio	Low	High

HSIL, high grade intraepithelial squamous lesion; N:C, nuclear:cytoplasmic.

honeycomb pattern, showing cytoplasmic streaming, nuclear polarity, and cytoplasmic vacuoles. Architectural features that help to distinguish benign mimics from neoplastic glandular lesions are sheets with pseudostratification, maintenance of polarity, prominent nucleoli, and less hyperchromasia.

Pre-neoplastic or neoplastic glandular cells show poorly oriented architecture, irregular nuclear membranes, decreased cytoplasm, loss of honeycomb pattern, nuclear crowding and overlap, loss of nuclear polarity, atypical single cells, and coarsely granular chromatin. Tight clusters of stretched cells with a high N:C ratio, hyperchromatic nuclei with fine nuclear chromatin and a thin rim of finely vacuolated cytoplasm upon changing plane of focus point towards a glandular origin. Moreover, nuclear enlargement with scant cytoplasm resulting in high N:C ratio, nuclear size variation, cellular crowding and stratification, nuclear hyperchromasia with coarse chromatin pattern and small or absent nucleoli in clean background are diagnostic features of endocervical AIS [18]. Apoptosis and mitoses can also be frequently seen in AIS, but the most helpful diagnostic clue would be ‘feathering’ at the periphery of the abnormal cell clusters.

Glandular lesion of the uterine cervix accounts for 0.1%–0.8% of the cervical smears, and 17%–80% of the cytologic diagnoses have significant follow-up results, 40%–50% of which coexist with squamous lesion. Clinically, the diagnosis of atypical glandular cells (AGC) warrants direct colposcopic biopsy with endocervical sampling and additional endometrial sampling for women older than 45 years. It is reported that the most common histologic diagnosis following cytologic diagnosis of AGC is SIL. Upon histologic correlation of AGC, about 15% have been reported to be associated with SIL, 1% with AIS, and 0.5% with adenocarcinoma [19]. This is attributed to the fact that it is most difficult to differentiate glandular abnormality from SIL with glandular involvement [20].

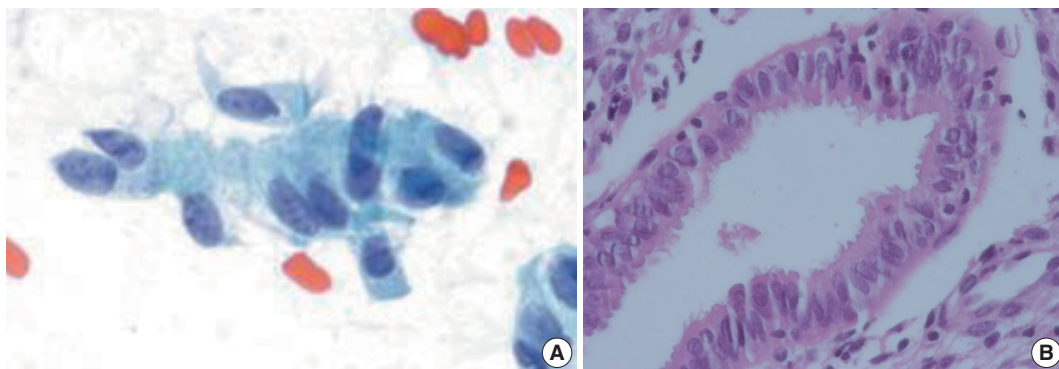


Fig. 4. Cytologic (A) and histologic (B) pictures of tubal metaplasia, showing cuboidal or columnar cells with basally oriented nuclei and cilia at the other end of the cytoplasm.

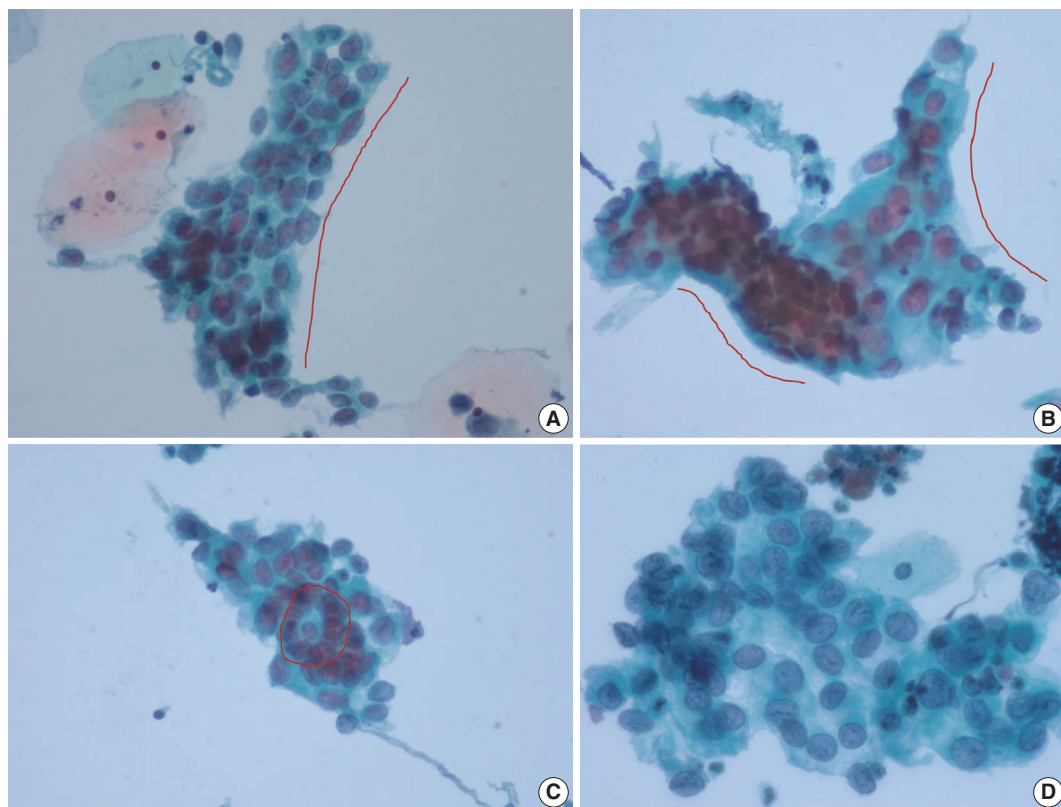


Fig. 5. The most frequent and helpful cytological features of high grade intraepithelial squamous lesion (HSIL) with glandular extension that are indicative of squamous origin. (A, B) The long axis of the peripheral nuclei are parallel to the longitudinal axis of the cellular cluster, arranged circumferentially rather than radially, with one sided flattening. (C) The nuclei often show horizontal polarity around gland opening. (D) Nuclear grooves in HSIL cells. The differential points from transitional metaplasia are nuclear irregularity, slightly thickened nuclear membrane, loss of polarity (absence of a streaming pattern), and increased nuclear:cytoplasmic ratio.

The most frequent and helpful cytological features of HSIL with glandular extension that are indicative of squamous origin are as follows: Syncytial clusters, sheets with loss of central polarity, oval nuclei, inconspicuous nucleoli, peripheral nuclear flattening, and nuclear grooves. The chromocenters in HSIL nuclei can often be misinterpreted as nucleoli, which may mislead to AGC [19]. The longitudinal axis of the peripheral nuclei are parallel to the long axis of the cellular cluster with one sided flattening (Fig. 5). Occasionally, the cellular clusters show whirling of the cells in the center so that the cells may appear to be piling up (Table 3) [17]. Also, singly scattered dysplastic squamous cells should be searched for in the background when HSIL should be differentiated from glandular lesion.

The most frequent reasons for misclassification of SIL as AGC would be few dysplastic squamous cells masked by abundant benign or AGC and sheets of dysplastic squamous cells peripherally lined by glandular cells, which should rightly be interpreted as glandular involvement of squamous lesion rather than AGC per se.

CONCLUSION

Interpretation of uterine cervical cytology can pose diagnostic difficulties because the transformation zone of the uterine cervix is vulnerable to many indigenous and exogenous factors. When evaluating cervical smears, it is important to spot tissue fragments and singly scattered cells, and careful examination of both components is essential. In evaluation of tissue fragments, polarity of the composing cells should be noted first, followed by the examination of homogeneity of the cells in size and shape. Finally, comparing whether the cells comprising the tissue fragments and the cells scattered in the background are the same cells should follow. Upon completion of examining the tissue fragments, single cells scattered in the background of the tissue fragments should be evaluated, including the cytoplasmic border, the amount of cytoplasm, N:C ratio, nuclear shape, nuclear membrane, and chromatin pattern. All these aspects should be considered comprehensively to reach the cytologic diagnosis, avoiding potential pitfalls. Additionally, it should always be

Table 3. Differential diagnostic points between HSIL with glandular involvement and glandular lesion

Cytologic feature	HSIL with glandular involvement	Glandular lesion
Architecture		
	Syncytial clusters	Loss of honeycomb pattern
	Peripheral nuclear flattening	Loss of nuclear polarity
	Whirling in the center	Nuclear crowding with overlapping
Nuclear features		
Chromatin pattern	Coarse	Fine
Nuclear grooves	Often present	Absent
Nucleoli	Absent	Often present
Cytoplasmic features		
Cytoplasmic processes	Present	Absent
Vacuolation	Absent	Present

HSIL, high grade intraepithelial squamous lesion.

kept in mind that when distinct nucleoli are seen, then the cytologic diagnosis of SIL is less likely. Rather, cells showing distinct nucleoli are either reactive, including various types of metaplasia, or overtly malignant cancer, either squamous or glandular in origin. Hyperchromatic crowded groups of cells showing nucleoli can be alarming at first, but careful evaluation of the architecture, nuclear membrane, and chromatin pattern can help avoid overdiagnosis. In summation, the most important key facilitating more accurate interpretation in spite of various diagnostic pitfalls would be sticking to the very basics of cytologic criteria of epithelial abnormality. Nuclear details such as chromatin pattern (fine or coarse), presence or absence of a prominent nucleolus, N:C ratio, and cytoplasmic differentiation (pale or dense) are important diagnostic features that may help distinguish those that are more likely in need of further management.

Ethics Statement

Not applicable.

Availability of Data and Material

All data generated or analyzed during the study are included in this published article (and its supplementary information files).

Code Availability

Not applicable.

ORCID

Eunah Shin <https://orcid.org/0000-0001-5961-3563>
 Jaeun Yu <https://orcid.org/0000-0003-1823-4908>
 Soon Won Hong <https://orcid.org/0000-0002-0324-2414>

Author Contributions

Conceptualization: ES, SWH. Data curation: JY. Methodology: ES. Super-

vision: SWH. Writing—original draft: ES. Writing—review & editing: JY. Approval of final manuscript: all authors.

Conflicts of Interest

E.S., a contributing editor of the *Journal of Pathology and Translational Medicine*, was not involved in the editorial evaluation or decision to publish this article. All remaining authors have declared no conflicts of interest.

Funding Statement

No funding to declare.

References

1. Acs G, Gupta PK, Baloch ZW. Glandular and squamous atypia and intraepithelial lesions in atrophic cervicovaginal smears: one institution's experience. *Acta Cytol* 2000; 44: 611-7.
2. Kaminski PF, Sorosky JL, Wheelock JB, Stevens CW Jr. The significance of atypical cervical cytology in an older population. *Obstet Gynecol* 1989; 73: 13-5.
3. Waddell CA. The influence of the cervix on smear quality. I: Atrophy. An audit of cervical smears taken post-colposcopic management of intraepithelial neoplasia. *Cytopathology* 1997; 8: 274-81.
4. Chivukula M, Shidham VB. ASC-H in Pap test: definitive categorization of cytomorphological spectrum. *Cytojournal* 2006; 3: 14.
5. Mokhtar GA, Delatour NL, Assiri AH, Gilliatt MA, Senterman M, Islam S. Atypical squamous cells, cannot exclude high-grade squamous intraepithelial lesion: cytohistologic correlation study with diagnostic pitfalls. *Acta Cytol* 2008; 52: 169-77.
6. Rader AE, Rose PG, Rodriguez M, Mansbacher S, Pitlik D, Abdulkarim FW. Atypical squamous cells of undetermined significance in women over 55: comparison with the general population and implications for management. *Acta Cytol* 1999; 43: 357-62.
7. McHugh KE, Reynolds JP, Suarez AA. Postmenopausal squamous atypia: cytologic features, hybrid capture 2 tests and contribution to the ASCUS pool. *Acta Cytol* 2018; 62: 418-22.
8. Ejersbo D, Jensen HA, Holund B. Efficacy of Ki-67 antigen staining in Papanicolaou (Pap) smears in post-menopausal women with atypia: an audit. *Cytopathology* 1999; 10: 369-74.
9. Abati A, Jaffurs W, Wilder AM. Squamous atypia in the atrophic cervical vaginal smear: a new look at an old problem. *Cancer* 1998; 84: 218-25.
10. Voytek TM, Kannan V, Kline TS. Atypical parakeratosis: a marker of dysplasia? *Diagn Cytopathol* 1996; 15: 288-91.
11. Nuovo GJ, Cottrill S, Richart RM. Occult human papillomavirus infection of the uterine cervix in postmenopausal women. *Am J Obstet Gynecol* 1989; 160: 340-4.
12. Yakoushina TV, Medina IM, Hoda RS. "String of pearls" appearance of blue blobs in postmenopausal atrophy on ThinPrep Pap test. *Diagn Cytopathol* 2009; 37: 738-9.
13. Abdulla M, Hombal S, Kanbour A, et al. Characterizing "blue blobs". Immunohistochemical staining and ultrastructural study. *Acta Cytol* 2000; 44: 547-50.
14. Sheils LA, Wilbur DC. Atypical squamous cells of undetermined significance: stratification of the risk of association with, or progression to, squamous intraepithelial lesions based on morphologic subcategorization. *Acta Cytol* 1997; 41: 1065-72.
15. Duggan MA. Cytologic and histologic diagnosis and significance of controversial squamous lesions of the uterine cervix. *Mod Pathol* 2000; 13: 252-60.

16. Selvaggi SM, Haefner HK. Microglandular endocervical hyperplasia and tubal metaplasia: pitfalls in the diagnosis of adenocarcinoma on cervical smears. *Diagn Cytopathol* 1997; 16: 168-73.
17. Torous VF, Pitman MB. Interpretation pitfalls and malignant mimics in cervical cytology. *J Am Soc Cytopathol* 2021; 10: 115-27.
18. Chaump M, Pirog EC, Panico VJ, d Meritens AB, Holcomb K, Hoda R. Detection of in situ and invasive endocervical adenocarcinoma on ThinPrep Pap Test: morphologic analysis of false negative cases. *Cytojournal* 2016; 13: 28.
19. Khan MY, Bandyopadhyay S, Alrajjal A, Choudhury MS, Ali-Fehmi R, Shidham VB. Atypical glandular cells (AGC): cytology of glandular lesions of the uterine cervix. *Cytojournal* 2022; 19: 31.
20. Lee KR, Manna EA, St John T. Atypical endocervical glandular cells: accuracy of cytologic diagnosis. *Diagn Cytopathol* 1995; 13: 202-8.

Expression of specific microRNAs in tissue and plasma in colorectal cancer

Allan Fellizar^{1,2}, Vivencio Refuerzo³, John Donnie Ramos^{1,4,5}, Pia Marie Albano^{1,4,5}

¹The Graduate School, University of Santo Tomas, Manila;
Departments of ²Pathology and Laboratories and ³Surgery, Mariano Marcos Memorial Hospital and Medical Center, Batac;
⁴Research Center for Natural and Applied Sciences, University of Santo Tomas, Manila;
⁵Department of Biological Sciences, College of Science, University of Santo Tomas, Manila, Philippines

Background: MicroRNAs (miRNA/miR) play significant roles in the regulation of cell differentiation, cell cycle progression, and apoptosis. They become dysregulated during carcinogenesis and are eventually released into the circulation, enabling their detection in body fluids. Thus, this study compared the miRNA expression in tissue and plasma samples of colorectal cancer (CRC) patients and clinically healthy controls and determined miRNA expression as a potential CRC biomarker. **Methods:** Using quantitative reverse transcription polymerase chain reaction (RT-qPCR), miR-21-5p, miR-29a-3p, miR-92a-3p, miR-135b-5p, miR-196b-5p, and miR-197-3p, expression was analyzed and compared between the malignant (n=41) and the adjacent neoplasm free mucosal tissues (n=41) of CRC patients. The findings were validated in plasma samples (n=36) collected from the same CRC patients prior to surgery or any form of treatment and compared to plasma from their age and sex-matched controls (n=36). **Results:** MiR-21-5p, miR-29a-3p, miR-92a-3p, and miR-196b-5p were upregulated and miR-135b-5p was downregulated in CRC malignant tissues compared to their expression in adjacent neoplasm-free tissue. This was further observed in the plasma of the same CRC cases compared to controls. MiR-92a-3p showed itself the most sensitive (0.93; p<.001) and most specific (0.95; p<.001) in detecting CRC in tissue. In plasma, miR-196b-5p was the most sensitive (0.97; p<.001) and specific (0.94; p<.001) in detecting CRC. Plasma miR-92a-3p and miR-196b-5p were the most sensitive (0.95; p<.001) and specific (0.94; p<.001) in the early detection of CRC. **Conclusions:** Results show that specific miRNAs dysregulated in malignant tissues are released and can be detected in the circulation, supporting their potential as non-invasive biomarkers of CRC.

Key Words: microRNA; Colorectal neoplasm; Liquid biopsy; Biomarker

Received: October 27, 2021 **Revised:** February 12, 2022 **Accepted:** February 19, 2022

Corresponding Author: Allan L. Fellizar, RMT, MSMT, Department of Pathology and Laboratories, Molecular Biology Laboratory, Mariano Marcos Memorial Hospital and Medical Center, City of Batac, 2906, Ilocos Norte, Philippines
Tel: +63-917-8734007, Fax: +63-77-600-8000, E-mail: allan.fellizar.gs@ust.edu.ph

Colorectal cancer (CRC) is a potentially preventable disease due to its slow development, unlike other solid tumor malignancies [1]. However, it remains a major cause of cancer-related deaths worldwide since approximately 90% of CRC patients are diagnosed only after presentation of signs and symptoms and are already in the more advanced stage of the disease [2]. GLOBOCAN reported over 1.9 million new CRC cases and 935,173 deaths in 2020 [3].

A screening program for CRC is probably the best way to mitigate the disease. It is estimated that over 95% of CRC cases would benefit from curative surgery if diagnosis is made at an early or premalignant polyp stage [4]. CRC screening programs worldwide are targeted at adults from 50–55 years of age, a

population at increased risk of adenomas and cancer. Screening is based on several methods with varied advantages and drawbacks and different economic impact. Existing screening modalities to diagnose CRC are most often impractical due to invasiveness and cost (e.g., colonoscopy) or insufficient diagnostic accuracy (e.g., fecal-based occult blood tests) [5,6].

The discovery of notable numbers of non-coding microRNAs (miRNA/miR) that are stable in tissues and body fluids such as plasma, serum, stool, and exosomes could lead to development of a novel approach to CRC detection using circulating miRNAs as early diagnostic biomarkers for CRC. MiRNAs are small non-coding RNAs involved in gene regulation and cancer development. These miRNAs modify cell proliferation, apoptosis, and

metastasis through their interaction with intracellular signaling networks [7]. Numerous studies [8,9] have discovered aberrantly expressed miRNAs in several human malignancies. Wikberg et al. [10] observed that plasma miRNA levels significantly increased approximately three years prior to presentation of symptoms and CRC diagnosis. This finding supports the potential of circulating miRNA to improve existing CRC risk prediction and screening strategies.

Up- and downregulation of miRNA expression are seen in CRC. Several miRNAs exhibit tissue-specific or development-stage-specific expression patterns and play potential roles in maintaining tissue identity and function. Similarly, miRNAs play a vital role in malignancy as tumor suppressors and oncogenes. Thus, discovery of novel miRNAs and validation of specific signature miRNAs in a specific population can potentially change the landscape of CRC diagnostics.

Numerous miRNAs have been identified as candidate biomarkers of CRC in several independent studies through sequencing and polymerase chain reaction (PCR) techniques [11-22]. Among the miRNAs, miR-21-5p, miR-29a-3p, miR-92a-3p, miR-135b-5p, miR-196b-5p, and miR-197-3p were validated in other populations; hence, these were tested in a group of Filipino CRC patients and clinically healthy controls.

MATERIALS AND METHODS

Study participants and samples

Formalin fixed paraffin embedded (FFPE) tissue samples surgically removed from patients with histologically confirmed CRC and seen at the Mariano Marcos Memorial Hospital and Medical Center (MMM-MC) in Ilocos Norte, Philippines from March 2018 to December 2018 were included in this study. Each FFPE tissue block positive for malignant cells was matched with neoplasm-free mucosal tissue removed from the same patient and designated as case and control, respectively. Successive 5- μ m-thick tissue samples were sectioned using a microtome (Leica Biosystems, Wetzlar, Germany), with the outer sections mounted on glass slides and then stained with hematoxylin and eosin (H&E). The inner sections (approximately 5 mg) were aseptically collected in nuclease-free microcentrifuge tube. The H&E-stained slides were evaluated by a pathologist to ensure that the tissue samples designated as cases and controls were strictly positive and negative for cancer cells, respectively.

Blood samples were also collected from the same CRC patients prior to their surgery or any form of treatment (cases). These were matched with blood samples from clinically healthy volun-

teers (controls) of the same age (± 2 years) and sex as the CRC patients. Controls were strictly not suspected of any type of malignancy at the time of physical or clinical assessment by a physician, had not undergone any colorectal resection except for sigmoid diverticular disease and had not been diagnosed with inflammatory bowel disease (IBD), chronic ulcerative colitis, or Crohn's disease. All blood samples were collected in K₂EDTA tubes (Becton Dickinson, Franklin Lakes, NJ, USA) and centrifuged immediately at 2,000 \times g for 10 minutes at 4°C. Hemolyzed blood samples and turbid plasma were excluded from the study. Plasma was separated and aliquoted into nuclease-free cryovials and then stored in a freezer at -80°C until analysis.

RNA isolation from FFPE tissues and plasma samples

Total RNA including miRNAs were isolated from FFPE tissues utilizing miRNeasy FFPE kit according to manufacturer's instructions (miRNeasy FFPE Handbook June 2015, <http://www.qiagen.com>). FFPE tissue sections were deparaffinized and then digested by proteinase K, followed by heat treatment. After centrifugation, the supernatant was collected and treated with DNase. After mixing with ethanol and buffer, the lysate was transferred into a RNeasy MinElute spin column where total RNA are bound. After washing twice, the RNA was eluted.

Plasma miRNA was isolated using the miRNeasy serum/plasma kit total RNA (Qiagen, Hilden, Germany) according to manufacturer's instructions. QIAzol was added to 100 μ L of plasma, incubated, and miRNeasy serum/plasma spike-in control *Caenorhabditis elegans* miR-39 miRNA mimic (1×10^8 copies/ μ L) (Qiagen) was added to each sample. Aqueous and organic phase separation was achieved using chloroform. The aqueous phase was extracted after centrifugation and addition of absolute ethyl alcohol. The mixture was transferred to RNeasy mini spin columns and centrifuged. Buffers RWT and RPE were used respectively on two consecutive steps to wash the spin columns with centrifugation. The total RNA including miRNA was eluted using RNase-free water applied directly at the center of the mini spin column silica membrane and centrifuged at full speed. The RNA eluates from tissue and plasma were stored at -20°C until subsequent analysis.

Reverse transcription of miRNA and preamplification of cDNA

MiRNAs from colorectal tissues and plasma were polyadenylated and reverse transcribed using the miScript II RT kit and miScript HiSpec buffer (Qiagen) following the manufacturer's procedure. RNase-free water (40 μ L) was added to the synthe-

sized cDNA (10 µL), and the mixture was aliquoted into PCR tubes and stored at -20°C until analysis.

MiScript PreAMP PCR Kit (Qiagen) was used to pre-amplify the cDNA target templates following manufacturer instructions. MiR-16 was analyzed to determine the optimal dilution for real-time quantitative reverse transcription polymerase chain reaction (RT-qPCR). Samples that generated Ct values between 10 and 24 needed no further dilution for target miRNAs using RT-qPCR. Efficiency of reverse transcription was measured using miRTC assay. Efficient reverse transcription for the miRTC primer assay was set at Ct values between 14 and 20.

Quantification of selected miRNAs by qRT-PCR

SNORD61 and *C. elegans* miR-39 primers for normalization of tissue and plasma miRNA, respectively, and 10× miScript primer assay mixes for hsa-miR-21-5p, hsa-miR-196b-5p, hsa-miR-135b-5p, hsa-miR-92a-3p, hsa-29a-3p, and hsa197-3p were ordered from Qiagen. Two microliters of pre-amplified cDNA was pipetted into a 96-well PCR plate, and 23 µL of reaction mix (12.5 µL 2× QuantiTect SYBR Green PCR master mix, 2.5 µL 10× miScript universal primer, 2.5 µL 10× miScript primer assay mix, and 5.5 µL RNase-free water) was added. Amplification was performed under the following conditions: initial activation step at 95°C for 15 minutes, denaturation at 94°C for 15 seconds, annealing at 55°C for 30 seconds, and extension at 70°C for 30 seconds for 40 cycles. All assays were performed in duplicate.

Data processing and analysis

The relative expression levels of the miRNAs interrogated were normalized to those of SNORD61 and cel-miR-39 and determined by the $2^{-\Delta\Delta\text{Ct}}$ method. Using GraphPad Prism 8.3 for Windows (GraphPad Software, San Diego, CA, USA, <http://www.graphpad.com>) and XLSTAT 2019.3.2 (Addinsoft, Paris, France), intergroup comparisons were analyzed by paired t tests and Mann-Whitney tests. Spearman correlation coefficient was used for correlation analysis. A p-value less than .05 (two-tailed) was considered statistically significant. The receiver operating characteristic (ROC) and the area under the ROC curve (AUC) with 95% confidence interval (CI) were generated, and the number of outliers per tissue and plasma group were determined by Robust Regression and Outlier Removal (ROUT) [23]. These discriminating performance calculations were carried out using GraphPad Prism 8.3 (GraphPad Software Inc., San Diego, CA, USA).

RESULTS

Clinicopathological characteristics of CRC patients

A total of 41 FFPE malignant tissues and their corresponding adjacent neoplasm-free mucosal tissues ($n = 41$) were collected from histologically confirmed Filipino CRC patients. EDTA-treated plasma samples from the same CRC patients ($n = 36$) were collected prior to surgery or any form of treatment and from their age- and sex-matched clinically healthy controls ($n = 36$). Table 1 shows the clinicopathologic characteristic of cases included in this study.

Expression patterns of selected miRNAs in CRC tissue and plasma

Table 2 shows the relative expression and fold regulation of the

Table 1. Clinicopathologic profile of cases

Characteristics	No (%) ($n = 41$)
Age	
<60	18 (44)
>60	23 (56)
Sex	
Male	18 (44)
Female	23 (56)
Location of tumor	
Rectum/cecum/rectosigmoid	34 (83)
Sigmoid ascending/transverse and descending	7 (17)
Histologic type	
Adenocarcinoma	33 (80)
Mucinous cell carcinoma/signet ring cell carcinoma	8 (20)
Histologic grade	
Well-differentiated	26 (63)
Moderately to poorly differentiated	15 (37)
TNM stage	
Stage I/II	20 (49)
Stage III/IV	21 (51)
Lymph node metastasis	
N0-N1	29 (71)
N2	12 (29)
Distant metastasis	
M0-M1	28 (68)
Mx	13 (32)
Tumor size	
<5 cm	18 (44)
>5 cm	23 (56)
Depth of tumor infiltration	
Muscularis propria	18 (44)
Muscularis propria into the pericolic adipose tissue and outside	23 (56)
Perineural invasion	
Absent	39 (95)
Present	2 (5)

Table 2. Relative expression, fold change, and fold regulation of selected miRNAs in tissue and plasma

miRNA	Mean expression in tissue			Mean expression in tissue after outlier removal			Mean expression in plasma			Mean expression in plasma after outlier removal			Fold change in plasma (n=36)	Fold change in tissue (n=41)	Fold regulation in tissue and plasma
	Malignant tissue (n=41)	Adjacent neoplasm-free tissue (n=41)	p-value	Malignant tissue ^a	Adjacent neoplasm-free tissue ^a	p-value	CRC cases (n=36)	Clinically healthy controls (n=36)	p-value	CRC cases ^a	Clinically healthy controls ^a	p-value			
miR-21-5p	9.35±8.28	5.49±6.44	<.001	8.76±7.44	1.43±1.25	<.001	5.84±6.56	2.05±4.15	<.001	5.82±6.65	0.44±0.47	<.001	8.40	4.23	Upregulated
miR-196b-5p	4.39±5.09	2.19±3.52	.026	2.61±2.79	0.96±1.06	.010	16.60±12.09	3.13±2.31	<.001	19.20±13.65	2.58±1.40	<.001	4.75	2.45	Upregulated
miR-92a-3p	4.45±3.56	0.79±1.35	<.001	3.38±2.02	0.59±0.57	<.001	7.63±8.29	2.24±2.93	<.001	5.18±4.32	1.43±1.11	<.001	2.50	7.41	Upregulated
miR-29a-3p	3.41±2.53	1.27±1.84	<.001	3.40±2.52	0.56±0.33	<.001	3.15±3.79	0.80±0.86	<.001	2.35±1.71	0.59±0.43	<.001	2.89	3.56	Upregulated
miR-135b-5p	1.06±1.64	2.64±2.58	<.001	0.32±0.43	2.47±2.35	<.001	0.89±0.99	3.98±4.06	<.001	0.74±0.69	2.96±2.23	<.001	0.44	0.17	Downregulated
miR-197-3p	3.33±3.36	4.80±7.38	.676	2.61±2.79	2.30±2.07	.681	3.86±3.04	3.45±3.50	.112	3.15±1.89	2.88±1.14	.656	1.32	0.78	Not significant

^aThe number of samples after the outlier removal from each miRNA varied depending on the number of samples (outlier) removed during the Robust Regression and Outlier Removal analysis.

miRNAs in malignant colorectal tissue. MiR-21-5p, miR-29a-3p, miR-92a-3p, and miR-196b-5p were upregulated in CRC tissues in relation to their adjacent neoplasm-free tissue. MiR-92a-3p showed the highest fold change ($FC = 7.41$, $p < .001$) in CRC tissue, followed by miR-21-5p ($FC = 4.23$, $p < .001$) and miR-29a-3p ($FC = 3.56$, $p < .001$). MiR-135b-5p was downregulated ($FC = 0.17$, $p < .001$) in CRC tissue compared to its adjacent neoplasm-free tissue. The relative expression of miR-197-3p in CRC tissue was not significantly different ($FC = 0.78$, $p = .676$) in relation to its adjacent neoplasm-free tissue.

To determine whether the dysregulated miRNAs in CRC tissue were released into the circulation, plasma from the same CRC patients was collected and tested for the specific miRNA under study prior to any form of treatment. Interestingly, expression patterns of miR-21-5p, miR-29a-3p, miR-92a-3p, miR-135b-5p, miR-196b-5p, and miR-197-3p in plasma of CRC

cases were similar to plasma from clinically healthy individuals (Table 2). MiR-21-5p showed the highest expression ($FC = 8.40$, $p < .001$) in CRC plasma, followed by miR-196b-5p ($FC = 4.75$, $p < .001$) and miR-29a-3p ($FC = 2.89$, $p < .001$). Similar to CRC tissue, miR-135b-5p was downregulated ($FC = 0.44$, $p < .001$) in CRC plasma compared to clinically healthy controls. The relative expression of miR-197-3p in CRC plasma was not significantly different ($FC = 1.32$, $p = .112$) in relation to control plasma.

To determine if the significant differences in miRNA expression levels in tissue and plasma were attributable to the presence of outliers, ROUT was performed. The residuals of the robust fit were analyzed to identify any outlier according to the false discovery rate approach for testing multiple comparisons. The ROUT coefficient was set at $Q = 1\%$. Table 2 shows that, upon outlier removal, the p-values between malignant and adjacent

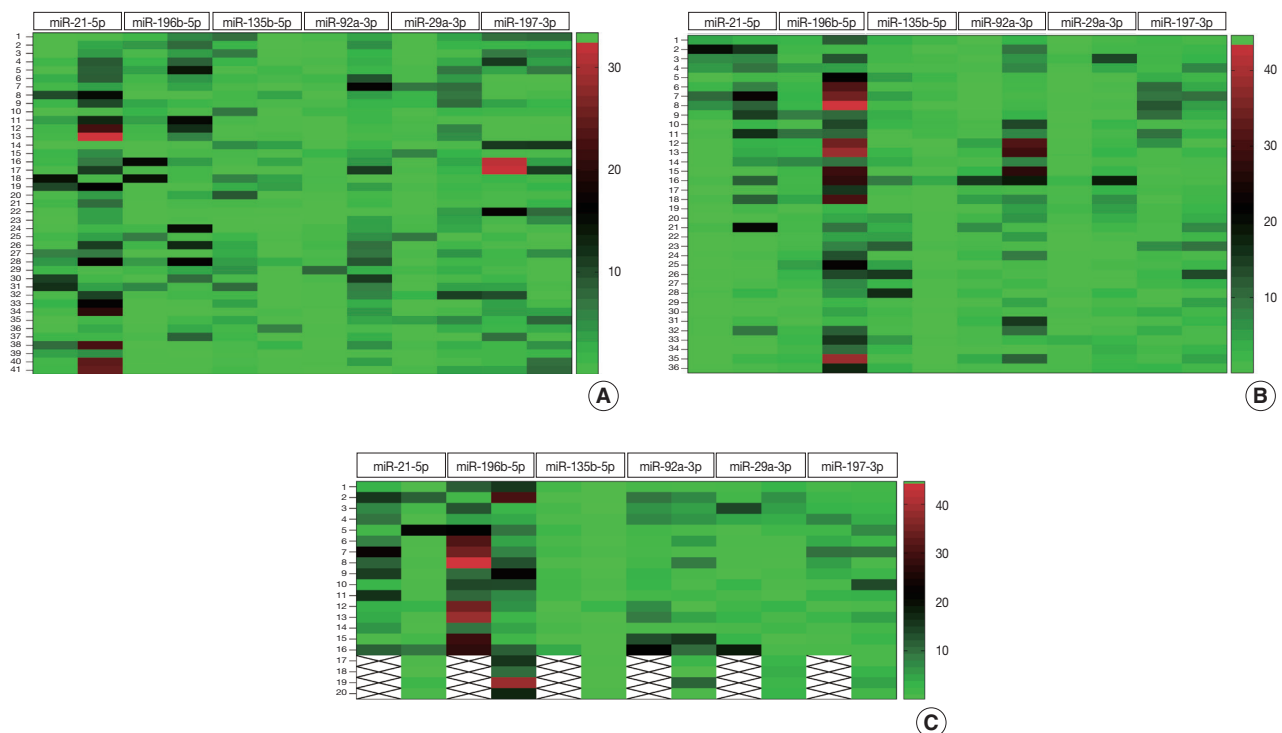


Fig. 1. Heatmap analysis showing differential expression of selected miRNA. (A) Heatmap of selected miRNA in malignant and neoplasm-free colorectal tissues. Each row (1-41) represents a tissue sample. (B) Heatmap of selected miRNA in colorectal cancer (CRC) plasma and clinically healthy control plasma. Each row (1-36) represents a plasma sample. (C) Heatmap of selected miRNAs in plasma of early (I/II) and late stages (III/IV) of CRC. Each row (1-20) represents a plasma sample. The first and second columns for each miRNA in each heatmap represent respective malignant and adjacent neoplasm-free tissues (A) plasma from CRC patients and healthy controls (B) and early ($n = 16$) and advanced ($n = 20$) stages (C). The color scale shows saturation and brightness based on the mean values of the data set. The largest mean values are shown in red (> 40), while the lowest mean values are shown in green (< 10). The mean intensities of miR-21-5p, miR-196b-5p, miR-92a-3p, and miR-29a-3p are stronger in malignant colorectal cancer tissue and plasma of CRC patients compared to controls. In contrast, miR-135b-5p has a lower intensity in malignant colorectal cancer tissue and plasma of CRC patients. The mean intensities of miR-21-5p, miR-196b-5p, miR-92a-3p, and miR-29a-3p are stronger in early stages compared to late stages of CRC. MiR-135b-5p and miR-197-3p have lower mean intensity in early stages compared to late stages of CRC.

neoplasm-free tissue and CRC and clinically health control plasma remained significantly different.

Ability of selected miRNAs to discriminate malignant from neoplasm-free mucosal tissue and plasma from CRC patients from clinically healthy controls

To determine discriminatory ability of miRNAs under study, heatmap analysis was performed. Fig. 1A shows that majority of the CRC tissues exhibited greater color intensities than normal adjacent tissues with respect to miR-21-5p, miR-196b-5p, miR-92a-3p, and miR-29a-3p expression. For miR-135b-5p, the color intensity appeared lighter in CRC compared to normal adjacent tissue.

Heatmap analysis (Fig. 1B) of plasma samples show that color intensity for miR-21-5p, miR-196b-5p, miR-92a-3p, and miR-29a-3p of CRC was stronger than color intensity for control plasma. For miR-135b-5p, the color intensity appeared lighter in CRC plasma than in control plasma. This color intensity pattern exhibited in CRC plasma is similar to that shown by malignant tissue.

Relative expression of selected miRNAs in early and advanced stage CRC

Relative expressions of miR-21-5p ($p = .531$), miR-29a-3p ($p = .473$), miR-92a-3p ($p = .578$), miR-135b-5p ($p = .611$), miR-196b-5p ($p = .769$), and miR-197-3p ($p = .879$) in tissues of patients with early-stage CRC were not significantly different from

those in tissues of patients with advanced stage CRC (Table 3). Conversely, levels of all miRNAs studied were useful to discriminate between early and advanced stage CRC using plasma. The relative plasma expressions of miR-21-5p ($p = .006$), miR-29a-3p ($p < .001$), miR-92a-3p ($p < .001$), and miR-196b-5p ($p < .001$) were significantly higher in early-stage CRC compared to advanced-stage CRC (Table 3). In contrast, significantly higher expression of miR-135b-5p ($p < .001$) and miR-197-3p ($p = .007$) was observed in plasma samples of patients with advanced CRC compared to early stage. MiR-197-3p, which failed to discriminate CRC plasma from clinically healthy plasma, was able to distinguish between early and advanced stages of CRC ($p = .007$). Heatmap analysis (Fig. 1C) showed the potential of specific miRNAs in discriminating early (I/II) from advanced (III/IV) stage CRC. The mean color intensities of miR-21-5p, miR-196b-5p, miR-92a-3p, and miR-29-3p are greater in the early stages compared to late stages of CRC. MiR-135b-5p and miR-197-3p have a lower mean color intensity in early stages compared to late stages of CRC.

Correlation of expression levels of miRNAs in tissues and plasma

Results show that expression levels of miR-196b-5p ($r = 0.02$, $p = .921$), miR-135b-5p ($r = 0.14$, $p = .430$) and miR-197-3p ($r = -0.24$, $p = .150$) in tissue and plasma were not correlated. A weak positive correlation was observed with miR-21-5p ($r = 0.33$, $p = .049$) while miR-92a-3p ($r = 0.54$, $p = .007$) and miR-29-3p

Table 3. Relative expression of selected miRNAs in tissue and plasma of patients with early (I/II) and advanced stage (III/IV) CRC

miRNA	Mean expression of miRNA in tissue		p-value	Mean expression of miRNA in plasma		p-value
	Early stage (n=20)	Advanced stage (n=21)		Early stage (n=16)	Advanced stage (n=20)	
miR-21-5p	10.13 ± 10.87	8.02 ± 7.39	.531	12.33 ± 5.33	7.14 ± 5.13	.006
miR-196b-5p	3.58 ± 2.53	5.02 ± 5.05	.769	10.76 ± 1.93	5.54 ± 2.35	< .001
miR-135b-5p	1.05 ± 1.63	0.76 ± 1.26	.611	2.34 ± 1.22	10.80 ± 3.76	< .001
miR-92a-3p	12.51 ± 11.89	14.90 ± 14.59	.578	9.92 ± 2.53	2.94 ± 2.95	< .001
miR-29a-3p	5.30 ± 3.19	5.06 ± 4.14	.473	6.67 ± 2.18	3.32 ± 2.18	< .001
miR-197-3p	1.18 ± 0.73	1.50 ± 1.49	.879	1.16 ± 1.03	2.60 ± 2.05	.007

miRNA (miR), microRNA; CRC, colorectal cancer.

Table 4. Correlation of the expression levels of selected miRNAs in tissue and plasma of CRC patients

Sample	miR-21-5p			miR-196b-5p			miR-135b-5p			miR-92a-3p			miR-29a-3p			miR-197-3p		
	Mean expression level	r	p-value	Mean expression level	r	p-value	Mean expression level	r	p-value	Mean expression level	r	p-value	Mean expression level	r	p-value	Mean expression level	r	p-value
Tissue	9.35 ± 8.28	0.33	.049	4.39 ± 5.09	0.02	.921	1.06 ± 1.64	0.14	.430	4.45 ± 3.56	0.54	.007	3.41 ± 2.53	0.52	.048	3.33 ± 3.36	-0.24	.150
Plasma	5.84 ± 6.56			16.60 ± 12.09			0.89 ± 0.99			7.63 ± 8.29			3.15 ± 3.79			3.86 ± 3.04		

miRNA (miR), microRNA; CRC, colorectal cancer.

Table 5. Diagnostic performance of the selected miRNA for CRC

miRNA	Diagnostic performance for CRC irrespective of cancer stage using tissue samples				Diagnostic performance for CRC irrespective of cancer stage using plasma samples				Diagnostic performance for early-stage CRC using plasma samples			
	AUC	Cutoff point	Sensitivity	Specificity	AUC	Cutoff point	Sensitivity	Specificity	AUC	Cutoff point	Sensitivity	Specificity
miR-21-5p	0.78	3.56	0.80	0.83	0.78	3.89	0.81	0.83	0.77	3.69	0.80	0.81
miR-196b-5p	0.64	0.97	0.68	0.71	0.94	4.96	0.97	0.94	0.94	5.24	0.95	0.94
miR-135b-5p	0.76	2.32	0.80	0.83	0.83	1.45	0.86	0.89	0.84	2.05	0.85	0.88
miR-92a-3p	0.89	1.40	0.93	0.95	0.76	1.39	0.81	0.81	0.95	1.79	0.95	0.94
miR-29a-3p	0.81	1.23	0.85	0.83	0.83	1.21	0.86	0.83	0.87	0.41	0.90	0.88
miR-197-3p	0.52	2.41	0.56	0.63	0.60	2.06	0.61	0.67	0.76	2.41	0.80	0.81

miRNA (miR), microRNA; AUC, area under the receiver operating characteristic curve; CRC, colorectal cancer.

($r = 0.52$, $p = .048$) expressions in CRC tissues and plasma presented a moderate correlation (Table 4).

Diagnostic potential of selected miRNAs in detection of CRC in tissue and plasma

AUC values of the ROC were computed for each miRNA to evaluate their diagnostic value in detection of CRC in tissues and plasma. In CRC tissue, miR-92a-3p obtained the highest AUC (0.89; 95% CI, 0.82 to 0.97), with a sensitivity of 0.93 and specificity of 0.95 (Table 5). In detecting malignancy using plasma samples, miR-196b-5p showed the highest AUC (0.94; 95% CI, 0.89 to 0.99) with a sensitivity of 0.97 and specificity of 0.94 (Table 5). In early detection of CRC using plasma samples, miR-92a-3p showed the highest AUC (0.95; 95% CI, 0.88 to 0.99), with a sensitivity of 0.95 and specificity of 0.94 (Table 5).

DISCUSSION

The identification of diagnostic molecular biomarkers is substantial in cancer research. Increasing evidence suggests that miRNAs play a vital role in regulating the development, differentiation, and progression of cancer. MiRNAs are well preserved in tissue even after formalin-fixation and paraffin-embedding. They can be efficiently extracted and assessed from tumors and body fluids such as serum, plasma, urine, stool, and saliva. The miRNAs analyzed in the current study have been identified in previous independent studies utilizing diverse study subjects (different races and populations) through sequencing and PCR techniques as candidate biomarkers for CRC. The differences and similarities in the expression patterns of these miRNAs in tissue and plasma across different study populations have been highlighted. Similarly, the current study determined the pattern of these miRNAs, thereby contributing to the current understanding of which specific signature miRNAs can be applied in the clinical setting.

The current study shows that miR-21-5p, miR-29a-3p, miR-92a-3p, and miR-196b-5p were significantly overexpressed while miR-135b-5p was underexpressed in malignant compared to neoplasm-free colorectal tissues. The above specific miRNAs were also dysregulated in the plasma of CRC patients but not in their matched clinically healthy controls. However, miR-197-3p expression in tumor tissue and plasma of cancer patients was not significantly different from that in controls.

MiR-21-5p plays an oncogenic role in the development and progression of CRC by modulating malignant processes such as proliferation, anti-apoptosis, cell cycle progression, and invasion in CRC cells through downregulation of *PTEN* protein expression [24]. Prostaglandin-endoperoxide synthase 2 (PGTS2) produces inflammatory mediator prostaglandin E2 (PGE2), which has been described as promoting colorectal tumor development. PGTS2-driven inflammatory responses induce tumor expression of miR-21-5p that can elevate PGE level by downregulating PGE2-metabolizing enzymes [25]. During CRC development, miR-21 also induces stemness by downregulating *TGFβR2* (transforming growth factor beta receptor 2) and stimulates invasion and metastasis by suppressing the *PDCD4* gene [26]. MiR-21 expression has been found to be upregulated in breast, lung, and gastric cancers including CRC and hematological malignancies [27]. This study agrees with previous findings that miR-21-5p is upregulated in tissues [27–29] and plasma or serum [29–32]. MiR-21-5p expression was 12 and 10 times higher in serum and stool, respectively, of CRC patients compared to those of healthy controls [31]. Meanwhile, Stiegelbauer et al. [32] observed a serological underexpression of miR-21-5p in CRC. Plasma miR-21-5p downregulation was also detected in invasive breast cancer [33].

It has been observed that miR-196b-5p is upregulated in acute lymphoblastic leukemia but downregulated in glioblastoma, cervical cancer, and B-cell lymphoma. This miRNA has been experimentally validated to regulate CRC cell migration and

metastasis through interaction with *GALNT5* and *HOXB7* genes [34]. Although they vary in expression levels, the miR-196 family of molecules is consistently overexpressed in oral cavity, esophageal, stomach, and intestinal cancer tissues [35]. Several investigations [36–38] support our findings that miR-196b expression levels in malignant tissues are significantly higher than in adjacent normal colorectal mucosa. MiR-196b-5p was also found to be elevated in serum exosomes of CRC and is associated with liver metastasis [35]. MiR-196b-5p is also more upregulated in serum of patients with CRC compared to that in adenoma patients or healthy individuals [36]. A few reports have shown that the miR-196 family can also act as tumor suppressors. For instance, miR-196a suppresses metastasis in breast cancers [37] and melanoma [38]. MiR-196-b has been found to be downregulated in different types of leukemia cells [39].

Upregulation of miR-29a in tissue and plasma of CRC patients was noted in the present study. Similarly, Brunet Vega et al. [40] noted that miR-29a along with 10 other miRNAs were significantly increased in malignant colorectal tissue samples compared with non-cancerous adjacent mucosa. In the same study, serum level of miR-29a was overexpressed in CRC patients but not in healthy controls. In a genome-wide miRNA profiling conducted by Giraldez et al. [41], in 63 plasma samples from newly diagnosed CRC patients, miR-29a was confirmed to be upregulated compared with controls. In contrast, downregulation of miR-29a has been observed in human lung cancer tissues. Liu et al. [42] demonstrated that expression level of miR-29a was significantly downregulated in 38 pairs of lung cancer tissues compared to adjacent normal tissue. MiR-29a-3p promotes CRC metastasis by regulating *MMP-2* gene and E-cadherin via the KLF-4 signaling pathway [43]. It has also been found to promote cell proliferation and epithelial-mesenchymal transition in breast cancer by targeting *TET-1* [44]. Conversely, miR-29a functions as a tumor suppressor by targeting the *MUC-1* in pancreatic cancer cell [45].

The miR-92 family, one of the four families that belong to the miR-17-92 cluster, has been shown to regulate formation of vascular endothelial cells and blood vessels. Aberrant expression of the miR-92a family has been observed in breast, lung, gastric, prostate, and pancreatic cancers [46]. MiR-92a-3p is implicated as a key oncogenic component in the miR-17-92 cluster during colorectal tumorigenesis [47]. MiR-92a promotes metastasis by suppressing *PTEN* gene expression and activation of the PI3K/AKT pathway [48]. The current study showed miR-92a-3p to be overexpressed in malignant tissue and plasma of CRC patients. Our study revealed that miR-92a-3p obtained the highest

sensitivity and specificity in detecting CRC in tissue. Tsuchida et al. [47] found in their study that miR-92 was more significantly upregulated in both colorectal adenoma and carcinoma compared to the other five miRNAs in the cluster. Along with miR-21 and miR-29a, miR-92a has been observed to be significantly upregulated in CRC tissues compared to normal colorectal mucosal tissue. Moreover, this study agrees with the results of Ng et al. [9] that miR-92a was upregulated in both plasma and tissue samples of CRC patients in comparison with healthy controls.

MiR-135b-5p, an oncogene, has a tumor-promoting effect by enabling proliferation and inhibiting apoptosis of CRC cells through negative regulation of the TGF- β signaling pathway [49]. Magalhaes et al. [50] experimentally validated that downregulation of the *APC* gene caused by miR-135b-5p led to higher transduction signaling within the β -catenin/Wnt pathway, causing a greater proliferative capacity of malignant cells. *APC* modulates β -catenin as an essential part of the multi-protein complex that marks it for proteasomal degradation. MiR-135b-5p expression in CRC tissue and plasma was downregulated in this study. Zekri et al. [51] obtained similar findings, wherein serum miR-135b-5p and miR-454 were the only downregulated miRNAs in CRC and colonic polyp groups compared to the IBD group. In contrast, Bastaminejad et al. [52] demonstrated that expression levels of miR-135b-5p in serum and stool of CRC patients were 32 and 16 times higher compared to healthy controls, respectively. While miR-135b-5p is known to be an oncogenic miRNA, it might have different binding affinities due to its numerous potential target genes [53].

Whether the miRNAs detected in circulation are products of tumor apoptosis or are secreted by the active tumor cell itself remains controversial. MicroRNAs released in the circulation are usually bound to Argonaute proteins, microvesicles, exosomes, or lipoproteins that offer different degrees of protection. Hence, circulating miRNAs exhibit half-lives ranging from minutes to hours, which might explain why their concentrations in circulation vary and why their expressions in the tumor and plasma of the same patient might not be correlated [54]. MiR-1224, for instance, is the most upregulated miRNA in CRC plasma samples, but its expression in its paired tumor sample is rather low. Several explanations have been offered regarding the non-correlation between tumor and plasma miRNA expression levels. Exosomal shifting between the tumor mass and fluid microenvironment is one possibility [55].

Cancer-associated circulating miRNAs might have originated from immunocytes in the tumor microenvironment or from some other response mediated by affected organs or system

[56,57]. Investigators suggest that tumor cells secrete a variety of miRNAs that act on immunocytes to modulate immune responses. In response, the immunocytes secrete miRNAs that either promote or inhibit tumor proliferation, migration, and apoptosis [58]. Lastly, technical issues such as sample type, biological and racial differences, and analytical and normalization methods can significantly contribute to the lack of or weak relational expression of specific microRNAs in tissue and plasma. Researchers found that serum samples can yield lower miRNA concentrations compared to plasma primarily due to the presence of cellular contaminants particularly from platelets.

CRC has been considered an extremely heterogeneous and dynamic disease characterized by multiple molecular pathways throughout its development. This can be attributed to the existence of cellular subpopulations between and within tumors of divergent genotype and phenotype expressions [59]. Chromosomal instability, microsatellite instability, aberrant DNA methylation, and DNA repair mechanisms are intricate processes involved in colorectal epithelial cell transformation and all confer on a tumor its distinctiveness [60]. This high degree of genomic diversity in CRC over time, including relationships between subpopulations within and between the tumor, inaccurately reflects the true molecular profile within the tumor tissue sample, forming a major obstacle in clinical practice [61]. Further, this tumor heterogeneity can introduce sampling bias, heightening the intricacies in validation of oncology biomarkers [62]. Molecular diagnostic studies that seek to recognize driver mutations within a tumor can be affected by the presence of multiple mutations within the same sample. Thus, it is imperative to prudently characterize tumor samples for research to avoid inexplicable results or outcomes.

There are certain limitations that need to be considered when interpreting the findings of this study. First is the small sample size in the context of miRNA-based biomarker identification and validation. Due to limited budget, the current study was only able to analyze a limited number of samples. Thus, a follow-up study to validate the current findings in a prospective set of samples in a blinded manner is recommended. Moreover, the research team has, in a separate study, applied artificial intelligence (AI) in the analysis of the data, wherein a set of samples has been used as a training set to create the AI models, and the remaining samples were used as test specimens to determine the diagnostic potential of the miRNAs. Second, this study was a single-institution study focused on a specific population in the Philippines, whose diet and lifestyle might not represent those of other ethnic regions of the country. Recruitment of CRC patients and controls

from different parts of the country is suggested to determine reproducibility of findings.

In conclusion, this study presented a proof of concept that dysregulated miRNAs in CRC tissues are observed in the circulation, supporting their potential as non-invasive biomarkers for early detection of CRC. Results of this study agree with those of previous studies using samples from other populations. However, clinical translation of miRNA as a non-invasive circulating biomarker requires highly sensitive, specific, reproducible, reliable, and robust assays to enable its accurate and precise quantification in tissue, plasma, serum, and other human body fluids. Critical pre-analytical and analytical variables such as individual biological variability, sample type, sample storage, miRNA extraction and purification, detection method, and normalization all need to be optimized.

Ethics Statement

All procedures were performed in accordance with the ethical standards of institutional and/or national research committee and with the 1964 Helsinki Declaration and its later amendments or comparable ethical standards. This study complied with all applicable ethical guidelines approved by the Research Ethics Review Committee of the Mariano Marcos Memorial Hospital and Medical Center (MMMh-RERC-18-005, March 2, 2018). Study participants gave their written informed consent and were assured of the confidentiality of the results.

Availability of Data and Material

The datasets generated or analyzed during the study are available from the corresponding author on reasonable request.

Code Availability

Not applicable.

ORCID

Allan Fellizar	https://orcid.org/0000-0002-1781-7418
Vivencio Refuerzo	https://orcid.org/0000-0002-1421-1840
John Donnie Ramos	https://orcid.org/0000-0002-1404-4093
Pia Marie Albano	https://orcid.org/0000-0002-5024-8819

Author Contributions

Conceptualization: AF, PMA. Data Curation: AF, VR, PMA. Formal Analysis: AF, PMA. Funding Acquisition: PMA, AF. Investigation: AF, VR, PMA. Methodology: AF, VR, JDR, PMA. Project Administration: PMA. Resources: AF, VR, PMA. Supervision: PMA, JDR. Validation: AF, VR, JDR, PMA. Visualization: AF, VR, JDR, PMA. Writing—original draft: AF, VR, JDR, PMA. Writing—review and editing: AF, VR, JDR, PMA.

Conflicts of Interest

The authors declare that they have no potential conflicts of interest.

Funding Statement

This study was funded by the Commission on Higher Education (CHED) of the Philippines and the Philippine Association of Medical Technologists (PAMET)-Safeguard (Procter & Gamble Philippines, Inc.) through its Post-graduate Scholarship Program *Dagdag Karunungan, Kinabukusan ng Kalusugan*.

Acknowledgments

We would like to express our gratitude to Robert Ternola, Caren Joy Bac-sid, and Patrick Jun Paul Lawan for their technical assistance.

References

- Kavousipour S, Khademi F, Zamani M, Vakili B, Mokarram P. Novel biotechnology approaches in colorectal cancer diagnosis and therapy. *Biotechnol Lett* 2017; 39: 785-803.
- Moreno CC, Mittal PK, Sullivan PS, et al. Colorectal cancer initial diagnosis: screening colonoscopy, diagnostic colonoscopy, or emergent surgery, and tumor stage and size at initial presentation. *Clin Colorectal Cancer* 2016; 15: 67-73.
- Sung H, Ferlay J, Siegel RL, et al. Global Cancer Statistics 2020: GLOBOCAN estimates of incidence and mortality worldwide for 36 cancers in 185 countries. *CA Cancer J Clin* 2021; 71: 209-49.
- Pawa N, Arulampalam T, Norton JD. Screening for colorectal cancer: established and emerging modalities. *Nat Rev Gastroenterol Hepatol* 2011; 8: 711-22.
- Ahmed FE, Ahmed NC. MicroRNAs as molecular markers for colon cancer: diagnostic screening in stool and blood. *Med Res Innov* 2017; 1: 1-20.
- Ju J. miRNAs as biomarkers in colorectal cancer diagnosis and prognosis. *Bioanalysis* 2010; 2: 901-6.
- Lin J, Chuang CC, Zuo L. Potential roles of microRNAs and ROS in colorectal cancer: diagnostic biomarkers and therapeutic targets. *Oncotarget* 2017; 8: 17328-46.
- Nagy ZB, Wichmann B, Kalmar A, et al. Colorectal adenoma and carcinoma specific miRNA profiles in biopsy and their expression in plasma specimens. *Clin Epigenetics* 2017; 9: 22.
- Ng EK, Chong WW, Jin H, et al. Differential expression of microRNAs in plasma of patients with colorectal cancer: a potential marker for colorectal cancer screening. *Gut* 2009; 58: 1375-81.
- Wikberg ML, Myte R, Palmqvist R, van Guelpen B, Ljuslinder I. Plasma miRNA can detect colorectal cancer, but how early? *Cancer Med* 2018; 7: 1697-705.
- Saini V, Dawar R, Suneja S, Gangopadhyay S, Kaur C. Can microRNA become next-generation tools in molecular diagnostics and therapeutics?: a systematic review. *Egypt J Med Hum Genet* 2021; 22: 4.
- Buhagiar A, Seria E, Borg M, Borg J, Ayers D. Overview of microRNAs as liquid biopsy biomarkers for colorectal cancer sub-type profiling and chemoresistance. *Cancer Drug Resist* 2021; 4: 934-45.
- Zuo Z, Jiang Y, Zeng S, et al. The value of microRNAs as the novel biomarkers for colorectal cancer diagnosis: a meta-analysis. *Pathol Res Pract* 2020; 216: 153130.
- Yau TO, Tang CM, Harriss EK, Dickens B, Polytrachou C. Faecal microRNAs as a non-invasive tool in the diagnosis of colonic adenomas and colorectal cancer: a meta-analysis. *Sci Rep* 2019; 9: 9491.
- Pardini B, Sabo AA, Birolo G, Calin GA. Noncoding RNAs in extracellular fluids as cancer biomarkers: the new frontier of liquid biopsies. *Cancers (Basel)* 2019; 11: 1170.
- Hibner G, Kimsa-Furdzik M, Francuz T. Relevance of microRNAs as potential diagnostic and prognostic markers in colorectal cancer. *Int J Mol Sci* 2018; 19: 2944.
- Carter JV, Galbraith NJ, Yang D, Burton JF, Walker SP, Galandiuk S. Blood-based microRNAs as biomarkers for the diagnosis of colorectal cancer: a systematic review and meta-analysis. *Br J Cancer* 2017; 116: 762-74.
- Yi R, Li Y, Wang FL, Miao G, Qi RM, Zhao YY. MicroRNAs as diagnostic and prognostic biomarkers in colorectal cancer. *World J Gastrointest Oncol* 2016; 8: 330-40.
- Wang DD, Chen X, Yu DD, et al. miR-197: a novel biomarker for cancers. *Gene* 2016; 591: 313-9.
- Zhi ML, Liu ZJ, Yi XY, Zhang LJ, Bao YX. Diagnostic performance of microRNA-29a for colorectal cancer: a meta-analysis. *Genet Mol Res* 2015; 14: 18018-25.
- Zhang H, Li P, Ju H, et al. Diagnostic and prognostic value of microRNA-21 in colorectal cancer: an original study and individual participant data meta-analysis. *Cancer Epidemiol Biomarkers Prev* 2014; 23: 2783-92.
- Yang X, Zeng Z, Hou Y, et al. MicroRNA-92a as a potential biomarker in diagnosis of colorectal cancer: a systematic review and meta-analysis. *PLoS One* 2014; 9: e88745.
- Motulsky HJ, Brown RE. Detecting outliers when fitting data with nonlinear regression: a new method based on robust nonlinear regression and the false discovery rate. *BMC Bioinformatics* 2006; 7: 123.
- Wu Y, Song Y, Xiong Y, et al. MicroRNA-21 (Mir-21) promotes cell growth and invasion by repressing tumor suppressor PTEN in colorectal cancer. *Cell Physiol Biochem* 2017; 43: 945-58.
- Mima K, Nishihara R, Yang J, et al. MicroRNA MIR21 (miR-21) and PTGS2 expression in colorectal cancer and patient survival. *Clin Cancer Res* 2016; 22: 3841-8.
- Yu Y, Kanwar SS, Patel BB, et al. MicroRNA-21 induces stemness by downregulating transforming growth factor beta receptor 2 (TGF-betaR2) in colon cancer cells. *Carcinogenesis* 2012; 33: 68-76.
- Feng YH, Tsao CJ. Emerging role of microRNA-21 in cancer. *Biomed Rep* 2016; 5: 395-402.
- Yamada A, Horimatsu T, Okugawa Y, et al. Serum miR-21, miR-29a, and miR-125b are promising biomarkers for the early detection of colorectal neoplasia. *Clin Cancer Res* 2015; 21: 4234-42.
- Bastaminejad S, Taherikalani M, Ghanbari R, Akbari A, Shabab N, Saidijam M. Investigation of microRNA-21 expression levels in serum and stool as a potential non-invasive biomarker for diagnosis of colorectal cancer. *Iran Biomed J* 2017; 21: 106-13.
- Almeida AL, Bernardes MV, Feitosa MR, et al. Serological under expression of microRNA-21, microRNA-34a and microRNA-126 in colorectal cancer. *Acta Cir Bras* 2016; 31 Suppl 1: 13-8.
- Jurkovicova D, Smolkova B, Magyerkova M, et al. Down-regulation of traditional oncomiRs in plasma of breast cancer patients. *Oncotarget* 2017; 8: 77369-84.
- Stiegelbauer V, Vychytilova-Faltejskova P, Karbiener M, et al. miR-196b-5p regulates colorectal cancer cell migration and metastases through interaction with HOXB7 and GALNT5. *Clin Cancer Res* 2017; 23: 5255-66.
- Lu YC, Chang JT, Huang YC, et al. Combined determination of circulating miR-196a and miR-196b levels produces high sensitivity and specificity for early detection of oral cancer. *Clin Biochem* 2015; 48: 115-21.
- Li X, Zhang G, Luo F, et al. Identification of aberrantly expressed miRNAs in rectal cancer. *Oncol Rep* 2012; 28: 77-84.
- Wu J, Lin B, Yu S, et al. Exosomal miR-196b-5p is a potential diagnostic marker for colorectal cancer with metachronous liver metastasis. *Transl Cancer Res* 2018; 7: 1482-90.
- Xu C, Gu L. The diagnostic effect of serum miR-196b as biomarker in colorectal cancer. *Biomed Rep* 2017; 6: 39-45.
- Li Y, Zhang M, Chen H, et al. Ratio of miR-196s to HOXC8 messenger

- ger RNA correlates with breast cancer cell migration and metastasis. *Cancer Res* 2010; 70: 7894-904.
38. Braig S, Mueller DW, Rothhammer T, Bosserhoff AK. MicroRNA miR-196a is a central regulator of HOX-B7 and BMP4 expression in malignant melanoma. *Cell Mol Life Sci* 2010; 67: 3535-48.
 39. Bhatia S, Kaul D, Varma N. Potential tumor suppressive function of miR-196b in B-cell lineage acute lymphoblastic leukemia. *Mol Cell Biochem* 2010; 340: 97-106.
 40. Brunet Vega A, Pericay C, Moya I, et al. microRNA expression profile in stage III colorectal cancer: circulating miR-18a and miR-29a as promising biomarkers. *Oncol Rep* 2013; 30: 320-6.
 41. Giraldez MD, Lozano JJ, Ramirez G, et al. Circulating microRNAs as biomarkers of colorectal cancer: results from a genome-wide profiling and validation study. *Clin Gastroenterol Hepatol* 2013; 11: 681-8.
 42. Liu X, Lv X, Yang Q, Jin H, Zhou W, Fan Q. MicroRNA-29a functions as a tumor suppressor and increases cisplatin sensitivity by targeting NRAS in lung cancer. *Technol Cancer Res Treat* 2018; 17: 1533033818758905.
 43. Tang W, Zhu Y, Gao J, et al. MicroRNA-29a promotes colorectal cancer metastasis by regulating matrix metalloproteinase 2 and E-cadherin via KLF4. *Br J Cancer* 2014; 110: 450-8.
 44. Pei YF, Lei Y, Liu XQ. MiR-29a promotes cell proliferation and EMT in breast cancer by targeting ten eleven translocation 1. *Biochim Biophys Acta* 2016; 1862: 2177-85.
 45. Trehoux S, Lahdaoui F, Delpu Y, et al. Micro-RNAs miR-29a and miR-330-5p function as tumor suppressors by targeting the MUC1 mucin in pancreatic cancer cells. *Biochim Biophys Acta* 2015; 1853: 2392-403.
 46. Li M, Guan X, Sun Y, et al. miR-92a family and their target genes in tumorigenesis and metastasis. *Exp Cell Res* 2014; 323: 1-6.
 47. Tsuchida A, Ohno S, Wu W, et al. miR-92 is a key oncogenic component of the miR-17-92 cluster in colon cancer. *Cancer Sci* 2011; 102: 2264-71.
 48. Ke TW, Wei PL, Yeh KT, Chen WT, Cheng YW. MiR-92a promotes cell metastasis of colorectal cancer through PTEN-mediated PI3K/AKT pathway. *Ann Surg Oncol* 2015; 22: 2649-55.
 49. Li J, Liang H, Bai M, et al. miR-135b promotes cancer progression by targeting transforming growth factor beta receptor II (TGFBR2) in colorectal cancer. *PLoS One* 2015; 10: e0130194.
 50. Magalhaes L, Quintana LG, Lopes DCF, et al. APC gene is modulated by hsa-miR-135b-5p in both diffuse and intestinal gastric cancer subtypes. *BMC Cancer* 2018; 18: 1055.
 51. Zekri AR, Youssef AS, Lotfy MM, et al. Circulating serum miRNAs as diagnostic markers for colorectal cancer. *PLoS One* 2016; 11: e0154130.
 52. Bastaminejad S, Taherikalani M, Ghanbari R, et al. Serum and stool miR-135b levels as a potential diagnostic biomarker for colorectal cancer. *Clin Exp Invest* 2020; 1: 1-6.
 53. Uddin MN, Li M, Wang X. Identification of transcriptional markers and microRNA-mRNA regulatory networks in colon cancer by integrative analysis of mRNA and microRNA expression profiles in colon tumor stroma. *Cells* 2019; 8: 1054.
 54. Reichholf B, Herzog VA, Fasching N, Manzenreither RA, Sowemimo I, Ameres SL. Time-resolved small RNA sequencing unravels the molecular principles of microRNA homeostasis. *Mol Cell* 2019; 75: 756-68.
 55. Cojocneanu R, Braicu C, Raduly L, et al. Plasma and tissue specific miRNA expression pattern and functional analysis associated to colorectal cancer patients. *Cancers (Basel)* 2020; 12: 843.
 56. Nagy ZB, Bartak BK, Kalmar A, et al. Comparison of circulating miRNAs expression alterations in matched tissue and plasma samples during colorectal cancer progression. *Pathol Oncol Res* 2019; 25: 97-105.
 57. Ma R, Jiang T, Kang X. Circulating microRNAs in cancer: origin, function and application. *J Exp Clin Cancer Res* 2012; 31: 38.
 58. De Rosa M, Rega D, Costabile V, et al. The biological complexity of colorectal cancer: insights into biomarkers for early detection and personalized care. *Therap Adv Gastroenterol* 2016; 9: 861-86.
 59. Balboa E, Carracedo A, Barros F. The complexity of colorectal cancer biology: putting bricks on the path to personalized medicine. In: *Colorectal cancer*. Khan JS, ed. Rijeka: Intech, 2014; 434-66.
 60. Nguyen HT, Duong HQ. The molecular characteristics of colorectal cancer: implications for diagnosis and therapy. *Oncol Lett* 2018; 16: 9-18.
 61. Diaz-Cano SJ. Tumor heterogeneity: mechanisms and bases for a reliable application of molecular marker design. *Int J Mol Sci* 2012; 13: 1951-2011.
 62. Buikhuisen JY, Torang A, Medema JP. Exploring and modelling colon cancer inter-tumour heterogeneity: opportunities and challenges. *Oncogenesis* 2020; 9: 66.

Frequent apocrine changes in pleomorphic adenoma with malignant transformation: a possible pre-malignant step in ductal carcinoma ex pleomorphic adenoma

Joon Seon Song¹, Yeseul Kim¹, Yoon-Se Lee², Seung-Ho Choi², Soon Yuhl Nam², Sang Yoon Kim², Kyung-Ja Cho¹

Departments of ¹Pathology and ²Otorhinolaryngology, Asan Medical Center, University of Ulsan College of Medicine, Seoul, Korea

Background: The most common type of carcinoma ex pleomorphic adenoma (CPA) is histologically equivalent to salivary duct carcinoma, which has an apocrine phenotype. Invasive CPA is often accompanied by non-invasive or *in situ* carcinoma, an observation that suggests the presence of precursor lesions. The aim of this study was to identify candidate precursor lesions of CPA within pleomorphic adenoma (PA). **Methods:** Eleven resected cases of CPA with residual PA and 17 cases of PA with atypical changes were subjected to immunohistochemistry (IHC) for p53, human epidermal growth factor receptor 2 (HER2), androgen receptor (AR), pleomorphic adenoma gene 1, gross cystic disease fluid protein-15 (GCDFP-15), and anti-mitochondrial antibody. **Results:** Invasive or *in situ* carcinoma cells in all CPAs were positive for AR, GCDFP-15, and HER2. Atypical foci in PAs corresponded to either apocrine or oncocytic changes on the basis of their reactivity to AR, GCDFP-15, and anti-mitochondrial antibody. Atypical cells in PAs surrounding CPAs had an apocrine phenotype without HER2 expression. **Conclusions:** Our study identified frequent apocrine changes in residual PAs in CPA cases, suggesting a possible precursor role of apocrine changes. We recommend the use of HER2 IHC in atypical PAs, and that clinicians take HER2 positivity into serious consideration.

Key Words: Carcinoma ex pleomorphic adenoma; Salivary duct carcinoma; Atypical pleomorphic adenoma; Apocrine changes

Received: January 25, 2023 Revised: March 7, 2023 Accepted: March 13, 2023

Corresponding Author: Kyung-Ja Cho, MD, PhD, Department of Pathology, Asan Medical Center, University of Ulsan College of Medicine, 88 Olympic-ro 43-gil, Seoul 05505, Korea
Tel: +82-2-3010-4545, Fax: +82-2-472-7898, E-mail: kjc@amc.seoul.kr

Carcinoma ex pleomorphic adenoma (CPA) is defined as carcinoma derived from pleomorphic adenoma (PA). Virtually all types of salivary gland carcinomas can occur within PAs, and can be classified as luminal, abluminal, or mixed type [1]. The most common form of CPA is high-grade carcinoma of a luminal type, which is histologically equivalent to salivary duct carcinoma (SDC). A significant proportion of SDCs are believed to arise in PAs [2]. These CPAs are thought to result from the accumulation of genetic instabilities in the luminal epithelial cells of either a long-standing primary or a recurrent PA. The existence of early CPA has been recognized and reported using a range of terms including 'precancerous foci,' 'non-invasive (intracapsular) carcinoma,' 'intraductal carcinoma,' 'intracapsular (*in situ*) carcinoma,' and 'intraductal precursor' [3-8]. Since the exact meaning of these terms varies slightly, confusion can arise. In this paper, we restrict the term "in situ" to intratubular or intraductal

carcinoma surrounded by benign myoepithelial cells, and do not apply it to CPA without extracapsular invasion.

The expression of androgen receptor (AR) and gross cystic disease fluid-15 (GCDFP-15) in SDCs was first reported in 1998 [9], and the apocrine nature of SDC has recently been described [10]. CPA frequently shows expression of AR [11,12], indicating that it shares the apocrine nature of SDC. Expression of AR has also been reported in a small number of studies on PA [12,13]. We attempted to identify the apocrine phenotype in atypical PA and residual PA in cases of CPA.

MATERIALS AND METHODS

Case selection

Five resected cases of CPAs with both invasive and *in situ* carcinoma (CisPA) and residual PA and six cases of CisPA only with

residual PA were selected from among 32 luminal-type CPA specimens collected at the Asan Medical Center, Seoul, Korea, between 2006 and 2017. Twenty-one cases without *in situ* carcinoma or residual PA, and 20 abluminal-type CPAs from the same period were excluded from the study. CisPAs were defined by the presence of areas of intratubular growth of markedly atypical cells, with expansion and distortion of surrounding myo-epithelial frames. Seventeen resected cases of PA with atypical changes were selected from the same period at random. The presence of cellular enlargement with nuclear pleomorphism, hyperchromasia, and prominent nucleoli, without structural abnormality, was regarded as atypical change in PA.

Immunohistochemistry

Representative areas from 28 cases were subjected to immunohistochemistry for p53 (1:1,500, clone DO-7, DAKO, Glostrup, Denmark), human epidermal growth factor receptor 2 (HER2; 1:8, clone 4B5, Ventana Medical Systems, Tucson, AZ, USA), AR (1:100, clone SP107, Cell Marque, Rocklin, CA, USA), pleomorphic adenoma gene 1 (PLAG1; 1:50, clone 3B7, Novus, Centennial, CO, USA), GCDFP-15 (1:50, clone 23A3, Neomarkers, Fremont, CA, USA), and anti-mitochondrial antibody (AM; 1:2,000, clone 113-1, Abcam, Cambridge, UK). Staining was carried out using the Benchmark XT automated immunohistochemistry system (Ventana Medical Systems). Expression in carcinoma cells and atypical cells was evaluated as follows: nuclear staining in $\geq 10\%$ of cells was defined as positive for p53, AR, and PLAG1. The positivity of p53 was scored as +1 when 10% to one-third of cells were positive; +2 when one-third to one-half of cells were positive; or +3 when, more than two-thirds of cells were positive [14]. HER2 was evaluated using the American Society of Clinical Oncology 2018 system [15] as follows: negative, score 0 (no staining or incomplete staining in $\leq 10\%$ of tumor cells) or score 1 (incomplete staining in $> 10\%$ of tumor cells); equivocal, score 2 (weak/moderate complete staining in $> 10\%$ of tumor cells); positive, score 3 (intense complete staining in $> 10\%$ of tumor cells). Cytoplasmic staining for GCDFP-15 and AM was graded from 0 to +3 according to the presence and intensity of the stain.

RESULTS

Patient characteristics

CPA specimens came from eight male and three female patients aged 35 to 78 years (mean, 57). Eight cases were located in the parotid gland and three cases occurred in the submandib-

ular gland. The mean tumor size was 2.6 cm (range, 1.5 to 4.3 cm). The mean time between symptom presentation and diagnosis was 123 months. Six patients received postoperative adjuvant radiotherapy. No patient developed recurrence or metastasis during the mean follow-up period of 66 months (range, 15 to 104 months). The 17 patients with PA included seven males and 10 females aged 29 to 73 years. The parotid gland was the most common site. These data are presented in Tables 1 and 2.

Immunoprofiles

The immunohistochemical results are summarized in Tables 1 and 2. Invasive or *in situ* carcinoma cells in all 11 CPAs were positive for AR and GCDFP-15, manifesting an apocrine nature. They were also positive for HER2, p53, and anti-mitochondrial antibody, and negative for PLAG1. The residual PA parts of CPA cases contained areas of apocrine phenotype and morphology including dense plump eosinophilic cytoplasm with snouts. HER2 expression was negligible in these components. The expression of p53 in the residual PAs was variable. Reaction to anti-mitochondrial antibody was strong in all cases, and PLAG1 was positive in one residual PA (Fig. 1).

Atypical cells in PA cases could be divided into either apocrine or oncocytic changes on the basis of reactivity to AR, GCDFP-15, and anti-mitochondrial antibody. Nine cases were positive for all, corresponding to apocrine changes, and eight cases were negative for AR or GCDFP-15 and strongly positive for anti-mitochondrial antibody, representing oncocytic changes. In the former group, the HER2 score was 1 or 0, while all cases in the latter group had a score of 0. All specimens with apocrine or oncocytic changes showed positive reactions to anti-mitochondrial antibody. There were variable positive reactions to p53 across the cases. In most specimens with oncocytic changes and in two apocrine cases, PLAG1 was expressed. These two types of metaplasia were sometimes difficult to distinguish by histology alone (Fig. 2). Interestingly, the acini of the submandibular glands stained diffusely positive for GCDFP-15, while the acini of the parotid gland did not, suggesting different constituents between the two glands.

DISCUSSION

The most common type of CPA is high-grade carcinoma, which is histologically equivalent to SDC. Several genetic studies into *PLAG1* or *HMG2* abnormalities in SDCs have suggested that a large proportion of SDCs arise in PAs regardless of the presence or absence of residual PA [2,16,17]. SDCs affect men more than

Table 1. Basic information and immunoprofiles of carcinoma ex pleomorphic adenomas

Case No.	Location	Sex/Age (yr)	Component	AR	GCDFP-15	HER2	p53	AM	PLAG1
1	Parotid	M/59	Inv. CPA	+	+1	3	+3	+2	-
			CisPA	+	-	2	+3	+1	-
			PA	+	+1	0	+1	+2	-
2	Parotid	M/48	Inv. CPA	+	-	3	+1	+2	-
			CisPA	+	-	3	+1	+2	-
			PA	+	+1	0	-	+2	-
3	Parotid	F/58	Inv. CPA	+	-	3	+2	+2	-
			CisPA	-	-	1	+2	+2	-
			PA	+	+	0	+2	+2	+
4	Parotid	M/44	Inv. CPA	+	+1	3	+1	+2	-
			CisPA	+	+1	3	+1	+2	-
			PA	+	+1	0	+1	+2	-
5	Parotid	M/69	Inv. CPA	+	+1	3	+3	+2	-
			CisPA	+	+1	3	+3	+2	-
			PA	+	+1	0	+2	+2	-
6	Parotid	M/62	CisPA	+	-	3	+1	+2	-
			PA	+	+3	-	+1	+2	-
7	SMG	F/78	CisPA	+	+1	3	+3	+2	-
			PA	+	+1	-	+1	+2	-
8	Parotid	M/35	CisPA	+	+2	2	+1	+2	-
			PA	+	+3	-	+1	+2	-
9	SMG	M/52	CisPA	+	+1	2	+3	+3	-
			PA	+	+1	-	+2	+3	-
10	SMG	F/52	CisPA	+	+1	2	+1	+2	-
			PA	-	+2	-	+1	+2	-
11	Parotid	M/55	CisPA	+	+2	3	+3	+2	-
			PA	+	+2	-	-	+1	-

AR, androgen receptor; GCDFP-15, gross cystic disease fluid protein-15; HER2, human epidermal growth factor receptor 2; AM, anti-mitochondrial antibody; PLAG1, pleomorphic adenoma gene 1; M, male; Inv. CPA, invasive carcinoma ex pleomorphic adenoma; CisPA, carcinoma in situ ex pleomorphic adenoma; PA, pleomorphic adenoma; F, female; SMG, submandibular gland.

Table 2. Basic information and immunoprofiles of atypical pleomorphic adenomas

Case No.	Location	Sex/Age (yr)	AR	GCDFP-15	HER2	p53	AM	PLAG1
1	SMG	M/29	+	+1	0	+1	+2	-
2	Parotid	F/70	+	+1	1	+3	+3	+
3	Parotid	M/40	+	+3	0	+3	+3	-
4	Parotid	M/55	+	+1	0	+2	+3	-
5	Parotid	F/56	+	+2	1	+1	+2	-
6	Parotid	M/76	+	+3	0	+3	+3	-
7	Parotid	F/64	+	+1	1	+1	+1	+
8	SMG	M/62	+	+1	1	+1	+1	-
9	Oropharynx	M/70	+	+3	1	+1	+3	-
10	SMG	F/42	-	-	0	+1	+1	+
11	Parotid	F/38	-	-	0	+1	+2	+
12	SMG	F/61	-	+1	0	+1	+2	-
13	Parotid	M/37	-	-	0	+1	+2	+
14	Parotid	F/73	-	-	0	+2	+1	+
15	Buccal	F/36	-	-	0	+1	+3	+
16	Parotid	F/64	-	-	0	+2	+3	+
17	Parotid	F/55	-	-	0	+2	+3	+

AR, androgen receptor; GCDFP-15, gross cystic disease fluid protein-15; HER2, human epidermal growth factor receptor 2; AM, anti-mitochondrial antibody; PLAG1, pleomorphic adenoma gene 1; SMG, submandibular gland; M, male; F, female.

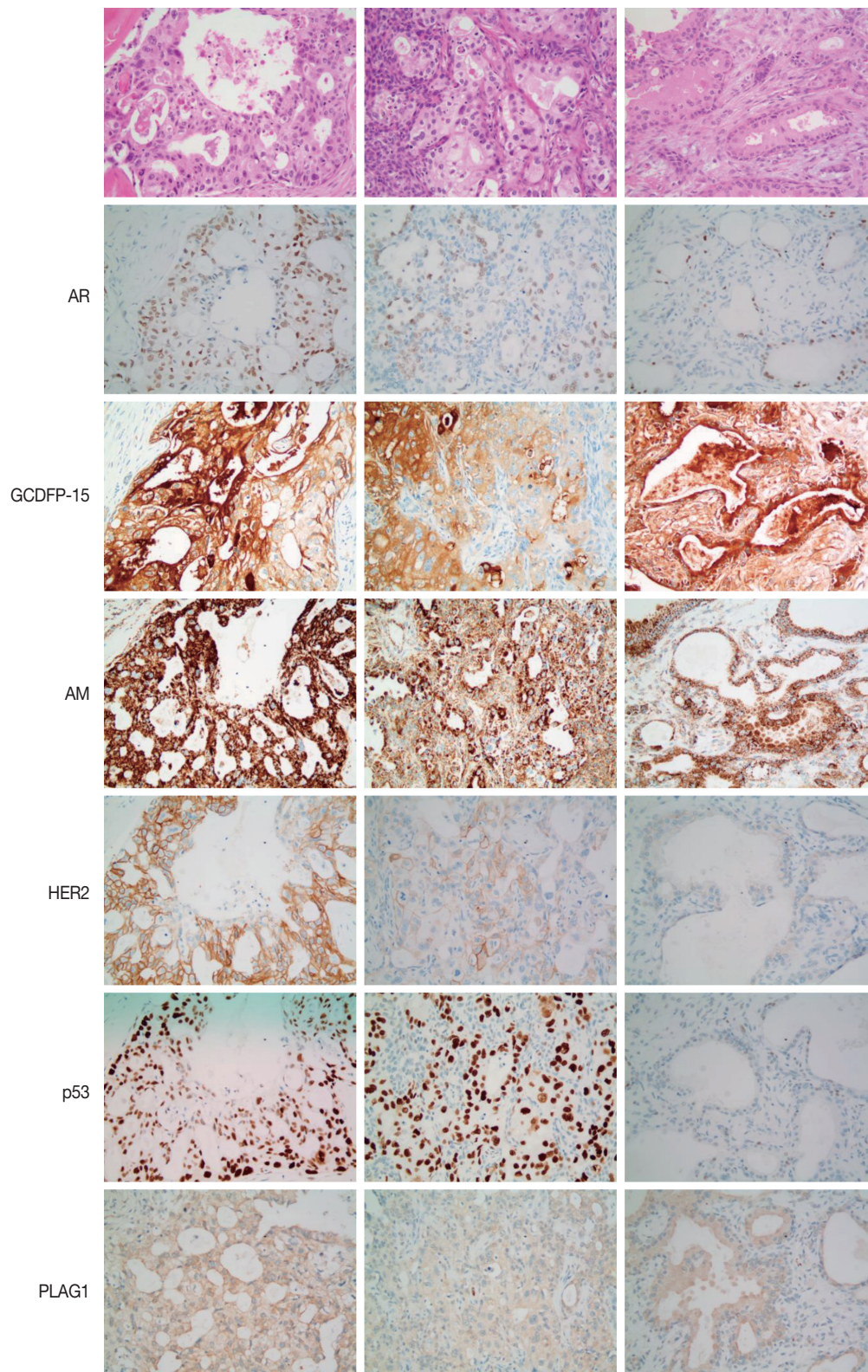


Fig. 1. Immunohistochemical results for carcinoma ex pleomorphic adenoma (left column), carcinoma in situ ex pleomorphic adenoma (middle column), and apocrine changes in residual pleomorphic adenoma (right column). All elements are positive for androgen receptor (AR), gross cystic disease fluid protein-15 (GCDFP-15), and anti-mitochondrial antibody (AM). The intensity of human epidermal growth factor receptor 2 (HER2) and p53 staining varies. Pleomorphic adenoma gene 1 (PLAG1) is negative in all cases.

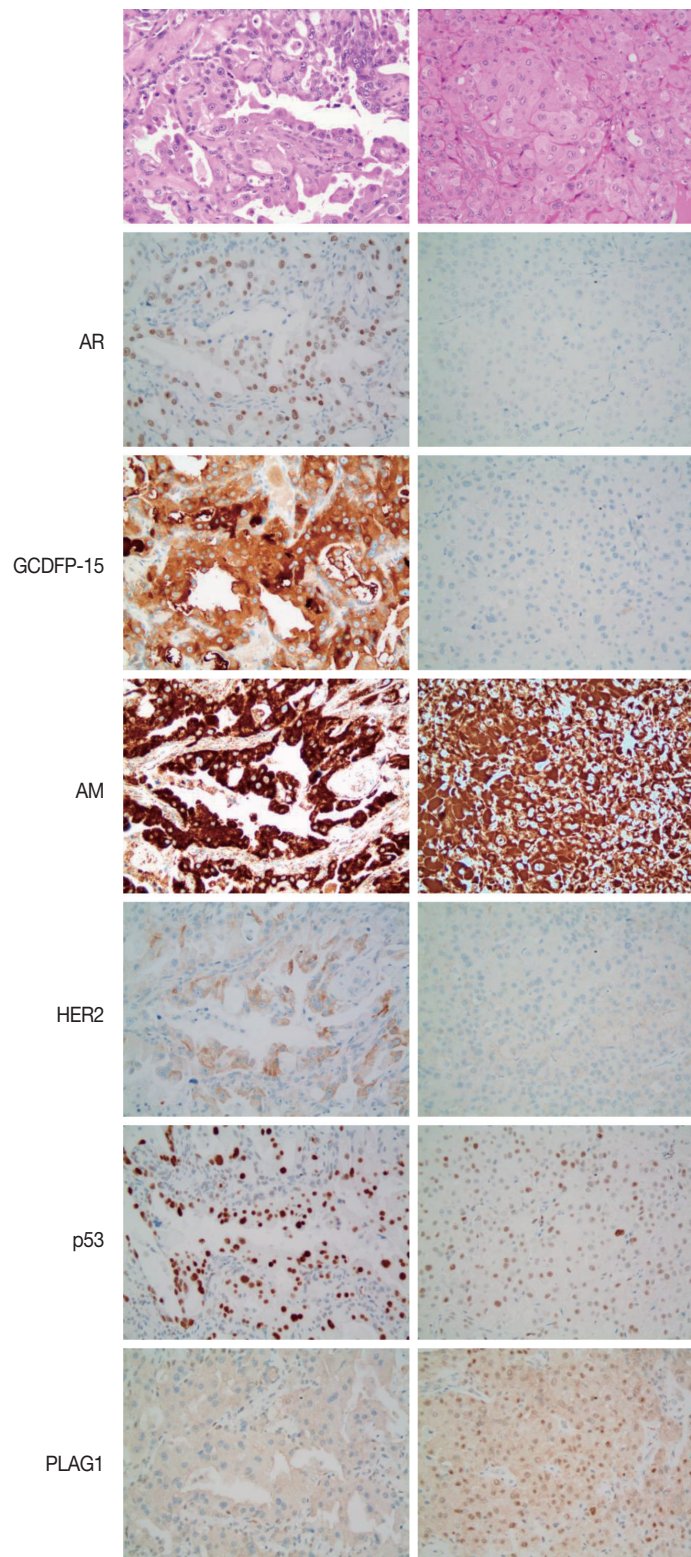


Fig. 2. Atypical changes in pleomorphic adenoma can be divided into the apocrine type (left column) and oncocytic type (right column) according to the immunohistochemistry results for androgen receptor (AR) and gross cystic disease fluid protein-15 (GCDFP-15). Both types are positive for antimitochondrial antibody (AM). Faint focal staining for human epidermal growth factor receptor 2 (HER2) can be seen in five apocrine cases and one oncocytic type. In all cases, p53 is positive. Pleomorphic adenoma gene 1 (PLAG1) is expressed in most oncocytic cases, but rarely expressed in the apocrine type.

women, and most of them show an apocrine phenotype with expression of AR [10]. We investigated whether there was an apocrine phenotype in the residual PA of CPAs and random PAs.

Our study confirmed that carcinoma cells of luminal-type CPA or CisPA were apocrine in nature, and there were apocrine changes in the residual PA components of these cases. These results suggested that apocrine changes might precede the development of CPA, although the pre-neoplastic potential of apocrine changes cannot be determined at present. In the female breast, apocrine carcinoma is rare, while benign apocrine changes are common [18]. The neoplastic potential of apocrine changes in the breast remains controversial. Jones et al. [19] conducted comparative genomic hybridization on apocrine hyperplasia, apocrine carcinoma in situ, and invasive apocrine carcinoma, and suggested that apocrine hyperplasia is a non-obligate precursor of apocrine carcinoma. Other authors, however, have described the difficulty of distinguishing atypical apocrine lesions from low-grade apocrine carcinoma in situ, and the biological significance of atypical apocrine lesions in the breast is unclear [20].

Apocrine changes or metaplasias are much rarer in the salivary gland than in the breast. Apocrine metaplasia in non-neoplastic salivary gland lesions has almost never been described. We found that the acini of the submandibular gland were diffusely positive for GCDFP-15, but they did not express AR. We found a similar report with respect to GCDFP-15 expression in the submandibular gland [21], and we hypothesize that there are differences in composition between the serous acini of the submandibular and parotid glands. Apocrine metaplasia is also a rare phenomenon in neoplasms of the salivary gland. Sclerosing polycystic adenosis (SPA), an uncommon proliferative lesion of the salivary gland, usually has an apocrine component, and 25.8% of these lesions develop ductal carcinoma, as reported in a review by Espinosa et al. [22] These authors described two new cases of intraductal epithelial proliferation with apocrine-like differentiation. For these reasons, many pathologists have considered SPA to be a tumorous lesion [23], and SPA is expected to be listed in the 5th edition of the *WHO Classification of Head and Neck Tumors* as 'sclerosing polycystic adenoma' [24]. A case of SPA with ductal carcinoma *in situ* and expression of GCDFP-15 and AR has also been reported, suggesting a pathogenesis similar to that of CPA [25].

In PAs, apocrine metaplasia has rarely been described, while oncocytic, sebaceous, squamous, and mucinous metaplasia are relatively well recognized [26,27]. Nakajima et al. [12] reported that AR expression was observed in seven of 23 PA cases, but the relationship between AR expression and histology was not

described. We could identify areas of apocrine changes in both residual PAs of CPAs and random PAs. The lesions often showed cystic changes and cytoplasmic snouts, but were sometimes histologically indistinguishable from oncocytic changes. Both changes are accompanied by cellular enlargement, rich eosinophilic cytoplasm, and large hyperchromatic nuclei with prominent nucleoli, with pathologists wavering between diagnoses of benign atypia and carcinoma in situ. Not only oncocytic but also apocrine-type cells stained strongly with anti-mitochondrial antibody, reflecting the abundance of intracytoplasmic mitochondria in both populations. The relevance of oncocytic changes in PA was not well established until Di Palma et al. [26] analyzed a case of PA with oncocytic changes using immunohistochemistry and microarray-based chromogenic in situ hybridization, and concluded that bizarre atypical cells are not malignant. They also decided, based on their expression of cytokeratin 8/18 and negativity for p63, that these cells were oncocytic epithelial cells. In contrast, non-apocrine oncocytic cells of the PAs in our series were all positive for PLAG1, suggesting that they had a myoepithelial nature.

Many pathologists have sought to identify early malignant changes in PAs using immunohistochemistry (IHC), including p53, HER2, and AR [3,4,6]. DeRoche et al. [13] reported that three of 41 PAs exhibited multifocal staining for HER2 and AR, but that the stained ductal epithelium showed no cytological atypia. They concluded that these markers could not be used to reliably predict early carcinomatous transformation. The significance of these lesions remains unclear. Meanwhile, an HER2 positivity score of 3 correlated well with marked cellular and structural atypia in our series, and no cases of PA with apocrine or oncocytic atypia expressed HER2. This finding is consistent with those of previous studies by Di Palma et al. [4] and Logasundaram et al. [8]. It is noteworthy that all three of these studies, including ours, the HER2 expression rate in CPA was high, while the documented HER2 immunopositivity or amplification rate in de novo SDC is approximately 30% [28,29], suggesting pathogenetic differences. We recommend the use of HER2 IHC in atypical PAs, and that clinicians take HER2 positivity into serious consideration.

We could not find any characteristic patterns of p53 overexpression in this series between PA and CPA, in contrast to a previous report on p53 positivity in focal carcinoma and atypical tumor cells in PA [3]. Other studies revealed that *TP53* mutations were accompanied by malignant transformation of PA [5,30], but protein expression was ubiquitous in both PAs and CPAs in our study. Expression of p53 alone did not indicate car-

cinomatous transformation.

In summary, we observed a similar apocrine phenotype in malignant and benign components of CPA, suggesting their relationship and a possible role of apocrine changes as a precursor to the development of carcinoma. Recognizing apocrine changes in PAs appears to be worth further investigation to facilitate the care of patients with PAs.

Ethics Statement

The study was approved by the institutional review board of Asan Medical Center (2021-1196), and the need for written informed consent was waived.

Availability of Data and Material

The datasets generated or analyzed during the study are available from the corresponding author on reasonable request.

Code Availability

Not applicable.

ORCID

Joon Seon Song <https://orcid.org/0000-0002-7429-4254>
 Yeseul Kim <https://orcid.org/0000-0001-8273-884X>
 Yoon-Se Lee <https://orcid.org/0000-0001-6534-5753>
 Seung-Ho Choi <https://orcid.org/0000-0001-9109-9621>
 Soon Yuhl Nam <https://orcid.org/0000-0002-8299-3573>
 Sang Yoon Kim <https://orcid.org/0000-0002-2162-7983>
 Kyung-Ja Cho <https://orcid.org/0000-0002-4911-7774>

Author Contributions

Conceptualization: KJC. Data curation: KJC, JSS. Formal analysis: JSS, YK. Funding acquisition: KJC. Investigation: JSS. Methodology: KJC. Project administration: JSS. Resources: YSL, SHC, SYN, SYK. Supervision: KJC. Validation: KJC, JSS. Visualization: JSS. Writing—original draft: KJC, JSS. Writing—review & editing: KJC, JSS. Approval of final manuscript: all authors.

Conflicts of Interest

J.S.S., a contributing editor of the *Journal of Pathology and Translational Medicine*, was not involved in the editorial evaluation or decision to publish this article. All remaining authors have declared no conflicts of interest.

Funding Statement

No funding to declare.

References

- Kim JW, Kwon GY, Roh JL, et al. Carcinoma ex pleomorphic adenoma of the salivary glands: distinct clinicopathologic features and immunoprofiles between subgroups according to cellular differentiation. *J Korean Med Sci* 2011; 26: 1277-85.
- Bahrami A, Perez-Ordóñez B, Dalton JD, Weinreb I. An analysis of *PLAG1* and *HMGA2* rearrangements in salivary duct carcinoma and examination of the role of precursor lesions. *Histopathology* 2013; 63: 250-62.
- Ohtake S, Cheng J, Ida H, et al. Precancerous foci in pleomorphic adenoma of the salivary gland: recognition of focal carcinoma and atypical tumor cells by p53 immunohistochemistry. *J Oral Pathol Med* 2002; 31: 590-7.
- Di Palma S, Skalova A, Vanieek T, Simpson RH, Starek I, Leivo I. Non-invasive (intracapsular) carcinoma ex pleomorphic adenoma: recognition of focal carcinoma by HER-2/neu and MIB1 immunohistochemistry. *Histopathology* 2005; 46: 144-52.
- Ihrler S, Weiler C, Hirschmann A, et al. Intraductal carcinoma is the precursor of carcinoma ex pleomorphic adenoma and is often associated with dysfunctional p53. *Histopathology* 2007; 51: 362-71.
- Ihrler S, Guntinas-Lichius O, Agaimy A, Wolf A, Mollenhauer M. Histological, immunohistological and molecular characteristics of intraductal precursor of carcinoma ex pleomorphic adenoma support a multistep carcinogenic process. *Virchows Arch* 2017; 470: 601-9.
- Di Palma S. Carcinoma ex pleomorphic adenoma, with particular emphasis on early lesions. *Head Neck Pathol* 2013; 7 Suppl 1: S68-76.
- Logasundaram R, Amarawickrama H, Premachandra D, Hellquist H. Intracapsular (in situ) carcinoma ex pleomorphic adenoma with unusual clinical and histological features. *Eur Arch Otorhinolaryngol* 2008; 265: 1563-6.
- Kapadia SB, Barnes L. Expression of androgen receptor, gross cystic disease fluid protein, and CD44 in salivary duct carcinoma. *Mod Pathol* 1998; 11: 1033-8.
- Williams L, Thompson LD, Seethala RR, et al. Salivary duct carcinoma: the predominance of apocrine morphology, prevalence of histologic variants, and androgen receptor expression. *Am J Surg Pathol* 2015; 39: 705-13.
- Nasser SM, Faquin WC, Dayal Y. Expression of androgen, estrogen, and progesterone receptors in salivary gland tumors: frequent expression of androgen receptor in a subset of malignant salivary gland tumors. *Am J Clin Pathol* 2003; 119: 801-6.
- Nakajima Y, Kishimoto T, Nagai Y, et al. Expressions of androgen receptor and its co-regulators in carcinoma ex pleomorphic adenoma of salivary gland. *Pathology* 2009; 41: 634-9.
- DeRoche TC, Hoschar AP, Hunt JL. Immunohistochemical evaluation of androgen receptor, HER-2/neu, and p53 in benign pleomorphic adenomas. *Arch Pathol Lab Med* 2008; 132: 1907-11.
- Schmitt FC, Soares R, Cirnes L, Seruca R. P53 in breast carcinomas: association between presence of mutation and immunohistochemical expression using a semiquantitative approach. *Pathol Res Pract* 1998; 194: 815-9.
- Wolff AC, Hammond ME, Allison KH, et al. Human epidermal growth factor receptor 2 testing in breast cancer: American Society of Clinical Oncology/College of American Pathologists clinical practice guideline focused update. *Arch Pathol Lab Med* 2018; 142: 1364-82.
- Chiosea SI, Thompson LD, Weinreb I, et al. Subsets of salivary duct carcinoma defined by morphologic evidence of pleomorphic adenoma, *PLAG1* or *HMGA2* rearrangements, and common genetic alterations. *Cancer* 2016; 122: 3136-44.
- Katabi N, Ghossein R, Ho A, et al. Consistent *PLAG1* and *HMGA2* abnormalities distinguish carcinoma ex-pleomorphic adenoma from its de novo counterparts. *Hum Pathol* 2015; 46: 26-33.
- D'Arcy C, Quinn CM. Apocrine lesions of the breast: part 2 of a two-part review. Invasive apocrine carcinoma, the molecular apocrine signature and utility of immunohistochemistry in the diagnosis of apocrine lesions of the breast. *J Clin Pathol* 2019; 72: 7-11.
- Jones C, Damiani S, Wells D, Chaggar R, Lakhani SR, Eusebi V. Molecular cytogenetic comparison of apocrine hyperplasia and apo-

- crine carcinoma of the breast. *Am J Pathol* 2001; 158: 207-14.
20. D'Arcy C, Quinn C. Apocrine lesions of the breast: part 1 of a two-part review: benign, atypical and in situ apocrine proliferations of the breast. *J Clin Pathol* 2019; 72: 1-6.
 21. Mazoujian G, Pinkus GS, Davis S, Haagensen DE Jr. Immunohistochemistry of a gross cystic disease fluid protein (GCDFP-15) of the breast: a marker of apocrine epithelium and breast carcinomas with apocrine features. *Am J Pathol* 1983; 110: 105-12.
 22. Espinosa CA, Rua L, Torres HE, Fernandez Del Valle A, Fernandes RP, Devicente JC. Sclerosing polycystic adenosis of the parotid gland: a systematic review and report of 2 new cases. *J Oral Maxillofac Surg* 2017; 75: 984-93.
 23. Gnepp DR. Salivary gland tumor "wishes" to add to the next WHO Tumor Classification: sclerosing polycystic adenosis, mammary analogue secretory carcinoma, cribriform adenocarcinoma of the tongue and other sites, and mucinous variant of myoepithelioma. *Head Neck Pathol* 2014; 8: 42-9.
 24. Skalova A, Hycza MD, Leivo I. Update from the 5th edition of the World Health Organization classification of head and neck tumors: salivary glands. *Head Neck Pathol* 2022; 16: 40-53.
 25. Petersson F, Tan PH, Hwang JS. Sclerosing polycystic adenosis of the parotid gland: report of a bifocal, paucicystic variant with ductal carcinoma in situ and pronounced stromal distortion mimicking invasive carcinoma. *Head Neck Pathol* 2011; 5: 188-92.
 26. Di Palma S, Lambros MB, Savage K, et al. Oncocytic change in pleomorphic adenoma: molecular evidence in support of an origin in neoplastic cells. *J Clin Pathol* 2007; 60: 492-9.
 27. Triantafyllou A, Thompson LD, Devaney KO, et al. Functional histology of salivary gland pleomorphic adenoma: an appraisal. *Head Neck Pathol* 2015; 9: 387-404.
 28. Han MW, Roh JL, Choi SH, et al. Prognostic factors and outcome analysis of salivary duct carcinoma. *Auris Nasus Larynx* 2015; 42: 472-7.
 29. Luk PP, Weston JD, Yu B, et al. Salivary duct carcinoma: clinicopathologic features, morphologic spectrum, and somatic mutations. *Head Neck* 2016; 38 Suppl 1: E1838-47.
 30. Valstar MH, Mast H, Ten Hove I, et al. Malignant transformation of salivary gland pleomorphic adenoma: proof of principle. *J Pathol Clin Res* 2021; 7: 432-7.

Clinicopathologic characterization of cervical metastasis from an unknown primary tumor: a multicenter study in Korea

Miseon Lee¹, Uiree Jo², Joon Seon Song², Youn Soo Lee¹, Chang Gok Woo³,
Dong-Hoon Kim⁴, Jung Yeon Kim⁵, Sun Och Yoon⁶, Kyung-Ja Cho²

¹Department of Pathology, St. Mary's Hospital, College of Medicine, The Catholic University of Korea, Seoul;

²Department of Pathology, Asan Medical Center, University of Ulsan College of Medicine, Seoul;

³Department of Pathology, Chungbuk National University Hospital, Chungbuk National University College of Medicine, Cheongju;

⁴Department of Pathology, Kangbuk Samsung Hospital, Sungkyunkwan University School of Medicine, Seoul;

⁵Department of Pathology, Inje University Sanggye Paik Hospital, Inje University School of Medicine, Seoul;

⁶Department of Pathology, Severance Hospital, Yonsei University College of Medicine, Seoul, Korea

Background: Research regarding cervical metastasis from an unknown primary tumor (CUP) according to human papillomavirus (HPV) and Epstein-Barr virus (EBV) status in Korea has been sporadic and small-scale. This study aims to analyze and understand the characteristics of CUP in Korea according to viral and p16 and p53 status through a multicenter study. **Methods:** Ninety-five cases of CUP retrieved from six hospitals in Korea between January 2006 and December 2016 were subjected to high-risk HPV detection (DNA in situ hybridization [ISH] or real-time polymerase chain reaction), EBV detection (ISH), and immunohistochemistry for p16 and p53. **Results:** CUP was HPV-related in 37 cases (38.9%), EBV-related in five cases (5.3%), and unrelated to HPV or EBV in 46 cases (48.4%). HPV-related CUP cases had the best overall survival (OS) ($p = .004$). According to the multivariate analysis, virus-unrelated disease ($p = .023$) and longer smoking duration ($p < .005$) were prognostic factors for poor OS. Cystic change ($p = .016$) and basaloid pattern ($p < .001$) were more frequent in HPV-related cases, and lymphoepithelial lesion was frequent in EBV-related cases ($p = .010$). There was no significant association between viral status and p53 positivity ($p = .341$), smoking status ($p = .728$), or smoking duration ($p = .187$). Korean data differ from Western data in the absence of an association among HPV, p53 positivity, and smoking history. **Conclusions:** Virus-unrelated CUP in Korea had the highest frequency among all CUP cases. HPV-related CUP is similar to HPV-mediated oropharyngeal cancer and EBV-related CUP is similar to nasopharyngeal cancer in terms of characteristics, respectively.

Key Words: Unknown primary neoplasms; Lymph node metastasis; Human papillomavirus virus; Epstein-Barr virus infections

Received: January 6, 2023 Revised: March 30, 2023 Accepted: April 12, 2023

Corresponding Author: Kyung-Ja Cho, MD, PhD, Department of Pathology, Asan Medical Center, University of Ulsan College of Medicine, 88 Olympic-ro 43-gil, Songpa-gu, Seoul 05505, Korea

Tel: +82-2-3010-4545, Fax: +82-2-472-7898, E-mail: kjc@amc.seoul.kr

Cervical metastasis from an unknown primary tumor (CUP) in the head and neck region is not rare. Reasons that primary tumors can avoid detection include small size, slow growth, hidden location, or involution [1,2]. The incidence of CUP in the West is approximately 1%–9% of all head and neck carcinomas [3–5]. Histologically, the most common type is squamous cell carcinoma, accounting for 75%–90% of all cases [6–8].

Human papillomavirus (HPV) [9,10] and Epstein-Barr virus (EBV) [11,12] are well-established carcinogenic viral agents in head and neck cancers and are increasingly associated with HPV infection [13,14]. HPV-mediated oropharyngeal cancer cases

have better survival rates than HPV-unrelated cases. The unique biologic behavior and natural history of diseases caused by these viruses necessitated the development of a new staging system [15]. The eighth edition of the American Joint Committee on Cancer (AJCC) introduced separate classification systems for unknown primary head and neck carcinomas, as follows: (1) EBV-positive, (2) HPV-positive, and (3) EBV-negative and HPV-negative [13,16].

A meta-analysis of 17 studies on head and neck squamous cell carcinomas of unknown primary cause reported that the HPV-positivity rate of CUP was 49%, which is 10% lower than the

rate of oropharyngeal carcinoma. The survival benefit of HPV positivity was also favorable [17]. In contrast, a recent Korean study revealed that HPV status did not significantly affect the survival rate in unknown primary head and neck cancer [18]. Previous studies in Korea offered similar results, reporting no significant survival benefit of HPV in oropharyngeal carcinoma [19,20]. These results may be attributed to the high smoking rate in Korea.

HPV infection and disruptive *TP53* mutations are considered non-overlapping events, so HPV infection has shown an inverse relationship with *TP53* mutations in various studies [21,22]. The *TP53* mutation rate in CUP or the relationship between the *TP53* mutation and HPV infection may also influence the behavior of CUP in Koreans.

To date, research in Korea has been sporadic and small-scale. We therefore sought to analyze and understand the clinico-pathological characteristics of CUP in Korea through a multicenter study. We intended to investigate the role of HPV and EBV in CUP in Korea with p16 or p53 expression.

MATERIALS AND METHODS

Patient selection and patient inclusion as CUP

Between January 2006 and December 2016, 159 patients diagnosed with metastatic carcinoma in cervical lymph nodes from the unknown primary site were analyzed across six hospitals (Asan Medical Center, Seoul St. Mary's Hospital, Sanggye Paik Hospital, Kangbuk Samsung Hospital, Chungbuk National University Hospital, and Severance Hospital, Yonsei University College of Medicine) in South Korea.

Among 159 cases, the primary sites in 64 cases were located after pathological diagnosis of lymph node metastasis. The remaining 95 cases were categorized as CUP, wherein the primary sites were not identified at the time of study initiation.

Hematoxylin and eosin-stained slides and formalin-fixed paraffin-embedded tissue were used for the analysis. Tissue microarrays (TMA) were constructed from representative parts of the tumor.

The research ethics committee of each institution deliberated on this process.

Clinicopathologic characteristics

Clinical data were collected through medical records, including age at diagnosis, sex, smoking history, follow-up duration, and clinical outcomes. Pathologists at each hospital reviewed the hematoxylin-and-eosin-stained slides of corresponding hospital cases; confirmed the lymph node location of the metastatic tu-

mor; and determined the size of the largest metastasis, extranodal extension, and N category. Histological findings were also analyzed, including keratinization, cystic change, basaloid pattern, and lymphoepithelial lesions.

Immunohistochemistry

Immunohistochemical (IHC) staining was performed on 4- μ m sections of TMA using the Ventana autostainer and UltraView DAB detection kit (Ventana Medical Systems, Tucson, AZ, USA), according to the manufacturer's instructions. The antibodies we used were p16INK4a (1:6, clone E6H4, mouse mAb, Ventana Medical Systems) and p53 (1:1,500, clone M7001, mouse mAb, Dako, Glostrup, Denmark). According to the eighth edition of the AJCC cancer staging manual, p16 immunostaining was positive when it showed greater than a +2/+3 intensity in >75% of tumor cells. Separately, the result of p53 was positive if nuclear staining was present in >10% of tumor cells.

In situ hybridization

EBV infection was evaluated by RNA in situ hybridization (ISH) (INFORM EBER, Ventana Medical Systems) and HPV infection was evaluated by DNA ISH (INFORM HPV III Family 16 Probe (B), Ventana Medical Systems). The INFORM HPV III Family 16 Probe (B) detects the following high-risk HPV types: 16, 18, 31, 33, 35, 45, 52, 56, 58, and 66. ISH was considered positive when >70% of tumor cells showed nuclear staining.

Real-time polymerase chain reaction

For cases wherein HPV ISH was unavailable, real-time polymerase chain reaction (RT-PCR) was performed. Nucleic acids were extracted from 10- μ m ($\times 5$) paraffin tissue sections, and the CFX96TM RT-PCR system (Bio-Rad Laboratories, Hercules, CA, USA) and Anyplex II HPV28 Detection system (31744024, Seegene, Seoul, Korea) were used. Anyplex II HPV28 detection (A) detects the following high-risk HPV types: 16, 18, 31, 33, 35, 39, 45, 51, 52, 56, 58, 59, 66, and 68.

Grouping of cervical metastases according to HPV and EBV status

Patient cases were divided into three groups according to HPV and EBV status, as follows: HPV-related CUP, EBV-related CUP, and CUP unrelated to both HPV and EBV. HPV-related CUP was defined by results of p16 overexpression via IHC, positive high-risk HPV via HPV ISH, or positive high-risk HPV via RT-PCR analysis. EBV-related CUP was defined by EBV

confirmation via EBV ISH. HPV-unrelated and EBV-unrelated CUP was defined by results negative for p16, HPV ISH, HPV RT-PCR, and EBV ISH. Cases were categorized as “not determined” when the HPV or EBV ISH test finding was unavailable.

N category

According to the eighth edition of the AJCC cancer staging manual, three different approaches were applied to cases with unknown primary tumors. As the primary T category is T0, the N category was determined by different staging systems according to EBV and HPV status, i.e., “nasopharynx” staging for EBV-related CUP, “HPV-mediated (p16+) oropharyngeal cancer” staging for HPV-related CUP, or “cervical lymph nodes and unknown primary tumors of the head and neck” staging for EBV-unrelated and HPV-unrelated CUP.

Statistical analysis

Fisher's exact test analyzed the variance between the three groups, which was then compared between them. Overall survival (OS) was counted from the first diagnosis of CUP to the date of death or final follow-up. Univariate and multivariate Cox proportional hazard regression models were used to identify a significant factor in predicting OS. Kaplan-Meier assessment was used to analyze OS, and the effect of groups on OS was investigated using the log-rank test. The variance ($p < .05$) significantly affecting OS in the univariate analysis was further tested through multivariate analysis. $p < .05$ was considered to be statistically significant. In the statistical comparison among groups according to viral status, cases that were “not determined” ($n = 7$) were excluded.

RESULTS

Clinicopathologic and immunohistochemical factors of CUP cases

The histologic type of all 95 CUP cases was squamous cell carcinoma. Fifty-two patients (54.8%) were aged ≥ 60 years. Among the 95 CUP cases, 77 were male (81.1%) and 18 were female (18.9%). Thirty patients were non-smokers (31.6%), 16 were past smokers (16.8%), 32 were current smokers (33.7%), and smoking status was not available for 17 patients (17.9%). Additionally, 19 patients (20.0%) had smoked for 1–20 pack-years, 16 patients (16.8%) had smoked for 21–40 pack-years, 10 (10.5%) had smoked for > 40 pack-years, and smoking duration data were not available for 20 patients (21.1%). The most frequent size of the largest metastatic lymph node was ≤ 3 cm

($n = 53$, 55.8%). Cervical level II lymph node involvement was identified in 68 patients (71.6%), with the highest frequency. Extranodal extension was identified in 35 patients (36.8%). Stage N1 ($n = 39$, 41.1%) was the most common stage. Keratinization was identified in 36 patients (37.9%), cystic changes were identified in 29 patients (30.5%), a basaloid pattern was identified in 37 patients (38.9%), and lymphoepithelial lesions were identified in 20 patients (21.1%). The p16 IHC finding was positive in 34 patients (35.8%) and negative in 54 patients (56.8%). The p53 IHC finding was positive in 51 patients (53.7%) and negative in 34 patients (35.8%) (Table 1).

High-risk HPV and EBV status by DNA ISH or RT-PCR and comparison with p16 and p53 positivity

EBV ISH was available in 86 cases and was positive in five cases (5.8%). HPV ISH or RT-PCR was available in 82 cases, and high-risk HPV was detected in 22 cases (26.8%).

Among the five EBV-positive cases, four (80%) were p53 positive, one (20%) was p53 negative, and none of the five cases showed p16 overexpression or identified high-risk HPV in RT-PCR or HPV ISH. A p16 overexpression status was significantly associated with high-risk HPV status. Among the 22 HPV-positive cases, 19 showed p16 overexpression, while 13 among the 60 HPV-negative cases showed p16 overexpression (90.5% vs. 21.7%, $p < .001$) (Table 2).

There was no significant relationship between p16 overexpression and p53 positivity ($p = .113$) nor between high-risk HPV infection and p53 positivity ($p = .203$).

Clinicopathologic comparison among three groups based on viral status

According to the IHC and ISH results, 37 cases (38.9%) were in the HPV-related group; five (5.3%) were in the EBV-related group; and 46 (48.45%) were in the HPV- and EBV-unrelated group, which displayed the greatest frequency of cases (Table 1).

The frequency of those < 60 years of age was high in the HPV-related CUP group ($n = 24$, 64.8%). Meanwhile, the frequency of patients aged ≥ 60 years was high in the HPV- and EBV-unrelated CUP group ($n = 33$, 71.7%), which showed a significant difference between groups ($p = .013$) (Table 1).

There was no significant difference in smoking status ($p = .738$) or smoking duration ($p = .187$) between groups divided by HPV/EBV status.

The ≤ 3 -cm cases showed the greatest frequency of the largest lymph node size across all three groups. In the EBV-related group, the largest lymph node size was ≤ 3 cm in all five cases. In the

Table 1. Characteristics according to the HPV and EBV status of cervical metastasis from an unknown primary tumor

	Total (n=95)	HPV-related (n=37, 38.9%)	EBV-related (n=5, 5.3%)	HPV and EBV-unrelated (n=46, 48.4%)	Not determined (n=7, 7.4%)	p-value
Age (yr)						.013
<50	12 (12.6)	7 (18.9)	1 (20.0)	4 (8.7)	0	
50–59	31 (32.6)	17 (45.9)	2 (40.0)	9 (19.6)	3 (42.9)	
60–69	26 (27.4)	8 (21.6)	2 (40.0)	15 (32.6)	1 (14.3)	
≥70	26 (27.4)	5 (13.5)	0	18 (39.1)	3 (42.9)	
Sex						.907
Male	77 (81.1)	31 (83.8)	4 (80.0)	37 (80.4)	5 (71.4)	
Female	18 (18.9)	6 (16.2)	1 (20.0)	9 (19.6)	2 (28.6)	
Smoking status						.738
Non-smoker	30 (31.6)	11 (29.7)	1 (20.0)	16 (34.8)	2 (28.6)	
Past smoker	16 (16.8)	7 (18.9)	0	9 (19.6)	0	
Current smoker	32 (33.7)	11 (29.7)	1 (20.0)	15 (32.6)	5 (71.4)	
NA	17 (17.9)	8 (21.6)	3 (60.0)	6 (13.0)	0	
Smoking duration (pack-years)						.187
Never-smoker	30 (31.6)	11 (29.7)	1 (20.0)	16 (34.8)	2 (28.6)	
1–20	19 (20.0)	9 (24.3)	0	7 (15.2)	2 (28.6)	
21–40	16 (16.8)	8 (16.2)	0	11 (19.5)	1 (14.3)	
≥41	10 (10.5)	1 (2.7)	1 (20.0)	7 (15.2)	1 (14.3)	
NA	20 (21.1)	10 (27.0)	3 (60.0)	7 (15.2)	0	
Lymph node size (cm)						.030
≤3.0	53 (55.8)	23 (62.2)	5 (100)	24 (52.2)	1 (14.3)	
>3.0, ≤6.0	28 (29.5)	6 (16.2)	0	20 (43.5)	2 (28.6)	
>6.0	7 (7.4)	5 (13.5)	0	2 (4.3)	0	
NA	7 (7.4)	3 (8.1)	0	0	4 (57.1)	
Lymph node level						
Level I	11 (11.6)	4 (10.8)	1 (20.0)	6 (13.0)	0	
Level II	68 (71.6)	30 (81.1)	4 (80.0)	28 (60.9)	6 (85.7)	
Level III	35 (36.8)	12 (32.4)	1 (20.0)	21 (45.7)	1 (14.3)	
Level IV	16 (16.8)	3 (8.1)	1 (20.0)	12 (26.1)	0	
Level V	9 (9.5)	1 (2.7)	2 (40.0)	5 (10.9)	1 (14.3)	
Level VI	0	0	0	0 (0)	0	
Retropharyngeal	2 (2.1)	0	1 (20.0)	1 (2.2)	0	
Axillary	1 (1.1)	0	0	1 (2.2)	0	
Supraclavicular	3 (3.2)	1 (2.7)	0	2 (4.3)	0	
Extranodal extension						.046
Positive	35 (36.8)	10 (27.0)	3 (60.0)	20 (43.5)	2 (28.6)	
Negative	44 (46.3)	25 (67.6)	2 (40.0)	15 (32.6)	2 (28.6)	
NA	16 (16.8)	2 (5.4)	0	11 (23.9)	3 (42.9)	
N category						.001
1	39 (41.1)	28 (75.7)	5 (100)	5 (10.9)	1 (14.3)	
2	1 (1.1)	1 (2.7)	0	0	0	
2a	6 (6.3)	0	0	6 (13.0)	0	
2b	5 (5.3)	0	0	5 (10.9)	0	
2c	2 (2.1)	0	0	2 (4.3)	0	
3	5 (5.3)	5 (13.5)	0	0	0	
3a	0	0	0	0	0	
3c	22 (23.2)	0	0	20 (43.5)	2 (28.6)	
NA	15 (15.8)	3 (8.1)	0	8 (17.4)	4 (57.1)	
Keratinization						.023
Present	36 (37.9)	11 (29.7)	0	24 (52.2)	1 (14.3)	
Absent	59 (62.1)	26 (70.3)	5 (100)	22 (47.8)	6 (85.7)	

(Continued to the next page)

Table 1. Continued

	Total (n = 95)	HPV-related (n = 37, 38.9%)	EBV-related (n = 5, 5.3%)	HPV and EBV-unrelated (n = 46, 48.4%)	Not determined (n = 7, 7.4%)	p-value
Cystic change						.016
Present	29 (30.5)	18 (48.6)	0	11 (23.9)	0	
Absent	66 (69.5)	19 (51.4)	5 (100)	35 (76.1)	7 (100)	
Basaloid pattern						<.001
Present	37 (38.9)	23 (62.2)	2 (40.0)	11 (23.9)	1 (14.3)	
Absent	58 (61.1)	14 (37.8)	3 (60.0)	35 (76.1)	6 (85.7)	
Lymphoepithelial lesion						.010
Present	20 (21.1)	8 (21.6)	4 (80.0)	7 (15.2)	1 (14.3)	
Absent	75 (78.9)	29 (78.4)	1 (20.0)	39 (84.8)	6 (85.7)	
p16 IHC						<.001
Positive	34 (35.8)	34 (91.9)	0	0	0	
Negative	54 (56.8)	2 (5.4)	5 (100)	46 (100)	1 (14.3)	
NA	7 (7.4)	1 (2.7)	0	0	6 (85.7)	
p53 IHC						.341
Positive	51 (53.7)	18 (48.6)	4 (80.0)	29 (63.0)	0	
Negative	34 (35.8)	17 (45.9)	1 (20.0)	16 (34.8)	0	
NA	10 (10.5)	2 (5.4)	0	1 (2.2)	7 (100)	
Follow-up duration (mo)						
Median	23.0	47.63	6.0	16.7	52.8	
Range	0.0–163.0	0–154	1–67	0–163	4–113	
Clinical outcome						
NED	56 (58.9)	27 (73.0)	2 (40.0)	22 (47.8)	5 (71.4)	.011
AWD	16 (16.8)	7 (18.9)	2 (40.0)	7 (15.2)	0	
DOD/DOC	23 (24.3)	3 (8.1)	1 (20.0)	17 (37.0)	2 (28.6)	

Values are presented as number (%) unless otherwise indicated.

In the statistical comparison among groups according to viral status, cases of 'not determined (n = 7)' are excluded.

HPV, human papillomavirus; EBV, Epstein-Barr virus; NA, not assessed; IHC, immunohistochemistry; NED, no evidence of disease; AWD, alive with disease; DOD, death of disease; DOC, death of other cause.

Table 2. Comparison of p16 overexpression and high-risk HPV detection

	HPV ISH or RT-PCR			Total
	Positive	Negative	ND	
p16				
Positive	19	13	2	34
Negative	2	47	5	54
ND	1	0	6	7
Total	22	60	13	95

HPV, human papillomavirus; ISH, in situ hybridization; RT-PCR, real-time-polymerase chain reaction; ND, not determined.

HPV- and EBV-unrelated group, the frequency of lymph nodes > 3 cm was highest (n = 22, 47.8%) among the three groups, and the frequency of cases with lymph nodes measuring 3–6 cm was particularly high (n = 20, 43.5%).

Level II lymph node involvement was most frequently observed across all three groups. Extranodal extension was infrequent in the HPV-related group (n = 10, 27.0%), while the HPV- and EBV-unrelated group (n = 20, 43.5%) and the EBV-related

group (n = 4, 80%) showed a significantly greater frequency (p = .046) (Table 1).

All five patients in the EBV-related group were stage N1, which was the most frequent stage in the HPV-related group (n = 28, 75.7%). In the HPV- and EBV-unrelated group, N3c (n = 20, 43.5%) was the most frequent stage, and the differences were statistically significant (p < .001) (Table 1).

Among histologic factors, cystic changes and the basaloid pattern were significantly frequently observed in the HPV-related group (n = 18, 48.6%, and n = 23, 62.2%, respectively). Lymphoepithelial lesions were significantly common in the EBV-related group (n = 4, 80%, p = .010). The histologic features in a representative case for the three groups are shown in Fig. 1.

The results of the p53 IHC were not significantly different between the groups based on viral status (p = .341) (Table 1).

Regarding the clinical outcomes, the proportion of patients with no evidence of disease (NED) was 73.0% (27/37) in the HPV-related group, representing the highest frequency among the groups. In the HPV- and EBV-unrelated group, the rate of

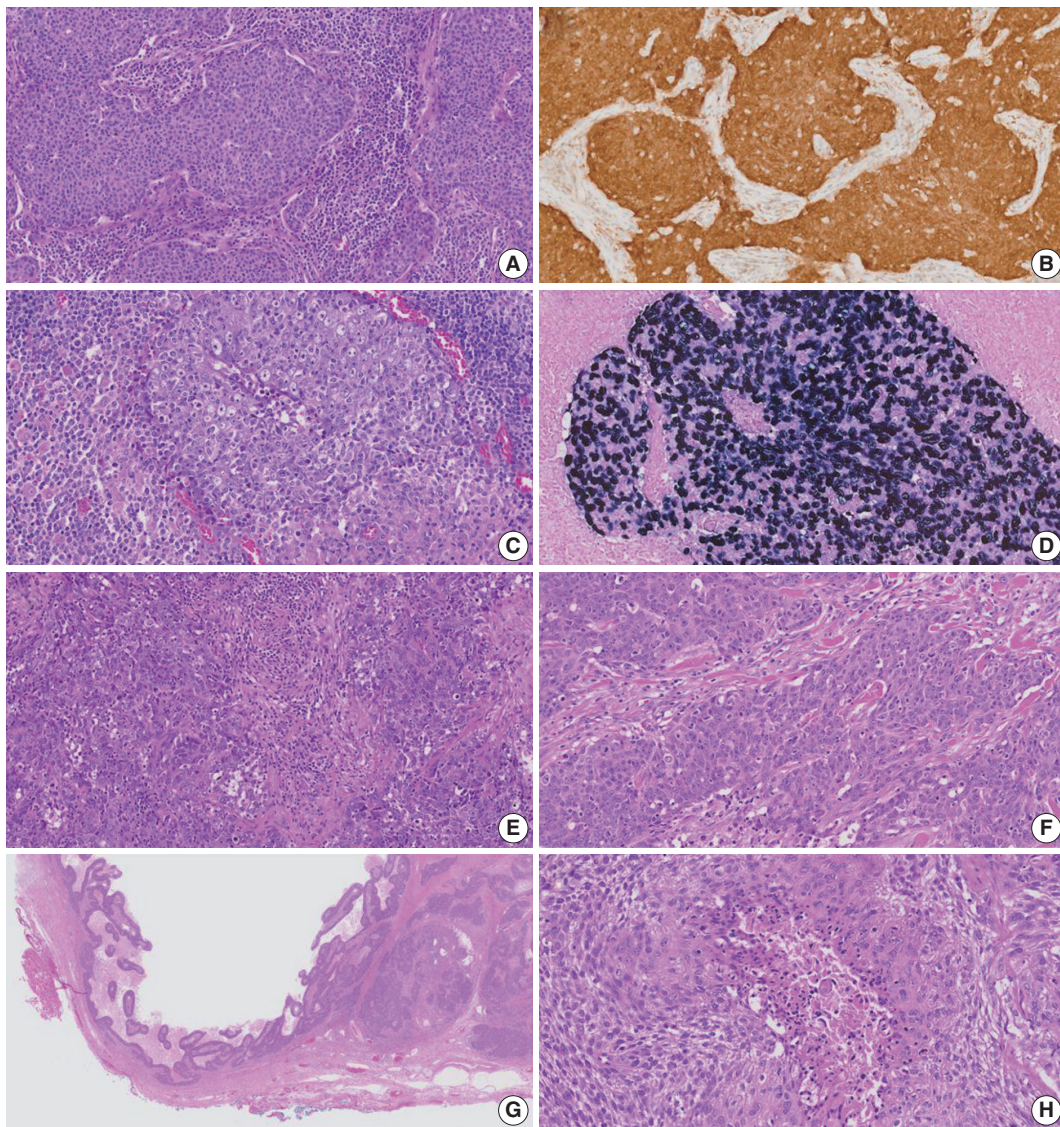


Fig. 1. Cervical lymph node metastasis from an unknown primary tumor (CUP). Human papillomavirus (HPV)-related CUP shows a basaloid pattern (A) and is positive for p16 immunohistochemistry (B). Epstein-Barr virus (EBV)-related CUP (C) was confirmed by EBV in situ hybridization (ISH) (D). HPV- and EBV-unrelated CUP (E, F) was defined as cases that are negative for p16, HPV ISH, HPV real-time polymerase chain reaction, and EBV ISH results. (G) Cystic change in the HPV-related CUP. (H) Keratinization in the HPV- and EBV-unrelated CUP.

death from disease (DOD)/death from other disease (DOC) was 37% (17/46), which was higher than that of the two virus-related groups. There was a significant difference in the clinical outcomes among the three groups ($p = .011$) (Table 1).

OS estimates in CUP

The univariate analysis revealed that ≥ 60 years of age ($p < .001$), current smoker ($p = .024$), > 40 pack-years ($p = .002$), presence of extranodal extension ($p = .001$), and HPV- and EBV-unrelated group status ($p = .005$) were significant factors for a poor prognosis. The presence of the basaloid pattern ($p = .042$) and

p16 IHC positivity ($p = .007$) were significant prognostic factors for good outcomes. Sex, largest lymph node size, the presence of keratinization, cystic changes, lymphoepithelial lesions, and p53 IHC positivity did not significantly affect the OS in the univariate analysis (Table 3).

In the multivariate analysis, long-term smoking (21–40 vs. ≤ 20 pack-years, $p = .014$; > 40 vs. ≤ 20 pack-years, $p = .038$) and HPV- and EBV-unrelated group vs. HPV-related group status (hazard ratio, 13.238; 95% confidence interval, 1.427 to 122.820; $p = .023$) were significant prognostic factors for poor outcomes (Table 3).

Table 3. Univariate and multivariate analyses on overall survival in cervical metastasis from an unknown primary tumor

Variable	Univariate		Multivariate	
	HR (95% CI)	p-value	HR (95% CI)	p-value
Age (≥ 60 yr vs. < 60 yr)	13.532 (3.137–58.374)	$< .001$	0.000 (0.000–5.590e128)	.929
Sex (male vs. female)	0.878 (0.256–2.960)	.825		
Smoking (current smoker vs. non- or past smoker)	2.990 (1.152–7.760)	.024	1.552 (0.209–11.545)	.668
Smoking				
Non-smoker, or 1–20 pack-years	1 (reference)			
21–40 pack-years	2.558 (0.894–7.315)	.080	11.893 (1.638–86.333)	.014
> 40 pack-years	5.362 (1.852–15.525)	.002	9.742 (1.131–83.944)	.038
Lymph node size (cm)	1 (reference)			
≤ 3.0				
$> 3.0, \leq 6.0$	1.471 (0.585–3.703)	.412		
> 6.0	0.457 (0.060–3.506)	.451		
Keratinization (present vs. absent)	1.529 (0.634–3.683)	.344		
Cystic change (present vs. absent)	0.438 (0.169–1.138)	.090		
Basaloid pattern (present vs. absent)	0.375 (0.146–0.965)	.042	3.130 (0.482–20.328)	.898
Lymphoepithelial lesion (present vs. absent)	0.512 (0.172–1.527)	.230		
Extranodal extension (present vs. absent)	9.017 (2.509–32.412)	.001	0.440 (0.055–3.488)	.470
Group				
HPV-related	1 (reference)			
EBV-related	6.608 (0.596–73.322)	.124	1.213e7 (0.000–1.018e142)	.918
HPV and EBV-unrelated	8.078 (1.859–35.106)	.005	13.238 (1.427–122.820)	.023
p16 IHC (positive vs. negative)	0.135 (0.031–0.585)	.007	-	
p53 IHC (positive vs. negative)	0.930 (0.375–2.304)	.875		

HR, hazard ratio; CI, confidence interval; HPV, human papillomavirus; EBV, Epstein-Barr virus; IHC, immunohistochemistry.

The Kaplan-Meier survival curves also estimated that OS was significantly better in non-smokers or past smokers than in current smokers ($p = .018$). Furthermore, groups who had smoked for < 20 pack-years, including non-smokers, showed the best OS, followed by those who had smoked for 21–40 pack-years, while those who had smoked for > 40 pack-years showed the worst OS ($p = .003$) (Fig. 2). However, in the analysis of individual groups, there was no significant OS difference in HPV-related CUP according to smoking status (non-smokers or past smokers vs. current smokers, $p = .160$) (non-smoker or < 20 vs. 21–40 vs. > 40 pack-years, $p = .340$). Among HPV- and EBV-unrelated CUP cases, non-smokers or past smokers tended to show better OS times than current smokers, but there was no significant difference ($p = .064$). There was also no significant OS difference in smoking duration (non-smoker or < 20 vs. 21–40 vs. > 40 pack-years, $p = .400$) among HPV- and EBV-unrelated CUP cases.

With the exception of HPV status, p16 alone was associated with a better OS ($p = .002$); however, there was no significant difference in OS between p53-positive and p53-negative patients ($p = .875$) (Fig. 2). The HPV-related CUP cases had the longest OS, and the HPV- and EBV-unrelated CUP patients had the worst prognosis, with a significant difference among the three groups ($p = .004$) (Fig. 3).

Cervical metastasis with subsequent confirmation of the primary tumors

Among the patients initially presenting with cervical metastasis with unknown primary tumors, 64 cases were found at the primary sites. Primary tumors were most frequently found at the oropharynx ($n = 25$, 89.3%), followed by at the hypopharynx and nasopharynx ($n = 5$, 7.8%, each). There were four cases (6.3%) of the esophagus; three cases (4.7%) of the oral cavity; and one case each (1.6%) of the pharynx, not specified, retropharynx, larynx, anus, and uterine cervix. Among them, 28 cases (43.8%) were identified as HPV-related tumors through p16 IHC or HPV-PCR tests. HPV-related primary tumors originated at the oropharynx, pharynx, not specified, anus, and uterine cervix. There were three cases of EBV-related tumors confirmed by EBV ISH, and the primary sites of all cases were the nasopharynx (Table 4). There was no significant difference in OS among the three groups according to viral status ($p = .073$) (Fig. 3). Clinical and pathologic characteristics according to viral status are presented with detailed tables in Supplementary Table S1.

DISCUSSION

This is the first multicenter study in Korea on CUP and has

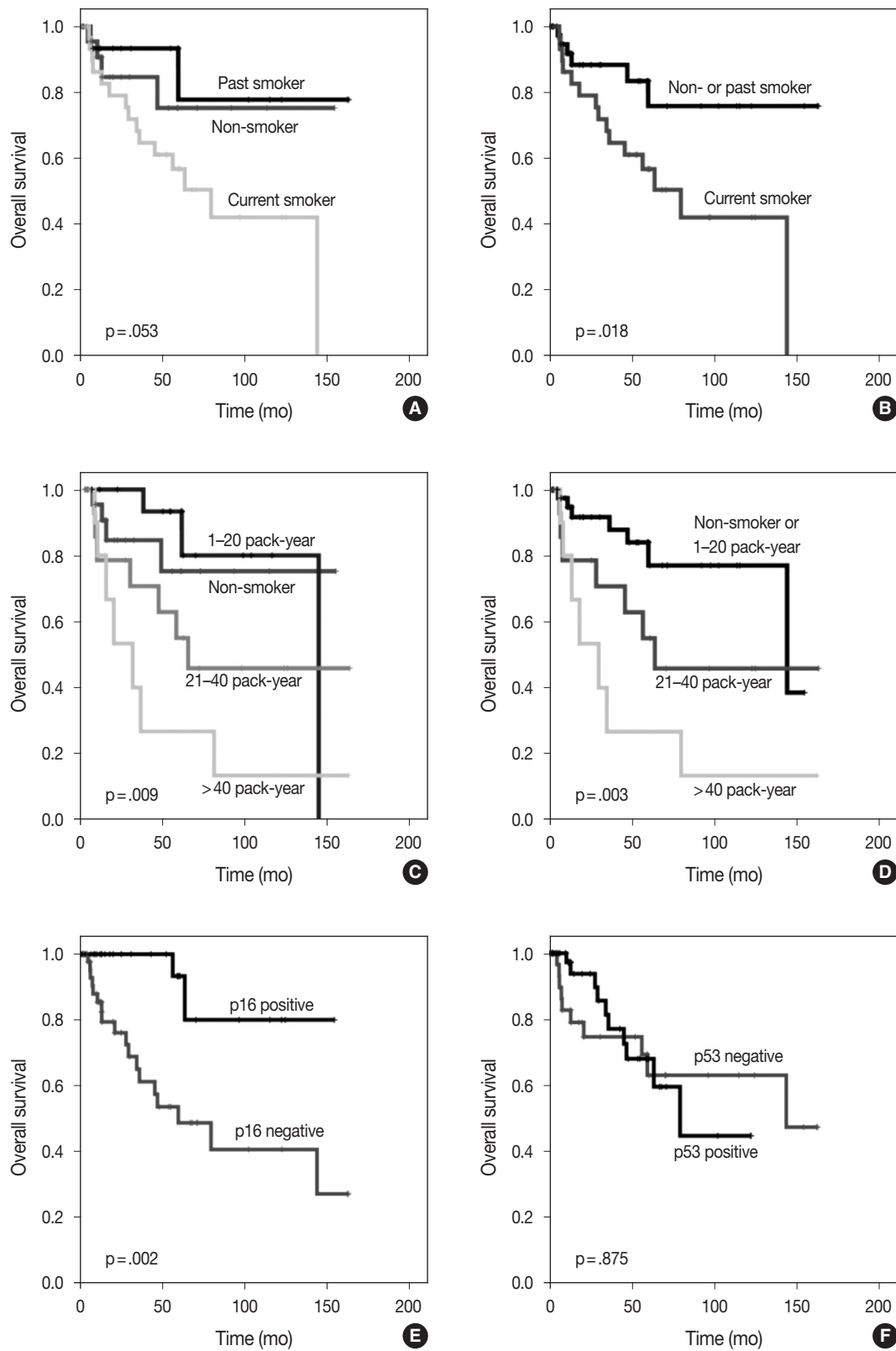


Fig. 2. Comparison of overall survival in cervical metastasis from an unknown primary tumor according to smoking status (A,B), smoking duration (C, D), and p16 (E) and p53 (F).

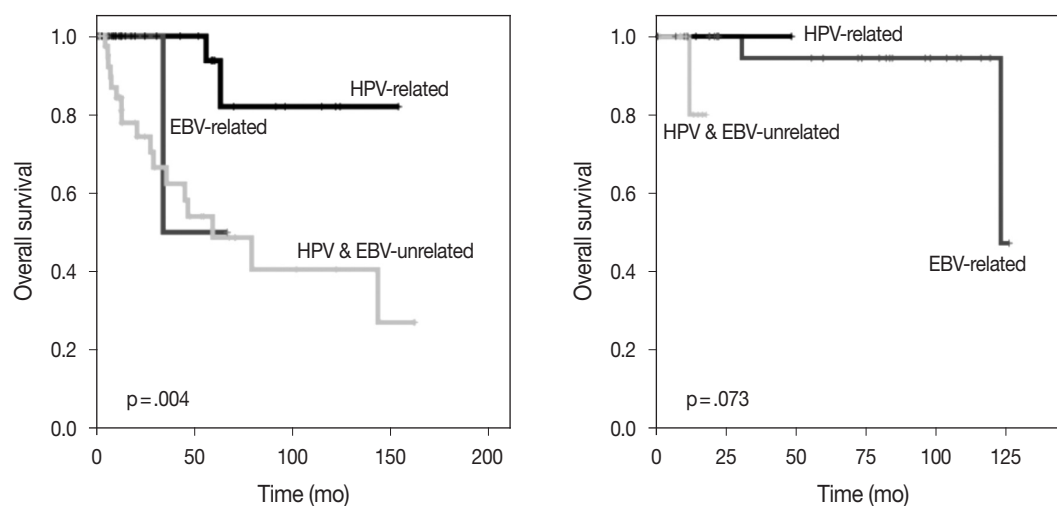


Fig. 3. Comparison of overall survival according to viral status in cervical metastasis from an unknown primary tumor and cervical metastasis with proven primary sites. (A) The human papillomavirus (HPV)-related cervical metastasis from an unknown primary tumor (CUP) cases had the longest overall survival, and the HPV- and Epstein-Barr virus (EBV)-unrelated CUP patients had the worst prognosis, with a significant difference among the three groups. (B) In cervical metastasis with proven primary sites, there was no difference in overall survival according to viral status.

Table 4. HPV and EBV status of cervical metastasis with proven primary sites

Primary site (n=64)	HPV-related (n=28, 43.8%)	EBV-related (n=3, 4.7%)	HPV & EBV-unrelated (n=10, 15.6%)	Not determined (n=23, 35.9%)
Oropharynx (n=41, 64.1%)	25 (89.3)	0	1 (10)	15 (65.2)
Hypopharynx (n=5, 7.8%)	0	0	1 (10)	4 (17.4)
Nasopharynx (n=5, 7.8%)	0	3 (100)	1 (10)	1 (4.3)
Oral cavity (n=3, 4.7%)	0	0	2 (20)	1 (4.3)
Pharynx, not specific (n=2, 3.1%)	1 (3.6)	0	0	1 (4.3)
Retropharynx (n=1, 1.6%)	0	0	0	1 (4.3)
Esophagus (n=4, 6.3%)	0	0	4 (40)	0
Larynx (n=1, 1.6%)	0	0	1 (10)	0
Anus (n=1, 1.6%)	1 (3.6)	0	0	0
Uterine cervix (n=1, 1.6%)	1 (3.6)	0	0	0

Values are presented as number (%).

HPV, human papillomavirus; EBV, Epstein-Barr virus.

noted several important findings. First, HPV-related cases constituted 38.9% of all CUP cases, which is approximately 10% lower than the frequency (49%) reported in a meta-analysis of 17 studies [17]. Second, HPV-related CUP in Korea showed better survival outcomes than HPV-unrelated CUP, per the studies in Western countries, including 978 cases in the United States [5] and 68 cases in the National Cancer Database [6]. Interestingly, a previous Korean study [18] reported opposing findings, a finding which might have been attributed to the small number of cases. A multicenter study is considered to have merits of case collection and reduction of bias due to the hospital size.

Although only 5 EBV-related CUP cases were analyzed in this study, virus-related CUP had a better prognosis than the virus-

unrelated group, and HPV-related CUP showed the best OS ($p = .004$) and a high NED status frequency (73.0%). Our results were consistent with the eighth edition of the AJCC staging system that accepted the unique biologic behavior and natural history of EBV- and HPV-related tumors. In addition, our results supported a unique staging system for cervical lymphadenopathy with an unknown primary tumor to apply to oropharynx and nasopharynx staging according to HPV and EBV status.

Characteristics of viral-related tumors were also well organized among CUP cases in Korea. HPV- and EBV-unrelated CUP cases showed the worst OS and a high DOD/DOC status frequency (37.0%, $p = .011$) among the three groups, with a high rate of extranodal extension ($p = .046$) and N staging ($p = .001$). HPV-

related CUP patients were younger than HPV-unrelated CUP patients ($p = .013$), and their lymph nodes showed a higher frequency of cystic changes ($p = .016$) and the basaloid pattern ($p < .001$) as seen in HPV-mediated oropharynx cancer. EBV-related CUP showed a high frequency of lymphoepithelial lesions ($p = .010$), as with nasopharynx cancer associated with EBV.

Dixon et al. [23] found no significant differences in OS ($p = .85$ and $p = .42$) and disease-free survival ($p = .87$ and $p = .58$) in CUP through the univariate analysis of smoking duration (≤ 10 vs. > 10 pack-years) and smoking status (current smoker vs. ex-smoker vs. never-smoker). Tribius et al. [7] found that a smoking history of > 10 pack-years showed a worse prognosis than that of ≤ 10 pack-years in HPV-DNA-positive and p16-positive CUP. In addition, HPV-DNA-positive and p16-positive CUP with a smoking history of > 10 pack-years showed a similar survival curve to HPV-DNA-negative or p16-negative groups ($p = .02$) [7]. In our study, smoking duration was a significantly worse prognostic factor for OS in the multivariate analysis of total CUP cases. The Kaplan-Meier survival curves also showed significant differences in OS according to smoking status (non-smokers or past smokers vs. current smokers, $p = .018$) and smoking duration (non-smoker or < 20 vs. $21-40$ vs. > 40 pack-years, $p = .003$). However, there was no significant difference in OS in the HPV-related CUP or virus-unrelated CUP groups according to smoking status or duration.

As a limitation of our study, HPV-related CUP was defined by three methods of RT-PCR, DNA ISH, and p16 IHC. RT-PCR is stable and reproducible. However, as the sensitivity is high, there is a possibility of contamination by surrounding HPV-infected normal epithelium or other samples [24]. DNA ISH is widely used in research due to its low price but shows different sensitivity and specificity values according to the type of probe for the target HPV [25]. The Ventana system was used in this study, but even with Ventana, different performances were achieved [26,27] owing to the varying quality-control procedures, laboratory experience, and techniques [28]. p16 positivity in IHC is used as a surrogate marker for high-risk HPV-associated tumorigenesis because p16 can be overexpressed by the loss of inhibitory feedback of the phosphorylated Rb protein, degraded by the E7 protein of high-risk HPV [29]. However, other processes, such as inflammation, regeneration, and *TP53* mutation, contribute to p16 overexpression [30,31]. The choice of one of the three methods varied across institutions and even within the same institution. In this study, 90.5% (19/21) of high-risk HPV-positive cases showed p16 overexpression, and 21.7% (13/60) of high-risk HPV-negative cases showed p16 overexpression. At

Johns Hopkins Hospital, which routinely uses both the HPV DNA ISH test and p16 IHC, they found p16-positive/HPV-DNA-negative cases in 18% of oropharyngeal squamous cell carcinoma [32], similar to the 16% identified in our study. They performed an additional RNA ISH assay for high-risk E6/E7 mRNA and confirmed the presence of active transcriptional active HPV in 84% of these cases. Judging from the characteristics of each method and the results of this study, the cause of the discrepancy in the cases showing p16 overexpression but DNA ISH negativity may be due to the false-negative result of DNA ISH from the background signal or due to the overexpression of p16 by another non-viral mechanism. HPV type 16 infection and disruptive *TP53* mutations did not seem to overlap, so HPV infection showed an inverse relationship with *TP53* mutations [21,22]. This study showed no inverse relationship between p53 and HPV infection. In this study, tumors showing nuclear staining in $\geq 10\%$ of the tumor cells are considered positive for p53 immunostaining. The reason for the cutoff of 10% was based on the analysis of multiple studies that found significant correlations between p53 overexpression and higher tumor grade [33,34], *TP53* gene mutations [35-37], or worse prognosis [38,39] when the threshold was set at 10%. However, the p53 immunostaining results in this study may not represent the entirety of the tumor due to being performed in the TMA. Different interpretations of p53 positivity among institutions may have resulted in different results in previous studies. Additionally, $> 10\%$ of p53 nuclear expression may not represent the *TP53* mutation of the tumor with rarity in this study. We lacked enough follow-up data and scale because we could only secure OS data. Although this is a multicenter study, its statistical power to understand CUP remains insufficient due to the small collection of data, which is the peculiarity of the low incidence of this entity.

In conclusion, virus-unrelated CUP in Korea had the highest frequency among CUP cases. Virus-related CUP had a better prognosis than the virus-unrelated group, and patients with HPV-related CUP showed the best OS. HPV-related CUP was similar to HPV-mediated oropharyngeal cancer and EBV-related CUP was similar to nasopharyngeal cancer in terms of clinicopathologic characteristics. In total CUP cases, longer smoking duration and virus-unrelated CUP were significant factors for poor prognosis.

Supplementary Information

The Data Supplement is available with this article at <https://doi.org/10.4132/jptm.2023.04.12>.

Ethics Statement

This study was approved by the Institutional Review Board of Asan Medical Center (2020-1722), and patient informed consent was waived, given the retrospective nature of the study. All procedures were performed in accordance with the 1964 Declaration of Helsinki and its later amendments or comparable ethical standards.

Availability of Data and Material

All data generated or analyzed during the study are included in this published article (and its supplementary information files).

Code Availability

Not applicable.

ORCID

Miseon Lee <https://orcid.org/0000-0002-6385-7621>
 Uiree Jo <https://orcid.org/0000-0001-6783-4016>
 Joon Seon Song <https://orcid.org/0000-0002-7429-4254>
 Youn Soo Lee <https://orcid.org/0000-0002-1653-6315>
 Chang Gok Woo <https://orcid.org/0000-0002-9131-3779>
 Dong-Hoon Kim <https://orcid.org/0000-0001-5722-6703>
 Jung Yeon Kim <https://orcid.org/0000-0002-7539-9242>
 Sun Och Yoon <https://orcid.org/0000-0002-5115-1402>
 Kyung-Ja Cho <https://orcid.org/0000-0002-4911-7774>

Author Contributions

Conceptualization: KJC. Data curation and interpretation: ML, UJ, JSS, YSL, CGW, DHK, JYK, SOY, KJC. Supervision: KJC. Writing—original draft: ML. Writing—review & editing: ML, KJC. Approval of final manuscript: all authors.

Conflicts of Interest

J.S.S., a contributing editor of the *Journal of Pathology and Translational Medicine*, was not involved in the editorial evaluation or decision to publish this article. All remaining authors have declared no conflicts of interest.

Funding Statement

This study was supported by the Korean Society of Pathologists (2021).

References

- Califano J, Westra WH, Koch W, et al. Unknown primary head and neck squamous cell carcinoma: molecular identification of the site of origin. *J Natl Cancer Inst* 1999; 91: 599-604.
- van de Wouw AJ, Jansen RL, Speel EJ, Hillen HF. The unknown biology of the unknown primary tumour: a literature review. *Ann Oncol* 2003; 14: 191-6.
- Strojan P, Ferlito A, Medina JE, et al. Contemporary management of lymph node metastases from an unknown primary to the neck: I. A review of diagnostic approaches. *Head Neck* 2013; 35: 123-32.
- Waltonen JD, Ozer E, Hall NC, Schuller DE, Agrawal A. Metastatic carcinoma of the neck of unknown primary origin: evolution and efficacy of the modern workup. *Arch Otolaryngol Head Neck Surg* 2009; 135: 1024-9.
- Cheraghloo S, Torabi SJ, Husain ZA, et al. HPV status in unknown primary head and neck cancer: prognosis and treatment outcomes. *Laryngoscope* 2019; 129: 684-91.
- Axelsson L, Nyman J, Haugen-Cange H, et al. Prognostic factors for head and neck cancer of unknown primary including the impact of human papilloma virus infection. *J Otolaryngol Head Neck Surg* 2017; 46: 45.
- Tribius S, Hoffmann AS, Bastrop S, et al. HPV status in patients with head and neck of carcinoma of unknown primary site: HPV, tobacco smoking, and outcome. *Oral Oncol* 2012; 48: 1178-84.
- Chernock RD, Lewis JS. Approach to metastatic carcinoma of unknown primary in the head and neck: squamous cell carcinoma and beyond. *Head Neck Pathol* 2015; 9: 6-15.
- Abogunrin S, Di Tanna GL, Keeping S, Carroll S, Iheanacho I. Prevalence of human papillomavirus in head and neck cancers in European populations: a meta-analysis. *BMC Cancer* 2014; 14: 968.
- Kreimer AR, Clifford GM, Boyle P, Franceschi S. Human papillomavirus types in head and neck squamous cell carcinomas worldwide: a systematic review. *Cancer Epidemiol Biomarkers Prev* 2005; 14: 467-75.
- Rickinson AB. Co-infections, inflammation and oncogenesis: future directions for EBV research. *Semin Cancer Biol* 2014; 26: 99-115.
- Chang ET, Adami HO. The enigmatic epidemiology of nasopharyngeal carcinoma. *Cancer Epidemiol Biomarkers Prev* 2006; 15: 1765-77.
- Piazza C, Incandela F, Giannini L. Unknown primary of the head and neck: a new entry in the TNM staging system with old dilemmas for everyday practice. *Curr Opin Otolaryngol Head Neck Surg* 2019; 27: 73-9.
- Marur S, D'Souza G, Westra WH, Forastiere AA. HPV-associated head and neck cancer: a virus-related cancer epidemic. *Lancet Oncol* 2010; 11: 781-9.
- Ang KK, Harris J, Wheeler R, et al. Human papillomavirus and survival of patients with oropharyngeal cancer. *N Engl J Med* 2010; 363: 24-35.
- Lydiatt WM, Patel SG, O'Sullivan B, et al. Head and neck cancers: major changes in the American Joint Committee on cancer eighth edition cancer staging manual. *CA Cancer J Clin* 2017; 67: 122-37.
- Ren J, Yang W, Su J, et al. Human papillomavirus and p16 immunostaining, prevalence and prognosis of squamous carcinoma of unknown primary in the head and neck region. *Int J Cancer* 2019; 145: 1465-74.
- Cho WK, Roh JL, Cho KJ, Choi SH, Nam SY, Kim SY. Predictors of survival and recurrence after primary surgery for cervical metastasis of unknown primary. *J Cancer Res Clin Oncol* 2020; 146: 925-33.
- Lee M, Kim SB, Lee SW, et al. Human papillomavirus prevalence and cell cycle related protein expression in tonsillar squamous cell carcinomas of Korean patients with clinicopathologic analysis. *Korean J Pathol* 2013; 47: 148-57.
- Ryu CH, Ryu J, Cho KH, et al. Human papillomavirus-related cell cycle markers can predict survival outcomes following a transoral lateral oropharyngectomy for tonsillar squamous cell carcinoma. *J Surg Oncol* 2014; 110: 393-9.
- Maruyama H, Yasui T, Ishikawa-Fujiwara T, et al. Human papillomavirus and p53 mutations in head and neck squamous cell carcinoma among Japanese population. *Cancer Sci* 2014; 105: 409-17.
- Westra WH, Taube JM, Poeta ML, Begum S, Sidransky D, Koch WM. Inverse relationship between human papillomavirus-16 infection and disruptive p53 gene mutations in squamous cell carcinoma of the head and neck. *Clin Cancer Res* 2008; 14: 366-9.
- Dixon PR, Au M, Hosni A, et al. Impact of p16 expression, nodal status, and smoking on oncologic outcomes of patients with head

- and neck unknown primary squamous cell carcinoma. *Head Neck* 2016; 38: 1347-53.
24. Boscolo-Rizzo P, Pawlita M, Holzinger D. From HPV-positive towards HPV-driven oropharyngeal squamous cell carcinomas. *Cancer Treat Rev* 2016; 42: 24-9.
 25. Augustin JG, Lepine C, Morini A, et al. HPV detection in head and neck squamous cell carcinomas: what is the issue? *Front Oncol* 2020; 10: 1751.
 26. Schlecht NF, Brandwein-Gensler M, Nuovo GJ, et al. A comparison of clinically utilized human papillomavirus detection methods in head and neck cancer. *Mod Pathol* 2011; 24: 1295-305.
 27. Keung ES, Souers RJ, Bridge JA, et al. Comparative performance of high-risk human papillomavirus RNA and DNA in situ hybridization on College of American Pathologists proficiency tests. *Arch Pathol Lab Med* 2020; 144: 344-9.
 28. Unger ER. In situ diagnosis of human papillomaviruses. *Clin Lab Med* 2000; 20: 289-301.
 29. Faraji F, Zaidi M, Fakhry C, Gaykalova DA. Molecular mechanisms of human papillomavirus-related carcinogenesis in head and neck cancer. *Microbes Infect* 2017; 19: 464-75.
 30. Khleif SN, DeGregori J, Yee CL, et al. Inhibition of cyclin D-CDK4/CDK6 activity is associated with an E2F-mediated induction of cyclin kinase inhibitor activity. *Proc Natl Acad Sci U S A* 1996; 93: 4350-4.
 31. Rietbergen MM, Snijders PJ, Beekzada D, et al. Molecular characterization of p16-immunopositive but HPV DNA-negative oropharyngeal carcinomas. *Int J Cancer* 2014; 134: 2366-72.
 32. Singhi AD, Westra WH. Comparison of human papillomavirus in situ hybridization and p16 immunohistochemistry in the detection of human papillomavirus-associated head and neck cancer based on a prospective clinical experience. *Cancer* 2010; 116: 2166-73.
 33. Hashmi AA, Hussain ZF, Hashmi SK, et al. Immunohistochemical over expression of p53 in head and neck Squamous cell carcinoma: clinical and prognostic significance. *BMC Res Notes* 2018; 11: 433.
 34. Mertens LS, Claps F, Mayr R, et al. The search for the optimal cut-off value of p53-immunohistochemistry to predict prognosis of invasive bladder cancer: a multi-center, multi-laboratory analysis. *Int J Surg Pathol* 2023; 31: 157-66.
 35. Tanboon J, Williams EA, Louis DN. The diagnostic use of immunohistochemical surrogates for signature molecular genetic alterations in gliomas. *J Neuropathol Exp Neurol* 2016; 75: 4-18.
 36. Hwang HJ, Nam SK, Park H, et al. Prediction of TP53 mutations by p53 immunohistochemistry and their prognostic significance in gastric cancer. *J Pathol Transl Med* 2020; 54: 378-86.
 37. Alsner J, Jensen V, Kyndi M, et al. A comparison between p53 accumulation determined by immunohistochemistry and TP53 mutations as prognostic variables in tumours from breast cancer patients. *Acta Oncol* 2008; 47: 600-7.
 38. Wang L, Yu X, Li J, Zhang Z, Hou J, Li F. Prognostic significance of p53 expression in patients with esophageal cancer: a meta-analysis. *BMC Cancer* 2016; 16: 373.
 39. Carlos de Vicente J, Junquera Gutierrez LM, Zapatero AH, Fresno Forcelledo MF, Hernandez-Vallejo G, Lopez Arranz JS. Prognostic significance of p53 expression in oral squamous cell carcinoma without neck node metastases. *Head Neck* 2004; 26: 22-30.

Thyroid pathology, a clue to PTEN hamartoma tumor syndrome

Yurimi Lee, Young Lyun Oh

Department of Pathology and Translational Genomics, Samsung Medical Center, Sungkyunkwan University School of Medicine, Seoul, Korea

Phosphatase and tensin homolog (*PTEN*) hamartoma tumor syndrome (PHTS) is a hereditary disorder caused by germline inactivating mutations in the *PTEN* tumor suppressor gene. As a type of PHTS, Cowden syndrome is associated with abnormalities of the thyroid, breast, uterus, and gastrointestinal tract. A 52-year-old-woman visited the outpatient clinic of our endocrinology clinic with multiple thyroid nodules and Hashimoto's thyroiditis. Computed tomography imaging revealed a multinodular mass measuring up to 3.5 cm in the left thyroid lobe, causing laryngotracheal airway displacement. The total thyroidectomy specimen revealed multiple follicular adenomas and adenomatous nodules with lymphocytic thyroiditis and lipomatous metaplasia in the background. The patient was suspected of PHTS based on her thyroid pathology, family history, and numerous hamartomatous lesions of the breast, uterus, and skin. Her diagnosis was confirmed through molecular testing. This case demonstrates that pathologists must be well acquainted with thyroid pathology in PHTS.

Key Words: PTEN; Hamartoma tumor syndrome; Thyroid pathology; Cowden

Received: January 10, 2023 **Revised:** February 27, 2023 **Accepted:** March 4, 2023

Corresponding Author: Young Lyun Oh, MD, PhD, Department of Pathology and Translational Genomics, Samsung Medical Center, Sungkyunkwan University School of Medicine, 81 Irwon-ro, Gangnam-gu, Seoul 06351, Korea
Tel: +82-2-3410-2805, Fax: +82-2-3410-0025, E-mail: yl.oh@samsung.com

Phosphatase and tensin homolog (*PTEN*) hamartoma tumor syndrome (PHTS) is a hereditary disorder caused by mutations in the *PTEN* tumor suppressor gene located on 10q23.3 [1]. It is a rare, autosomal dominant spectrum of disease, causing hamartomatous overgrowth of tissues in the thyroid, gastrointestinal tract, and skin. Patients with this disease are at increased risk of thyroid, breast, endometrial, renal, and possibly colorectal cancers [2-4]. PHTS includes Cowden syndrome (CS), Bannayan-Riley-Ruvalcaba syndrome (BRRS), *PTEN*-related Proteus syndrome (PS), and Proteus-like syndrome. CS is the most common PHTS, usually presenting in young to middle-aged adults. Thyroid pathologic findings in patients with CS are distinctive and characteristic [1,5,6]. Recognition of CS by a pathologist is critical for cancer screenings and genetic counseling.

We encountered a patient who presented with unusual thyroid pathology, suspicious of CS. We aim to demonstrate that thyroid pathology can be a clue for diagnosing PHTS, including clinical and immunophenotypical features and molecular testing results. Our observations will aid pathologists and clinicians in properly diagnosing PHTS.

CASE REPORT

A 52-year-old-woman visited our endocrinology clinic with multiple thyroid nodules. She had undergone a right lobectomy for benign nodules 30 years prior. She had remaining left multiple thyroid nodules diagnosed as nodular hyperplasia from fine-needle aspiration cytology in 2005. She received ultrasonography (US) and computed tomography (CT) exams in 2021 to evaluate the surgical site for symptoms of neck swelling. The US revealed an enlarged left lobe with numerous iso- and hypoechoic nodules. Several nodules had cystic changes, while others were solid with well-defined margins and increased vascularity. The intermediate and low suspicion nodules measured up to 3.5 cm. In addition, the CT revealed multinodular masses in the left thyroid lobe, causing laryngotracheal airway displacement (Fig. 1A, B). The patient underwent a subsequent core needle biopsy on the 3.5 cm-sized, intermediate suspicious mass in the left lobe.

The core needle biopsy of the thyroid revealed monomorphic microfollicular cells with fibrous capsules. A follicular neoplasm was suspected, and a left thyroid gland lobectomy was performed.

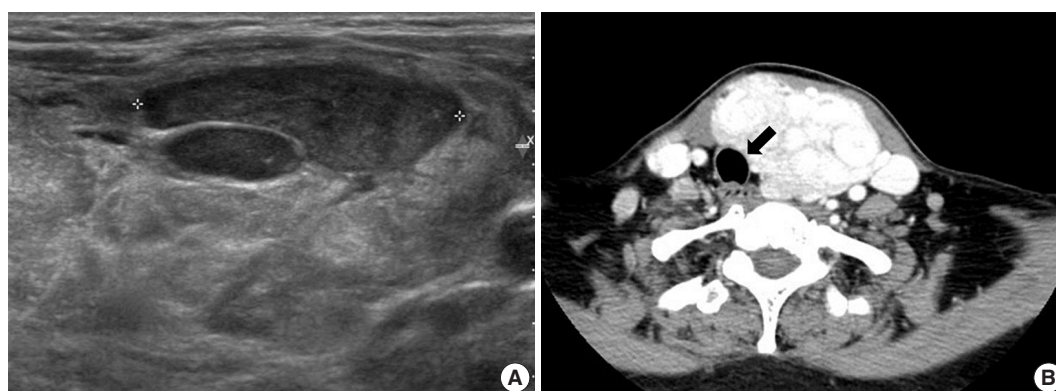


Fig. 1. Radiologic and core needle biopsy images of the thyroid. (A) Thyroid ultrasound image showing multiple hypoechoic solid nodules with well-defined margins. (B) Thyroid computed tomography revealing multinodular masses in the left thyroid lobe displacing the laryngotracheal airway (arrow).

The resected specimen of the left lobe was enlarged, measuring 9 × 7 cm, and consisted of well-circumscribed nodular lesions (Fig. 2A).

Grossly, multiple well-circumscribed tan nodular lesions with suspicious encapsulation and unencapsulated small nodules with calcification and infarction were identified. Adjacent to the nodules, yellowish fatty components were present. The nodules were too numerous with inconspicuous margins to determine the exact number.

Microscopically, follicular adenomas with monomorphic microfollicular patterns of growth (Fig. 2B, C), numbering more than 20 up to 3.5 × 2.3 cm in size, were identified. They were well-demarcated with a fibrous capsule containing medium to large vessels. Capsular or vascular invasion was not observed. In addition, numerous adenomatous hyperplasias without a thin fibrous band were noted. A mixture of lipomatous metaplasia with mixed mature fat and follicles and chronic lymphocytic thyroiditis was characteristic (Fig. 2D, E). A 0.5-cm-sized lymphoepithelial cyst composed of stratified squamous epithelium linings, lymphoid germinal centers, and luminal debris with cholesterol clefts was present in the background of the adjacent chronic lymphocytic thyroiditis (Fig. 2F). Based on these aspects, it was considered to exhibit hamartomatous morphology, and PHTS was suspected. According to the literature indicating PTEN staining for sensitive and specific detection of CS, PTEN immunohistochemistry was performed. In addition, to exclude papillary thyroid carcinoma, the slides showing subtle nuclear atypia were subjected to HBME-1, CD56, cytokeratin 19, and galectin-3 immunohistochemical staining. Small adenomatous nodules with mild nuclear atypia maintained CD56 expression and were negative for HBME1. Galectin-3 and cytokeratin 19 were focally expressed in areas of thyroiditis and fibrosis with calcifications,

but were considered negative.

Proliferative thyroid lesions were all negative for PTEN proteins, whereas the normal background thyroid tissue was positive (Fig. 3A, B). PTEN proteins in normal tissue and endothelial cells within the tumor exhibited nuclear and cytoplasmic expression, but the loss of expression was observed in the follicular adenoma components (Fig. 3C, D).

The immunohistochemistry result of PTEN was compatible with PHTS. Further examination of the patient's history revealed a family history of uterine disease and thyroid cancer in her mother and aunt. Moreover, the patient had received sclerotherapy for an arteriovenous malformation in 2002, a hysterectomy for leiomyomas in 2011, a polypectomy for multiple gastric polyps, and an excisional biopsy of the breasts for intraductal papillomas in 2021. Reviewing her medical history, we found that the endometrial glands of the uterus specimen showed nuclear atypia, crowding, and complex architecture with loss of PTEN expression. Her breast specimen exhibited a PTEN loss within the intraductal papilloma. Under the recommendation of clinical correlation and genetic counseling for the PHTS, the patient underwent an additional endoscopy exam and skin biopsy. The patient had a lipoma in the proximal jejunum, fundic gland polyps in the stomach, and multiple facial plaques diagnosed as syringomas in her forehead.

The next-generation sequencing analysis revealed a heterozygous germline mutation in chromosome 10q23 (c.260_281delinsCATAT). A subsequent genetic analysis by polymerase chain reaction and direct sequencing revealed that the mutation induces a frameshift and leads to a stop codon ending the transcription process (p.Gln87Profs*14). The mRNA reference sequence was NM.000314.4. Therefore, the patient's diagnosis was confirmed as PHTS.

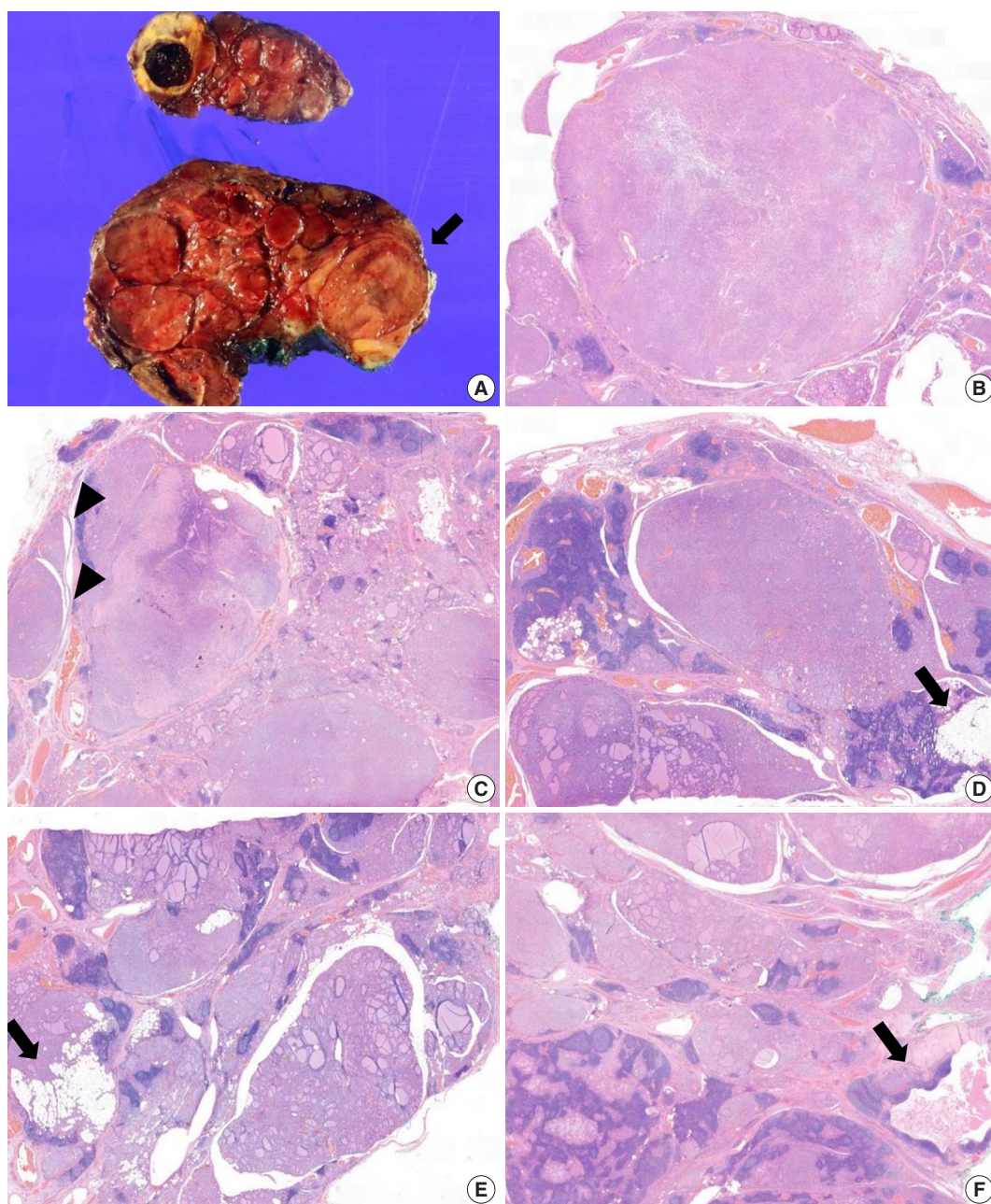


Fig. 2. Thyroid gross and histologic findings of Cowden syndrome. (A) Multiple well-circumscribed nodular lesions with suspicious encapsulations (arrow) and yellowish fat components. (B) Follicular adenomas with a monomorphic microfollicular pattern of growth are identified and well-demarcated with a fibrous capsule. (C) Multiple microadenomas with or without a thin fibrous band (arrowheads). (D, E) Adenomatous nodules, small to medium-sized adenomas with a microfollicular pattern, lipomatous metaplasia (arrows), and chronic lymphocytic thyroiditis are intermixed. (F) Multiple adenomatous hyperplasias and a lymphoepithelial cyst (arrow), considered a hamartomatous component, are noted.

DISCUSSION

PTEN encodes a tumor suppressor, a dual-specificity phosphatase that downregulates the anti-apoptotic/pro-proliferative phosphatidylinositol 3kinase/protein kinase B signaling pathway, and the mitogen-activated kinase pathway [1,7]. Inactivation

of PTEN occurs through frameshift mutations, inactivating missense mutations, and copy number losses, typically in exons 5, 7, and 8 [4]. PHTS includes CS, BRRS, which is a congenital disorder characterized by macrocephaly [8] and PS, which is a hereditary disorder displaying characteristic hyperostosis [8]. Based on the clinical manifestations, our patient was suspected

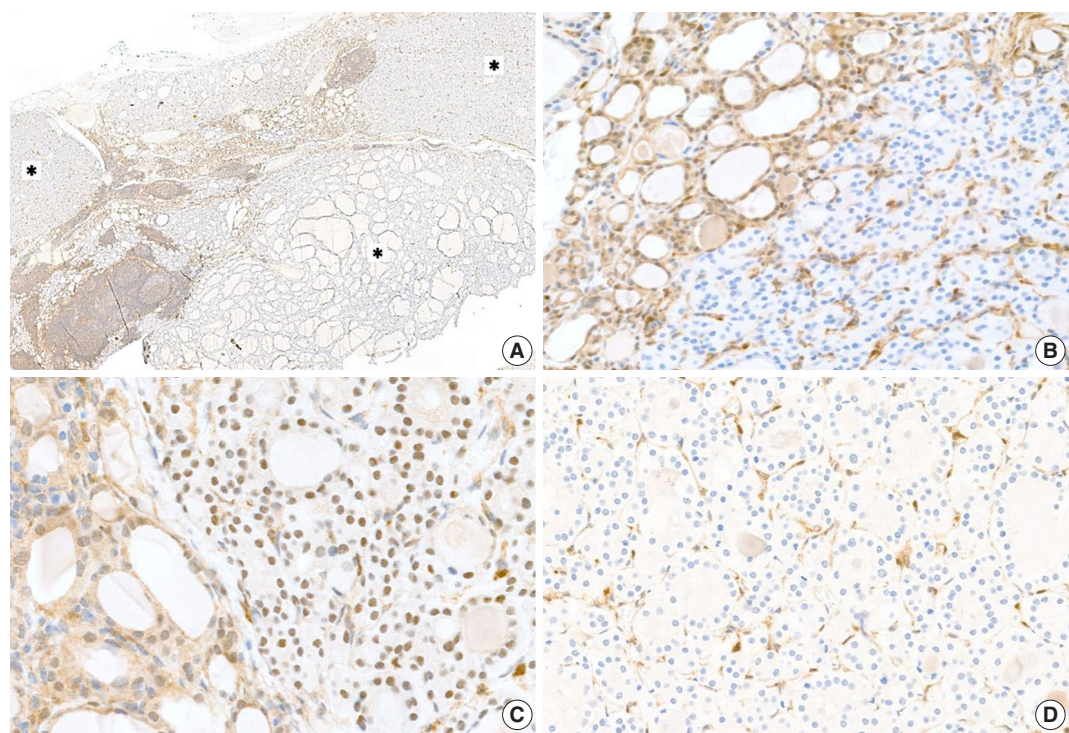


Fig. 3. Phosphatase and tensin homolog (PTEN) immunohistochemistry. (A) A low-magnification image showing heterogeneous PTEN expression between normal tissue and proliferative lesions (asterisks). (B) The contrast of PTEN expression in the left upper area and PTEN loss in the right lower area. (C) Nuclear and cytoplasmic expression of PTEN identified in several normal areas. (D) Loss of expression of PTEN with positive vascular endothelial cells representing the internal control.

Table 1. Cowden syndrome/PTHS testing criteria (NCCN Guidelines version 3.2019) [9]

Major criteria	Minor criteria ^a
Breast cancer	Autism spectrum disorder
Endometrial cancer	Colon cancer
Follicular thyroid cancer	≥3 esophageal glycogenic acanthoses
Multiple GI hamartomas or ganglioneuromas	Lipomas
Macrocephaly	Intellectual disability
Macular pigmentation of the glans penis	Papillary or follicular variant of papillary thyroid cancer
Mucocutaneous lesions	Thyroid structural lesions (e.g., Adenoma, nodules, goiter)
One biopsy-proven trichilemmoma	
Multiple palmoplantar keratoses	Renal cell carcinoma
Multifocal or extensive oral mucosal papillomatosis	Single GI hamartoma or ganglioneuroma
Multiple cutaneous facial papules	Testicular lipomatosis
	Vascular anomalies (including multiple intracranial developmental venous anomalies)

PHTS, phosphatase and tensin homolog hamartoma tumor syndrome; NCCN, National Comprehensive Cancer Network; GI, gastrointestinal.

^aInsufficient evidence exists in the literature to include fibrocystic disease of the breast, fibromas, and uterine fibroids as diagnostic criteria.

of CS among PHTS.

According to the National Comprehensive Cancer Network guidelines for CS/PTHS, genetic testing can be recommended when a patient satisfies one major and more than three or four minor criteria (Table 1) [9]. Genetic testing was relevant for our patient as she had multiple gastrointestinal hamartomas and cutaneous facial papules among the major criteria, and a lipoma,

thyroid structural lesions, and vascular anomaly meeting the minor criteria. Mucocutaneous lesions are present in 90% to 100% of CS cases [1,4,6], and cutaneous lesions are usually the first signs of the disease [4,10], with facial papules being the most frequent lesions [4].

Thyroid nodules, adenomas, and goiters have been reported in 30% to 68% of adults and 2% to 14% of children with *PTEN*

mutations [2,11,12]. Several studies have provided detailed descriptions of the clinical features and pathology of thyroid nodules in *PTEN* mutation carriers [2]. Harach et al. [5] were the first to note the histologic findings of multiple adenomatous goiters and multiple follicular adenomas, including adenolipomas, particularly in children and young adults, should alert clinicians to the possibility of CS [1]. In a pathologic study evaluating thyroidectomy specimens from patients with CS and BRRS, Laury et al. [6] observed that multiple adenomatous nodules were the most common finding (75%), followed by papillary thyroid carcinomas (60%), lymphocytic thyroiditis (55%), C-cell hyperplasia (55%), and follicular carcinoma (25%) [13]. For the diagnostic criteria of PHTS, only follicular thyroid cancer is specified as a major criterion because it appears to be over-represented in mutation carriers (25%) compared with the general population (15%) [2].

Thyroid lesions in patients with CS mainly manifest in females and present at a younger age (mean diagnosis age, 33.7 years) compared to sporadic thyroid nodules [14]. Grossly, solid yellow-tan thyroid nodules are identified with variations in size and number. Specifically, the thyroid nodules in CS do not present with abundant colloids as seen in sporadic goiters. Microscopically, the nodules are well-delineated, with no, partial, or complete encapsulation and variable growth patterns. The nodules present with microscopic features of follicular adenomas, cellular hyperplastic nodules, adenolipomas or lipomatous metaplasias, Hurthle cell or clear cell nodules, C-cell hyperplasia, papillary microcarcinomas, or follicular carcinoma in the background of chronic lymphocytic thyroiditis. The adenomatous nodules have a microfollicular architecture composed of small cellular follicles without a capsule. Meanwhile, follicular adenomas present with a well-defined fibrous capsule and possess an architectural pattern that differs from the surrounding thyroid tissue without capsular or vascular invasion. While these thyroid pathologic findings are not specific to CS patients [13], *PTEN* immunohistochemistry can be helpful for the identification of CS. *PTEN* immunohistochemical staining shows a complete or heterogeneous loss in adenomatous nodules, specifically in CS patients.

Although CS has a reported incidence of 1 in 200,000 [15], it seems that the prevalence has been underestimated because of the complex clinical criteria and non-specific manifestations that are similar to those found in the general population. However, the diagnosis of CS is essential because these patients have an increased cancer risk [13]. The projected estimated lifetime risks of cancer in individuals with PTHS range from 85%–89% for any cancer, 67%–85% for female breast cancer, 6%–38% for thyroid can-

cer, 2%–28% for endometrial cancer, 2%–34% for renal cancer, and 9%–20% for colorectal cancer [16–19]. The characteristic thyroid pathology and *PTEN* immunohistochemistry are indicators of PHTS, diagnosis of which is crucial for initiation of cancer screenings and genetic counseling.

To summarize, we report a case of a patient who presented with unusual thyroid pathology, exhibiting numerous follicular adenomas, adenomatous nodules with cellular and microfollicular proliferations intermixed with lipomatous metaplasia, and lymphocytic thyroiditis. The patient was diagnosed with PTHS based on the loss of *PTEN* immunohistochemical staining not only in the thyroid specimen but also in the breast and uterus specimens, and the diagnosis was confirmed by the molecular study. This case indicates the importance of recognizing the thyroid histologic findings of PTHS to suspect CS.

Ethics Statement

The research was approved by the Institutional Review Board of Samsung Medical Center (Protocol code: 2022-03-149; Date of approval: March 30, 2022) with a waiver of informed consent.

Availability of Data and Material

The datasets generated or analyzed during the study are available from the corresponding author on reasonable request.

Code Availability

Not applicable.

ORCID

Yurimi Lee <https://orcid.org/0000-0002-1820-5923>

Young Lyun Oh <https://orcid.org/0000-0002-9127-4642>

Author Contributions

Conceptualization: YLO. Data curation: YL. Formal analysis: YLO, YL. Funding acquisition: YLO. Investigation: YLO, YL. Methodology: YLO, YL. Project administration: YLO. Resources: YLO. Software: YL. Supervision: YLO. Validation: YLO, YL. Visualization: YL. Writing—original draft: YL. Writing—review & editing: YLO, YL. Approval of final manuscript: all authors.

Conflicts of Interest

The authors declare that they have no potential conflicts of interest.

Funding Statement

No funding to declare.

References

1. Cameselle-Teijeiro J, Fachal C, Cabezas-Agricola JM, et al. Thyroid pathology findings in Cowden syndrome: a clue for the diagnosis of the *PTEN* hamartoma tumor syndrome. *Am J Clin Pathol* 2015; 144: 322–8.
2. Pilarski R, Burt R, Kohlman W, Pho L, Shannon KM, Swisher E. Cowden syndrome and the *PTEN* hamartoma tumor syndrome: systematic review and revised diagnostic criteria. *J Natl Cancer Inst*

- 2013; 105: 1607-16.
3. Pilarski R. PTEN hamartoma tumor syndrome: a clinical overview. *Cancers (Basel)* 2019; 11: 844.
4. Son JH, Chung BY, Jung MJ, Choi YW, Kim HO, Park CW. Cowden disease: case report and review of the literature. *Ann Dermatol* 2019; 31: 325-30.
5. Harach HR, Soubeyran I, Brown A, Bonneau D, Longy M. Thyroid pathologic findings in patients with Cowden disease. *Ann Diagn Pathol* 1999; 3: 331-40.
6. Laury AR, Bongiovanni M, Tille JC, Kozakewich H, Nose V. Thyroid pathology in PTEN-hamartoma tumor syndrome: characteristic findings of a distinct entity. *Thyroid* 2011; 21: 135-44.
7. Chen CY, Chen J, He L, Stiles BL. PTEN: tumor suppressor and metabolic regulator. *Front Endocrinol (Lausanne)* 2018; 9: 338.
8. Yehia L, Eng C. PTEN hamartoma tumor syndrome. In: Adam MP, Ardinger HH, Pagon RA, et al., eds. *GeneReviews*. Seattle: University of Washington, Seattle, 1993.
9. Daly MB, Pilarski R, Yurgelun MB, et al. NCCN guidelines insights: genetic/familial high-risk assessment: breast, ovarian, and pancreatic, version 1.2020. *J Natl Compr Canc Netw* 2020; 18: 380-91.
10. Oh JG, Yoon CH, Lee CW. Case of Cowden syndrome associated with eccrine angiomatous hamartoma. *J Dermatol* 2007; 34: 135-7.
11. Pilarski R, Stephens JA, Noss R, Fisher JL, Prior TW. Predicting PTEN mutations: an evaluation of Cowden syndrome and Bannayan-Riley-Ruvalcaba syndrome clinical features. *J Med Genet* 2011; 48: 505-12.
12. Tan MH, Mester J, Peterson C, et al. A clinical scoring system for selection of patients for PTEN mutation testing is proposed on the basis of a prospective study of 3042 probands. *Am J Hum Genet* 2011; 88: 42-56.
13. Barletta JA, Bellizzi AM, Hornick JL. Immunohistochemical staining of thyroidectomy specimens for PTEN can aid in the identification of patients with Cowden syndrome. *Am J Surg Pathol* 2011; 35: 1505-11.
14. Hoda SA. Diagnostic pathology and molecular genetics of the thyroid: a comprehensive guide for practicing thyroid pathology. *Am J Clin Pathol* 2019; 152: 115.
15. Nelen MR, Kremer H, Konings IB, et al. Novel *PTEN* mutations in patients with Cowden disease: absence of clear genotype-phenotype correlations. *Eur J Hum Genet* 1999; 7: 267-73.
16. Tischkowitz M, Colas C, Pouwels S, Hoogerbrugge N; PHTS Guideline Development Group; European Reference Network GENTURIS. Cancer Surveillance Guideline for individuals with PTEN hamartoma tumour syndrome. *Eur J Hum Genet* 2020; 28: 1387-93.
17. Bubien V, Bonnet F, Brouste V, et al. High cumulative risks of cancer in patients with PTEN hamartoma tumour syndrome. *J Med Genet* 2013; 50: 255-63.
18. Nieuwenhuis MH, Kets CM, Murphy-Ryan M, et al. Cancer risk and genotype-phenotype correlations in PTEN hamartoma tumor syndrome. *Fam Cancer* 2014; 13: 57-63.
19. Tan MH, Mester JL, Ngeow J, Rybicki LA, Orloff MS, Eng C. Lifetime cancer risks in individuals with germline PTEN mutations. *Clin Cancer Res* 2012; 18: 400-7.



What's new in bone and soft tissue pathology 2023: guidelines for molecular testing

Farres Obeidin

Department of Pathology, Northwestern University Feinberg School of Medicine, Chicago, IL, USA

Received: March 16, 2023

Accepted: March 20, 2023

Corresponding Author: Farres Obeidin, MD
 Department of Pathology, Northwestern University
 Feinberg School of Medicine, Chicago, IL, USA
 E-mail: farres.obeidin@nm.org

ORCID

Farres Obeidin

<https://orcid.org/0000-0001-8461-9238>

This article has been published jointly, with consent, in both Journal of Pathology and Translational Medicine and PathologyOutlines.com.

Abstract

Our understanding of bone and soft tissue tumors has thoroughly evolved as a consequence of modern molecular techniques. DNA and RNA sequencing methods play an important diagnostic and therapeutic role in sarcoma pathology. Herein, we discuss current guidelines and best practices for molecular testing in bone and soft tissue tumors.

COMMON MOLECULAR METHODS

While translocation driver events are very rare in epithelial malignancies, they occur in up to 25% of sarcomas. As a result, molecular techniques for identifying recurrent translocations currently play an important diagnostic role in bone and soft tissue pathology.

Fluorescence in-situ hybridization (FISH)

FISH uses a fluorescently labeled probe targeted towards a specific genetic sequence. The fluores-

cent probe can then be assessed in situ using a fluorescence microscope. Dual-color dual-fusion probes are designed towards a particular gene fusion target, while dual-color break-apart probes have greater utility for gene fusions in which the partner may not be known (e.g. *EWSR1*). Large gene amplifications and deletions may also be detected by comparing the ratio of lost target signals to a control signal (e.g. *MDM2*).

Reverse-transcriptase polymerase chain reaction (RT-PCR)

PCR-based tests utilize PCR amplification of certain primer sequences that can be built to accommodate a set of gene rearrangements. This is particularly useful for larger panels that use known genetic breakpoints, but this method generally lacks the ability to detect new fusion partners.

Next-generation sequencing (NGS)

NGS has become standard for detection of both prognostic and therapeutic mutations. In sarcoma, new RNA-based methods, including hybrid-capture and anchored multiplex PCR, offer better detection for gene rearrangements. These methods have the added benefit of detecting new gene partners, which is particularly useful with promiscuous genes like *EWSR1*. The development of various commercial platforms for NGS fusion testing has significantly increased the availability of this test to pathologists. Additionally, tertiary institutions with large sample volume in bone and soft tissue pathology may opt to bring these methods in-house to improve turnaround times.

Methylation testing

Initially developed for usage in the diagnosis of brain tumors, methylation testing has expanded

to begin to include soft tissue and bone tumors. Methylation tests use an array chip to detect the methylation patterns of thousands of CpG islands to produce a “signature” for a particular tumor. Through statistical methods, these signatures can be clustered into groups of similar tumors, providing a tentative “cell of origin” diagnosis (Fig. 1). While still in its infancy, methylation has great potential for future diagnostics in soft tissue and bone.

TESTING GUIDELINES FOR SPECIFIC TUMOR CLASSES

The constantly growing number of translocation-driven soft tissue and bone tumors in the literature necessitates judicious use of diagnostic genetic testing. By employing a morphology-based approach, pathologists can triage mesenchymal neoplasms for both diagnostic and therapeutic testing. The following review takes a “line of differentiation” approach to decide on appropriate testing strategies.

Adipocytic

- *MDM2* amplification is the key differentiating factor between lipoma and well-differentiated/dedifferentiated liposarcoma (Fig. 2). *MDM2* amplification may also rarely be seen in other high-grade sarcomas; as such, caution is warranted when interpreting this finding without the presence of a well-differentiated liposarcoma component.
- *RB1* deletion (tested by loss of RB1 on immunostaining or NGS) is pathognomonic for spindle cell/pleomorphic lipoma and may be seen in about 50% of atypical spindle cell/pleomorphic lipomatous tumor.
- Myxoid liposarcoma is driven by translocations



Fig. 3. New NGS methods are highly sensitive and specific for translocations and can also be used to detect new fusions with previously undescribed partners. This example shows the readout from the NGS software demonstrating a fusion of the *USP6* gene with the *SERPINF1* gene in a case of nodular fasciitis.

Vascular

- Fusion testing is not required but helpful in the diagnosis, particularly in the case of the low-grade malignancies and hemangioendotheliomas.
- Epithelioid hemangioma is defined by recurrent fusions involving *FOS* and *FOSB*. Fusion testing is not required but can be useful in more cellular cases with atypical cytologic features.
- Epithelioid hemangioendothelioma: *WWTR1::CAMTA1* fusion or rarely *TFE3::YAP1* fusion; these malignant tumors show more primitive vascular differentiation, epithelioid morphology, intracytoplasmic lumens, and a distinct myxohyaline stroma that distinguishes them from epithelioid angiosarcoma. The *CAMTA1* fusion or IHC stain may be used to confirm the diagnosis.
- Pseudomyogenic hemangioendothelioma: *FOSB* gene fusions, usually with *SERPINE1* or *ACTB*; histologically, shows a rhabdomyoblastic-like appearance but stains for keratins and vascular markers.
- Angiosarcoma, like other high-grade sarcomas, shows complex genomic changes. The presence of *MYC* gene amplifications (tested by IHC, FISH, or NGS) is seen in most cases of post-irradiation or lymphedema-associated angiosarcoma. This finding is very useful in distinguishing post-irradiation atypical vascular lesions from true angiosarcoma.

Pericytic and smooth muscle

- While the diagnosis of glomus tumors is generally based on morphology, examples of deep, gastrointestinal, or malignant glomus tumors may confound the diagnosis. Most glomus tumors (including malignant variants) show recurrent fusions involving the *NOTCH* family of genes, most commonly *MIR143::NOTCH1/2/3*.
- Distinct from classical leiomyosarcoma, inflammatory leiomyosarcoma is a low-grade malignancy that has been shown to have a recurrent karyotypic pattern that is best seen on mRNA microarray technology, such as OncoScan™. These neoplasms show a near-haploid genotype that is thought to be a relevant driver of the disease process. Some tumors may show whole genome duplication afterwards, resulting in a pseudo-hyperdiploid karyotype that may signal transformation to a higher-grade malignancy. Recent studies have demonstrated a number of cases with rhabdomyoblastic IHC staining, and new terminology (inflammatory rhabdomyoblastic tumor) has been suggested.

Skeletal muscle

- Molecular testing in rhabdomyoblastic tumors is best utilized in the differentiation of embryonal and alveolar rhabdomyosarcoma. Both tumors may have a solid small round blue cell morphology and skeletal muscle staining with IHC. Myogenin IHC tends to be more diffuse in alveolar rhabdomyosarcoma; however, definitive diagnosis requires molecular detec-

tion of the typical *FOXO1* fusion with either *PAX3* or *PAX7* in alveolar rhabdomyosarcoma. Embryonal rhabdomyosarcoma may show recurrent mutations in the *RAS* family of genes or *DICER1* in some syndromic patients. The distinction between the alveolar and embryonal subtypes is necessary because of the variation in prognosis and treatment.

- Spindle cell rhabdomyosarcoma falls into three distinct molecular groupings. Congenital and infantile tumors are most often translocation-driven, with fusions involving *VGLL2*, *SRF*, *READ1*, *NCOA2*, and *CITED2*. Another subset of tumors in adolescents and young adults shows mutations in the *MYOD1* gene. The third category does not have recurrent genetic abnormalities. Additionally, some intraosseous variants may show *EWSR1*, *FUS*, or *MEIS1::NCOA2* rearrangements.

Gastrointestinal stromal tumor (GIST)

- All GISTs should be tested for mutational status, as these mutations predict response to treatment and prognosis.
- Mutations most commonly occur in *KIT* (exons 9, 11, 13, 14, or 17) and second most commonly in *PDGFRA* (exons 12, 14, and 18).
- Immunostaining for cKIT (CD117) does not imply the presence of a *KIT* mutation.
- SDH-deficient GISTs are negative for *KIT* and *PDGFRA* mutations and show mutations in *SDHA*, *SDHB*, *SDHC*, or *SDHD*. These mutations are typically screened by assessing for loss of SDHB IHC staining, which picks up

mutations in any of the four genes. SDH-deficient GISTs are more common in younger patients in the stomach.

- Some GISTs will instead show mutations in *RAS* family genes.
- A small proportion of GISTs may be negative for all four of these mutations, called quadruple wild-type GIST.

Uncertain differentiation and round cell tumors

- Undifferentiated round to spindle cell tumors and those with monomorphic cytology should be considered for large panel NGS fusion testing. IHC has been found to show much overlap in this category of tumors, and NGS testing offers the ability to pick up non-classical examples as well as discover new fusion partners.
- Currently, Ewing and Ewing-like round cell sarcomas can be split into six overall categories (Table 1). New fusion partners continue to be discovered, and the particular fusion may affect treatment and prognosis. Certain neoplasms show bi-immunophenotypic staining patterns that may lead to confusion. Molecular testing can be confirmatory.
- Angiomatoid fibrous histiocytoma: *EWSR1::ATF1*, *FUS::ATF1*, or *EWSR1::CREB1*; a low-grade malignancy with EMA and desmin co-positivity and prominent lymphoid cuffing.
- Ossifying fibromyxoid tumor: Most commonly *PHF1* rearrangements (50% of cases), rarely rearrangements in *BCOR* or *SUZ12*, suggesting a genetic overlap with endometrial stromal sarcoma; low-grade malignancy with prominent peritumoral metaplastic bone formation

and often co-positivity for keratins, S100, or desmin.

- Myoepithelial neoplasms of soft tissue: *EWSR1* or *FUS* rearrangements with several different partners; keratin and S100 co-positivity with myxoid to myxocollagenous background and bland round to spindle cells. *INI1* is lost in a subset. These tumors show different genetics to salivary gland myoepithelial neoplasms, which are often governed by *PLAG1* rearrangements.
- Extraskelatal myxoid chondrosarcoma: *NR4A3* rearrangement, most commonly with *EWSR1*. Keratin, S100, neuroendocrine, or myoepithelial markers may be nonspecifically positive. Morphologic and immunophenotypic overlap with myoepithelial neoplasms may cause diagnostic difficulty, and because of the presence of *EWSR1* as a partner in both, NGS testing is recommended to assess the partner gene to distinguish these two.
- Phosphaturic mesenchymal tumor: in patients with clinical evidence of hypophosphatemia and/or osteomalacia, serum testing may be performed for increased FGF23 secretion. Most of these tumors show fusions involving *FN1::FGFR1* or *FN1::FGF1*.
- *NTRK* gene rearrangements have been seen in an increasing spectrum of mesenchymal tumors. The prototypical infantile fibrosarcoma is defined by *ETV6::NTRK3*. However, *NTRK* fusions have now been seen in cellular mesoblastic nephroma as well as various myxoid soft tissue tumors with bland cytology and possible co-positivity for S100 and CD34, including lipofibromatosis-like neural tumor. Some uterine and soft tissue neoplasms with fibrosarcoma-like morphology also define a new subset

of *NTRK*-rearranged sarcomas.

- A subset of PEComa is driven by rearrangements in *TFE3*; often not required for the diagnosis, as the combination of myogenic and melanocytic markers is specific enough in most instances to diagnose PEComa.
- Recent studies have shown that the majority of true intimal sarcomas show amplifications in *MDM2*, similar to well/dedifferentiated liposarcoma. Intimal sarcoma may have variable differentiation and immunostaining. The presence of a luminal mass in the pulmonary or cardiac vasculature should prompt FISH testing for *MDM2* to confirm the diagnosis.

Bone and cartilage

- The diagnosis of primary bone lesions is still based most heavily on the morphology coupled with the radiological imaging.
- Some distinct exceptions where molecular testing can be diagnostically useful:
 - Aneurysmal bone cyst: *USP6* gene rearrangements; cystic, giant cell-rich neoplasm with reactive woven bone formation.
 - Low-grade central osteosarcoma/parosteal osteosarcoma: *MDM2* amplifications; low-grade osteoblastic tumors that, similar to well-differentiated liposarcoma, have potential to dedifferentiate. *MDM2* testing by FISH can help to distinguish from reactive or benign bone-forming tumors.
 - Giant cell tumor of bone/chondroblastoma: both show unique and specific mutations in *H3F3A* or *H3F3B*. IHC testing is useful as a molecular adjunct.
 - Conventional chondrosarcoma: *IDH1* or *IDH2* mutations in a subset of chondrosarcoma; can be diagnostically useful in small biopsies and dedifferentiated examples.
 - Mesenchymal chondrosarcoma: *HEY1::NCOA2* fusion; small round blue cell sarcoma with cartilaginous maturation.

Table 1. Ewing and Ewing-like round cell sarcomas

Category	Molecular abnormalities
Classic Ewing sarcoma and Ewing family tumors	<i>EWSR1::FL1</i> <i>EWSR1::ERG</i> <i>EWSR1::FEV</i> <i>EWSR1::ETV1</i> <i>ESWR1::ETV4</i> <i>FUS::ERG</i> <i>FUS::FEV</i>
<i>CIC</i> -rearranged sarcoma	<i>CIC::DUX4</i> <i>CIC::FOXO4</i> <i>CIC::LEUTX</i> <i>CIC::NUTM1</i> <i>CIC::NUTM2B</i>
<i>BCOR</i> -rearranged sarcoma	<i>BCOR::CCNB3</i> <i>BCOR</i> internal tandem duplication <i>BCOR::MAML3</i>
<i>GLI1</i> -altered sarcoma	<i>GLI1::MALAT1</i> <i>GLI1::ACTB</i> <i>GLI1</i> amplifications or other rearrangements
Non-Ewing family gene fusions	<i>EWSR1::PATZ1</i> <i>EWSR1::NFATC2</i> <i>EWSR1::SP3</i> <i>EWSR1::SMARCA5</i>
Unclassified round cell sarcoma	Fusion negative or unknown

Meet the Author

Dr. Obeidin has been an author for PathologyOutlines since 2018 and part of the PathologyOutlines editorial board since January 2022. He is currently an Assistant Professor of Pathology at Northwestern University Feinberg School of Medicine. He obtained his M.D. at the Medical College of Georgia and then completed his Anatomic and Clinical Pathology residency at Northwestern University. He then completed a fellowship in General Surgical Pathology and Bone and Soft Tissue Pathology at the University of California, Los Angeles.

